Streptomyces natalensis: Characterisation and Growth Optimisation

Thesis Presented by

Therese Mc Cormack, B.Sc., M.Eng.Sc.

School of Biotechnology
Dublin City University

Submitted as the requirement for the M.Sc. degree from
Dublin City University
December 2001

Supervisor : Dr. Patricia Kieran

Head of School : Prof. Richard O'Kennedy

I hereby certify that this material, which I now submit for assessment on the programme of study leading to the award of M.Sc. in Biotechnology is entirely my own work and has not been taken from the work of others save and to the extent that such work has been cited and acknowledged within the text of my work.

Signed: Thérèse Mc Cormack I.D. No.: 97 97 07 43

Date: 18/01/02

TABLE OF CONTENTS

ACKNOWLEDGEMENTS

I cannot submit this thesis without thanking so many people who have been there for me over the last few years.

To Patricia Kieran, my supervisor. I want to thank you for offering me the postgraduate position and giving me the opportunity to challenge myself, not to mention the chance to come back to DCU, my second home. For all your support throughout my most difficult times of the past few years. You have been more than a supervisor to me....

To Donal O'Shea (for his contribution to the image analysis work), Alan Pearson (in particular for his contribution to the Lasentec data), Brian Glennon (for his guidance throughout) and Ben Austen - thank you.

To all my pals in DCU – well what can I say?!! The end of the journey...sad, isn't it? You have all been there in one way or another to support me (sometimes literally!!) over the years. I don't think that you'll ever really know how much you mean to me. I can't say that I'm going to miss you all 'cause you know as well as I do that I'll be in to see you all at every opportunity!! I don't think that I could have falling profits in the Slipper on my conscience either.....!!! Seriously though, for all the 'deep and meaningfuls' (Alan, Paul...well actually probably all of you at some stage or other!). For all the laughs, nights out (slagging my dancing – that didn't 'impress me much'...though!!) and chats....I wish you all the very best in the future. I could name you all but I think referring to the directory for the department would be a better option!

To my friends from home (Fiona and Suzanne), from UCD (Shane and Niamh), from school (Denise, Emma, Susie, Noel, Justin, Joe, John-Paul), from Trinity and from my house (Dave, Mark and Lucy) – 'Thank God she's finished', I hear you say! Yes, I know...actually starting to worry now about what I'm going to talk about..hmmm! Thank you all for being there and listening! To Denise – a huge 'thank you' for all your help in the final stages of this thesis!

Finally to my family – my dad, Noel, (for all your encouragement), my mum, Margaret, (for always being there on the other end of the phone!), my sister, Elaine (for being my best friend, I'm so proud of you graduating as a qualified nurse) and my brothers, Shane (for your text messages…) and Noel (for having the attitude you have to life!!).

I know there are other people I should thank but I do really want to finally finish this thesis (!!) and as funds are running low - the amount of paper that would be involved….well I just can't afford it at the moment! So, to those people a big 'thank you'….. you know who you are.

So that's it! I finish this thesis and start a new road as 'Miss Mc Cormack' - has a nice ring to it! What do you think?……

ABSTRACT

Streptomyces natalensis is an actinomycete which produces the antifungal agent pimaricin (also known as natamycin) as a secondary metabolite. This research involves an investigation into the growth and morphology of *Streptomyces natalensis* in submerged culture with a view to optimising both characteristics. Four maintenance and cultivation techniques were investigated, involving the use of different inoculum sizes and different inoculum media, in a preliminary attempt to optimise growth and pimaricin production. An algorithm was developed and validated to characterise the morphology of the organism, (in terms of hyphal elements, clumps or pellets) using an Optimas Image Analyser (a semi-automated image analysis system). Further, this system and a Lasentec Focused Beam Reflectance Measurement (FBRM) probe were comparatively evaluated in terms of their potential to develop a morphological profile of the organism.

On the basis of the work performed it was determined that maintenance and cultivation techniques significantly affected growth and secondary metabolite production. It was concluded that YED was the preferred inoculum medium in terms of biomass and subsequent pimaricin production levels. Two fermentation media, SPG and phosphate-limited medium, were considered suitable for production of the secondary metabolite. Recorded pimaricin levels were, however, significantly lower than those obtained by other researchers. Cultivation of the organism in YEME medium, using a spore inoculum, resulted in high levels of biomass (~ 5 g/L).

Validation of the image analysis technique included an investigation of the sensitivity of the results to (i) the level of microscopic magnification employed, (ii) sample dilution (iii) the number of entities counted. Ensuring that 10-15 % of the total area available in the region of interest was occupied by entities of interest, as used by Treskatis *et al.* (1997), it was determined that x10 (as opposed to x4 magnification) gave a more accurate representation of the morphology present. Also, having investigated samples of up to 1000 entities, it was concluded that measurement of 600 entities was sufficient to accurately portray the morphological state of the organism.

Volume-based analysis of the morphological data (as opposed to number-based) was found to be beneficial in terms of providing a more accurate portrayal of the existing morphology, using the image analyser. Hyphal contribution, on this basis, was discovered to be negligible. During the early stages of a batch fermentation, numbers and sizes of both 'larger' and 'smaller' entities increase, followed by a subsequent reduction (and corresponding increase) in the former and latter, respectively, upon entry of the organism into the stationary phase.

Limited trials performed using the FBRM probe suggested the potential of this system for on-line morphological measurements of fermentation organisms. However this work also highlighted the inherent difficulty of drawing direct comparisons between data collected using an image analyzer and those resulting from the FBRM.

NOMENCLATURE

Symbol	Definition	Units
$Y_{x/s}$	Biomass yield per gram substrate	g/g substrate
R_{vb}	Biomass production rate	g/L.h
d	Equivalent diameter	μm
A	Measured area of entity	μm^2
n	Number of particles	(-)
$Y_{p/s}$	Product yield per gram substrate	g/g substrate
$Y_{p/x}$	Product yield per gram biomass	g/g biomass
α	Significance level	(-)
$\Delta_{\alpha,n}$	Width of confidence band	(-)
φ	Uncertainty in any variable	(-)

ABBREVIATIONS

ALI	Analytical Language for Images
ATCC	American Type Culture Collection
CBS	Central Bureau voor Schimellcultures
CCD	Charged Couple Device
CFW	Calcoflour White
C	Clumps
DNA	Deoxyribonucleic acid
DNS	Dinitrosalicyclic acid
FBRM	Focused Beam Reflectance Measurement
H	Hyphae
NCIMB	National Collections of Industrial and Marine Bacteria
NRRL	Northern Regional Research Laboratory
OD	Optical Density
P	Pellets
ppm	Parts per million
rpm	Revolutions per minute
SE	Structuring element
SPG	Soya Peptone, Glucose
STR	Stirred Tank Reactor
TBO	Tomato paste Based Oatmeal
UV	Ultra violet
vvm	Volumes/volumes/minute
YED	Yeast Extract, Dextrose
YEME	Yeast Extract, Malt Extract
YEPD	Yeast Extract, Peptone, Dextrose

LIST OF FIGURES

LIST OF TABLES

CHAPTER 1
INTRODUCTION

Streptomyces natalensis, a member of the Actinomycetes, was first discovered in Natal in 1955. The organism produces an anti-fungal agent, pimaricin, (also called natamycin), which is used as a preservative in the food and beverage industries. Many studies have been carried out on the growth of *Streptomycetes*, in general, as they are accredited with producing 80% of the total antibiotics produced by the Actinomycetes, and are therefore of great commercial importance.

Research into media composition has focussed primarily on the optimisation of antibiotic production. This is because a medium which produces optimal biomass levels often results in low antibiotic yields due to catabolite repression. However, very few studies have involved *S. natalensis*. Work by Mahon (1990) and Mc Cabe (1990) at DCU focussed mainly on the production of pimaricin, not growth optimisation. However, O'Shea (1998) carried out preliminary media studies for the optimisation of *S. natalensis* growth. More recently, (Martin, 1978) phosphate has been reported to regulate the production of many antibiotics and the effectiveness of both a complex SPG medium and a well defined, phosphate-limited medium has been used with *S. natalensis* by researchers in Leon, Spain, (Aparicio *et al*, 1999). Using a spore inoculum (obtained by initially cultivating the organism on tomato-based oatmeal plates) to inoculate a YEME medium has shown greatly increased biomass and pimaricin levels. This work serves as a reference point for studies conducted in this project.

In addition to biomass levels, another important parameter, from both a biological and engineering point of view, is organism morphology. *Streptomyces* display a diverse range of morphologies in submerged fermentation, from the free filamentous form to tightly packed pellets. The morphology formed depends on a number of factors, including the organism, medium composition, inoculum size, and aeration and agitation conditions. For example, Mc Cabe (1990) found that a medium containing glucose, soya peptone, and $CaCO_3$ resulted in very small dense pellets with the addition of soya bean meal resulted

in dispersed growth. Cell morphology has a marked effect on broth rheology. Long filaments tend to interlock, giving rise to increased broth viscosity, which often leads to insufficient mixing conditions and the formation of 'stagnant' zones in a fermentation vessel where oxygen can become a limiting factor. Pelleted growth results in broths of reduced viscosity. However, the formation of large dense pellets can also result in oxygen starvation, as oxygen is unable to diffuse to the centre of the pellet. Traditional manual methods of morphological characterisation have many drawbacks. However, with the development of image analysis systems, the process has become less time consuming, less error prone, and less subjective.

In this project, 250 mL Erlenmyer shake flasks were used to cultivate the organism using various inoculum media and different inoculum sizes. An algorithm was developed and validated to specifically characterise the morphology of the organism, using a semi-automated image analysis system. Both this image analysis system and a Lasentec FBRM probe were used to characterise *S. natalensis* during inoculum studies. A comparative evaluation of the potential of both instruments to develop a morphological portrayal of the organism in submerged culture was performed.

CHAPTER 2

ACTINOMYCETES: CHARACTERISATION AND GROWTH OPTIMISATION

2.1 INTRODUCTION

2.2 THE ACTINOMYCETES

Considerable confusion has surrounded the bacteria belonging to the order 'Actinomycetales'. As early as 1887, the actinomycetes or 'ray fungi' in Greek, appeared in the literature and were commonly referred to as fungi by the mycologists and as bacteria by the bacteriologists (Sokatch and Ornston, 1986). This confusion arose from the ability of the bacteria to form a mycelium consisting of narrow hyphae, approximately 1μm in diameter, which sometimes produced spores of similar dimension (Williams, 1990). It is this characteristic which distinguishes the actinomycetes from other bacteria. Taxonomists, such as Lechevalier and Lechevalier (1967, 1981) studying the characteristics of the actinomycetes confirmed them as prokaryotes. General features common to the actinomycetes include: sensitivity to the most common antibacterial agents; when present, the flagellae are similar to bacterial flagellae; they have no nuclear membrane separating the nucleus from the cytoplasm and they have a cell wall similar to those of bacteria (Gottlieb, 1973).

However, there is much variation in the morphology of these bacteria. Most species produce a primary mycelium, which grows on or into agar or, in some cases, away from the medium, the latter being referred to as a secondary mycelium. There are also some genera, such as Mycobacterium, in which mycelia are non-existent. Microcolonies consisting of rod-shaped filaments have also been observed. Variations among the bacteria have been noted as regards hyphal development. Fragmentation of the hyphae occurs at different times in different species, resulting in different types of colonies being formed. Soft colonies are typical of early fragmentation, whereas colonies with a leathery texture are more characteristic of late fragmentation. In species such as *Streptomyces*, fragmentation rarely occurs as filament development for this species is strong (Gottlieb, 1973).

2.2.1 CLASSIFICATION OF THE ACTINOMYCETES

The vast majority of Actinomycetes are oxidative, aerobic and reproduce asexually. Numerous researchers (*e.g.* Cross and Goodfellow, 1973; Lechevalier and Lechevalier, 1965), have been involved in separating the bacteria into genera using morphological, physical and chemical criteria. Morphological studies have been carried out at a microscopic level which permits observation without distortion of the hyphal spread. The presence of endospores with a high heat resistance is another distinguishing characteristic of the Actinomycetes. Chemical studies primarily involve observations of the cell wall and its components. Specifically knowledge of phospholipid patterns and the presence of sugars in the cell wall cast light on the separation of the bacteria into genera (Lechevalier and Lechevalier, 1981).

2.2.2 FUNCTIONS OF THE ACTINOMYCETES

Although the Actinomycetes have been found in a variety of environments, they are found with the greatest frequency as saprophytes in the soil. Numbers vary from soil to soil with the majority of a population found in the top few inches (Gottlieb, 1973). The presence of their hyphae aids crop production by acting as binders for individual clay particles found in the soil. They also act as decomposers of organic matter in soil and of lignocellulose from plant residues. Mesophilic and thermophilic species produce cellulases, xylanases, amylases, liganases and proteases (Demain, 1988). Some genera of the Actinomycetes can be found in fresh water. These genera are well adapted to this environment, having motile spores (the Actinoplanes) or spores which are hydrophilic and non-motile (the Micromonospora).

Some genera have also been shown to play a vital role in the decomposition of composts. These genera include Actinomycetes which are thermophilic, with optimum growth at temperatures between 50°C and 60°C. While beneficial in the waste removal process, inhalation of their spores can cause forms of allergic alveolitis, or 'farmer's lung', as it is more commonly known (Blyth, 1973). Demain (1988) reports on the use of Actinomycetes as enhancers of plant growth, although the mechanisms involved are unknown. *Frankia* has been acknowledged as playing an important role in symbiotic nitrogen fixation.

Although the Actinomycetes play a beneficial role in nature, such as producing glucose isomerase for the production of high fructose corn syrups (Demain, 1988), they also exert detrimental effects. These are usually in the form of plant and animal diseases. The

Streptomyces, *e.g. S. scabies* and *S. ipomoea* are responsible for the formation of scabs on the common potato and the sweet potato, respectively. Reduction of the soil pH through the introduction of sulphur, eliminates these pathogens. *A. bovis* is responsible for a disease known as "lumpy jaw" in cattle, while *A. israeli*, produces the same disease in humans. *Mycobacterium tuberculosis* causes one of the best known human diseases, which had a high mortality rate in the 1940s (Gottlieb, 1973).

2.2.3 THE STREPTOMYCETES

Due to its wide distribution in nature, *Streptomyces* is the best recognised genus of the family *Streptomycetaceae*. Members of this family are aerobic and gram-positive and form a mat of mycelia when grown on agar. Hyphae are characterised as both aerial (secondary) and substratal. Typically, the mycelium is 0.5 - 2μm thick (Dietz, 1986). *Streptomyces* hyphae are 1 – 5 μm in diameter and may be several millimetres long. The *Streptomycetaceae* mycelia may bear spores with most genera of the family having mycelia bearing chains of arthrospores (aerial spores) enclosed in thin fibrous sheaths. In the case of *Streptomyces,* these spore chains are long (> 50 spores) (Cross and Goodfellow, 1973). Individual spores have been reported (Kalakoutskii and Pouzharitskaja, 1973) to be resistant to dessication, repeated freezing and thawing and ultrasound. In general, the *Streptomyces* are mesophiles of the lower range, having optimum growth temperatures between 25°C and 35°C and optimum pH of between pH 5.0 and pH 9.0, with a peak at pH 7.0 (Bader, 1986).

2.3 THE PRODUCTION OF SECONDARY METABOLITES

2.3.1 ANTIBIOTICS

Actinomycetes have been exploited for the production of extremely valuable secondary metabolites, antibiotics. Williams (1990) reported that about two thirds of the 6000 known antibiotics are produced by the Actinomycetes with 80% produced by the *Streptomyces* species alone. The production of antibiotics is strain specific and their chemical make-up is diverse. Production is detected by growing isolates from the soil on media in a laboratory.

From the mid-1940s to the mid-1960s, the rate of discovery of new antibiotics was tremendous. The first antibiotic to be produced was penicillin, produced by the fungal strain, *Penicillium*. The second antibiotic to be isolated was streptomycin, effective against

tuberculosis, the disease caused by a mycobacterium. This was the first commercially successful antibiotic produced by an Actinomycete (Claridge, 1979). Isolation of strains producing new antibiotics is very important today but the rate of discovery has decreased dramatically since the 1960s. It has become increasingly more difficult to find new antibiotics with rare Actinomycetes being examined as a result.

2.3.2 THE GROWTH CYCLE

Originally, it was thought that the logarithmic phase of the metabolic growth cycle of microorganisms was principally concerned with cell growth and reproduction and the stationary phase corresponded to reduced/no metabolic activity. However, during the 1920s and the 1930s, this assumption was found to be incorrect with the stationary phase producing an abundance of complex organic compounds, having no apparent part to play in the growth of the developing microorganism. The concept of primary and secondary metabolites was introduced by Bu'lock and Demain in the 1960s and the 1970s. Primary metabolites are generally defined as those products, such as amino acids and sugars, which are produced during logarithmic growth or the trophophase, while secondary metabolites are those produced during the stationary phase of the growth cycle, also referred to as the idiophase (Rose, 1979).

The ability to produce secondary metabolites is most prevalent among bacteria, especially the Actinomycetes, as well as filamentous fungi. Many suggestions have been made to explain why microorganisms produce secondary metabolites. One explanation is that they are required as food reserves but this does not help to explain their chemical diversity. It was thought that antibiotics were used to protect the microorganisms in their natural environments. However, the currently accepted explanation is that they are produced to reduce metabolic problems which would arise if intermediates were allowed to accumulate in the microorganism. Instead, they are converted to secondary metabolites which allow the synthesis of low molecular weight compounds to be produced without interruption (Rose, 1979). Secondary metabolites produced by the Actinomycetes include almost all known structural classes of commercially important antibiotics, namely aminoglycosides, anthracyclines, chloramphenicol, β-lactams, macrolides and tetracyclines (Okami and Hotta, 1988). These antibiotics have a large and important role to play in human and animal health care, the fermentation industry and in natural science.

2.3.3 BIOSYNTHESIS OF SECONDARY METABOLITES

At this stage it is important to observe in more detail the evolution of the antibiotics (secondary metabolites) in the Actinomycetes. This is achieved by studying the biosynthetic pathways in the microorganism. The catabolism of glucose, being the main pathway, results in the formation of available intermediates which can be used as precursors for primary and consequently, secondary metabolite production (Turner, 1973).

As previously mentioned, antibiotics produced by the Actinomycetes are chemically diverse (Williams, 1990) and it is processes such as methylation and oxidation/reduction and halogenation reactions which are responsible for this diversity. A characteristic feature of the Actinomycetes is the incorporation of the intact skeleton of glucose into their secondary metabolites. This can be seen in the aminoglycosides *e.g.* streptomycin. Incorporation of part of the skeleton occurs in the macrolide antibiotics *e.g.* erythromycin. Nucleoside antibiotics, structurally related to essential nucleosides, incorporate ribose (made available by the pentose phosphate cycle for biosynthetic purposes). Chloramphenicol and novobiocin are examples of two aromatic secondary metabolites produced by a condensation reaction. In these cases, use is made of a tetrose which is released by the pentose phosphate pathway and which condenses with a triose to give shikimic acid (the precursor of these aromatic secondary metabolites). Another route, less common among the actinomycetes but which leads to tetracycline production, is referred to as the polyketide route (Turner, 1973). A variation of this route, the polypropionate route, is peculiar to the Actinomycetes. A well known product of this biosynthetic pathway is the aglycone of erythromycin (a glycoside). The biosynthetic route which leads to the production of steroids and terpenes appears to be ignored by the Actinomycetes. However, a gaseous compound which contributes to the earthy smell of these microorganisms has a structure suggesting that it is a degraded sesquiterpenoid. Interestingly, compounds of fully sesquiterpenoid structure have recently been obtained. This presents the possibility that, in the future, Actinomycetes producing terpenes may be isolated (Turner, 1973).

Okami and Hotta (1988) report that antibiotic synthesis is affected by carbon catabolite regulation (glucose effect). This is the inactivity or inhibition of the synthesis of catabolite enzymes, caused by glucose (Martin, 1978). Examples of antibiotics which have been found to be negatively regulated by carbon catabolites are actinomycin, kanomycin and puromycin.

Antibiotic-producing organisms generally have self-resistance mechanisms so that they can survive in the presence of the antibiotics which they produce themselves. Self-resistance patterns have been observed in various strains of Actinomycetes which aid in their characterisation and in the determination of the antibiotics they produce. The correlation between antibiotic resistance (self-resistance) patterns and the types of antibiotics produced suggests that there is a close genotypic linkage between antibiotic resistance and biosynthetic genes. Native antibiotic resistance of actinomycetes has been reported to be usually stable, (Okami and Hotta, 1988).

2.3.4 GENETIC INVOLVEMENTS IN ANTIBIOTIC PRODUCTION

Okami and Hotta (1988) also reported on the possible involvement of plasmids in antibiotic production. Observed loss of antibiotic production after plasmid curing treatment (Hopwood *et al.*, 1986) and the detection of plasmids in various antibiotic-producing strains *e.g.* strains of *S. coelicolor*, supported this possibility. It is now possible to clone antibiotic biosynthesis genes *using Streptomyces* host-vector systems. Evidence suggests that these genes are involved in directing enzymes which catalyse pathways following the primary metabolic pathways. Loss of antibiotic productivity during subculturing or preservation of strains is common among the Actinomycetes. Another feature common to the Actinomycetes is genetic exchange. New antibiotics have been found by interspecific recombination of genes.

Improving the yield of antibiotics produced by *Streptomycetes* can be achieved by induced mutagenesis. This method is very efficient and flexible, *i.e.* it can be used with any species regardless of the knowledge concerning parameters which influence antibiotic yields. However, it must also be remembered that improved yields may be obtained by careful control of the fermentation conditions, such as temperature, pH, aeration and nutrient availability (Mc Cabe, 1990). Mutagens such as UV light and ethyl methanesulphonate have been used to induce changes in the DNA, resulting in an increase in the number and activity of biosynthetic enzymes, or introduces a new, more efficient route to the desired product, *i.e.* the antibiotic (Hopwood *et al.*, 1986).

2.3.5 THE POLYENE MACROLIDE ANTIBIOTICS

2.3.5.1 INTRODUCTION

Pimaricin is an antifungal antibiotic produced by *Streptomyces natalensis*. It is a polyene macrolide antibiotic *i.e.* a submember of a class of antibiotics known as the macrolides. Grisebach 1978 reports that, originally, the macrolides were defined as a group of lipophilic basic antibiotics, possessing a medium-sized lactone ring. The introduction of new macrolide antibiotics broadened this definition to encompass a heterogenous group of compounds whose only common feature is the macrocyclic lactone ring. However, in 1957, Woodward suggested the term 'macrolide' to describe antibiotics having the following features :

- 12-, 14-, 16-membered lactone ring
- Few double bonds and no nitrogen in the ring
- Numerous ring substitutions, which include one to three sugars, either attached to the ring or to themselves

Most of the macrolide antibiotics are produced by *Streptomyces* species and examples include erythromycin (produced by *S. erythreus*), pimaricin (produced by *S. natalensis*) and tylosin (isolated from *S. fradiae*). Tylosin belongs to the subclass of the largest macrolides, *i.e.* those containing the 16-membered lactone rings.

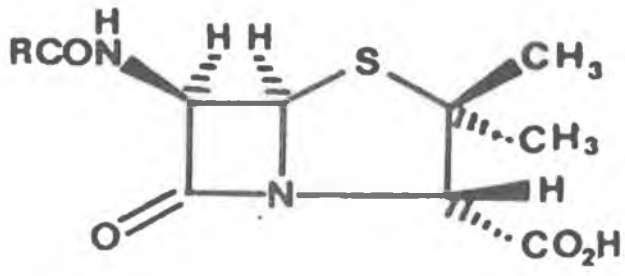

Figure 2.1 The β-lactam ring structure of polyene macrolide antibiotics (*from* Abraham, 1978).

2.3.5.2 CLASSIFICATION OF THE POLYENE MACROLIDE ANTIBIOTICS

As previously mentioned, the polyene macrolides form a large group belonging to the macrolide class of antibiotics. Their structure consists of macrocyclic rings closed by a lactone ring. The lactone ring, consisting of 26 – 28 atoms, is similar to that found in another subclass of the macrolides, the non-polyene macrolides (Crandall and Hamill, 1986). Erythromycin is an example of the non-polyene macrolides having a 14- or 16-membered macrolide ring. The presence of a chromophore of 3-7 alternate double bonds, forming part of the macrolide ring in the polyene macrolides and its absence in the non-polyene macrolides, helps to distinguish between the two macrolide subclasses. Another feature of the polyene macrolides is the presence of an amino sugar. Two sugars which have been found to date are mycosamine (found in pimaricin, for example) and perosamine. Perosamine does not occur with the same frequency as mycosamine, being found only in perimycin. Neutral sugars, found in non-polyene macrolides, have not been found in the polyene macrolides. This is another distinguishing characteristic between the two subclasses (Martin, 1979).

A further classification of these antibiotics is on the basis of the number of consecutive conjugated bonds in the chromophore, the antibiotics being classified as tetraenes (4), pentaenes (5), hexaenes (6) and heptaenes (7). Pimaricin is a tetraene, since it has four alternating double bonds (Thomas, 1976). The chromophores of the polyene macrolides have a strong ultraviolet and short visible radiation absorption in the 280 to 410 nm region. The main absorption band is resolved into four peaks (common to all polyene macrolides); in most instances the peak occuring at the longest wavelength is the strongest and the narrowest of the four (common to most of this subclass).

In general, for the polyene macrolides the solubility and the colour of the pure antibiotic are determined by the chromophore. As the number of double bonds in the chromophore increases, the chromophore becomes increasingly more hydrophobic and, hence, has limited solubility in water. However, antibiotics have been found to be soluble in solvents such as dimethylformamide, dimethyl sulphoxide and in aqueous solutions of alcohols (Thomas, 1976). It has been noted that polyene macrolide antibiotic solutions can be carefully diluted with water, since no visible precipitation occurs at concentrations of less than 50 $\mu g\ ml^{-1}$, although they do exist as micellar suspensions in aqueous media. The polyene macrolides are stable in the absence of heat, light and moisture. It has been observed that microorganisms

producing polyene macrolides also may co-produce non-polyene macrolides. For example, strains of *Streptomyces noursei* have produced cyclohexamide and nystatin. These non-polyene macrolides are antibacterial (unlike the polyene macrolides which are antifungal). They have little effect on the analysis and assay of polyene macrolides although they may affect their toxicity. However, as a result of the above co-production of antibiotics, special extraction procedures are necessary in order to obtain high yields of the required antibiotic.

2.3.5.3 PIMARICIN, A POLYENE MACROLIDE ANTIBIOTIC

Pimaricin, also referred to as natamycin, is produced from *Streptomyces natalensis,* a Streptomyces strain which was isolated in 1955, from soil taken near the town of Pietermaritzburg in Natal, South Africa (Borden *et al.*, 1995). Four years later, in Chattanooga, Tennessee, the antibiotic tennectin was produced from another Streptomyces strain. Studies have indicated that both pimaricin (natamycin) and tennectin are the same antibiotic (Bridger, 1968). The empirical formula for pimaricin (Figure 2.2) is $C_{34}H_{49}NO_{14}$ and its molecular weight is approximately 658 (Mahon, 1990). Aqueous solutions of pimaricin have been found to be less stable than aqueous suspensions of the same (Thomas, 1976).

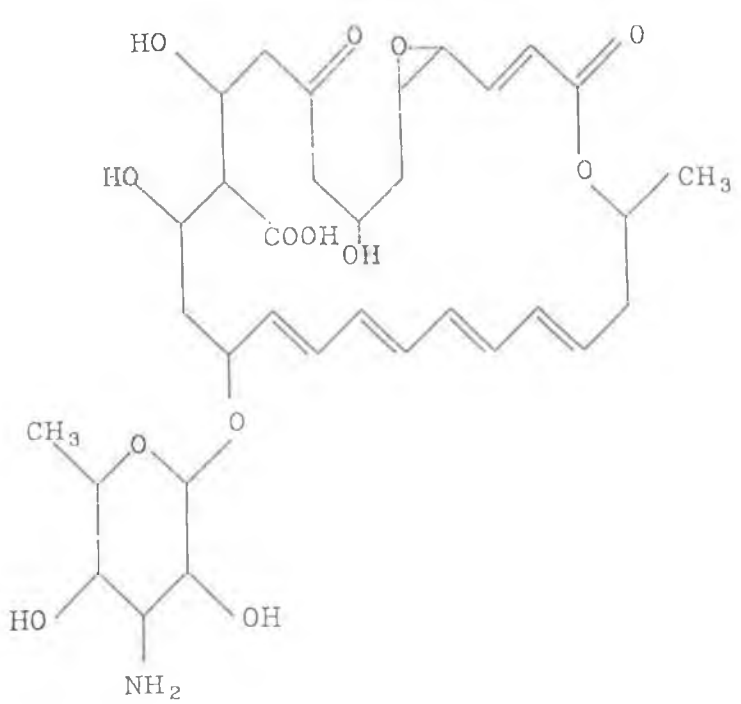

Figure 2.2 Structure of pimaricin (*from* Mahon, 1990).

2.3.5.4 FUNCTIONS OF THE POLYENE MACROLIDE ANTIBIOTICS

Martin (1979) discusses the industrial significance of the polyene macrolides. They have been used in combination with other drugs but, more recently, there has been a tendency to restrict their use in this manner. They are used topically but can be toxic, resulting in the administration of smaller doses of these therapeutic agents.

The degree of light and temperature sensitivity of the polyene macrolides makes them generally unsuitable for treatment of fungal diseases in plants and crops, with one exception. Aureofungin has been used against post-harvest diseases as well as seedborne and plantation diseases (Thomas, 1976). Pimaricin has been used as a preservative in the food and beverage industry. Holley (1981), carried out experiments using Italian Dry Sausage to study the effectiveness of pimaricin as a preservative. A pimaricin spray was found to be an effective antifungal agent in both Genoa and Casalingo salami, although, it was noted that the mold growth was replaced by yeast colonies.

Tuinstra and Traag (1982), considered the use of pimaricin as a cheese preservative. The outward appearance of the cheese product was improved by pimaricin inhibition of mold growth and of the subsequent accumulation of mycotoxins. Another advantage of the use of pimaricin over food preservatives such as sorbic acid, is that treatment does not affect the overall taste of the food.

2.4 PRODUCTION OF ANTIBIOTICS BY STREPTOMYCETES

Media

Optimisation of fermentation conditions is required for high yields of polyene macrolides. It is essential that the medium contains sources of carbon and nitrogen. Glucose, starch and British gum are examples of carbon sources which have been used for the production of the secondary metabolites, pimaricin, nystatin and amphotericin, respectively (Martin, 1979). Slow feeding of the carbon source helps to produce greatest yields of the antibiotics by bypassing carbon catabolite regulation as previously mentioned (Section 2.3.3). Higher respiration and glucose utilisation rates but decreased biomass accumulations are associated with these types of fermentations. Complete exhaustion of sugar from the medium results in failure of the organism to further produce antibiotics as extensive disruption of the mycelia occurs.

Farid *et al.* (2000) performed a limited series of experiments on the effect of various mono-, di- and poly-saccharides on growth and antibiotic production levels in *S. natalensis*. The organism was allowed to grow on the various media (at a sugar concentration of 20 g/L) for 96 hours. On the basis of pimaricin production, the sugars were ranked as follows: glucose > glycerol > xylose > malt extract > ribose > dextrin > starch > galactose. As glucose was concluded to be the best of these carbon source for pimaricin production, an investigation into whether the antibiotic yield could be improved by varying the glucose concentration was undertaken. It was determined that, at concentrations above 20 g/L, pimaricin production was significantly reduced.

Martin (1979), discusses the importance of other carbon sources such as short-chain organic acids and alcohols. These are biosynthetic precursors of the polyene antibiotics. Acetate, propionate or malonate alone do not support production of candicidin but when they are used in the presence of glucose, synthesis of the antibiotic is stimulated. It has been concluded that the acetate and propionate, together with the glucose, provide precursors of aminosugars which are needed for antibiotic production.

Martin (1979) also discusses the choice of an appropriate nitrogen source. Soybean meal and soya peptone are the most commonly used undefined sources of nitrogen due to their slow hydrolysis. Corn meal, corn steep liqour, casein and yeast extract have also been used. The levels of phosphates and trace element are especially important as these may be inhibitory. For example, phosphate concentrations of 5 mM have been reported to be inhibitory to polyene macrolide antibiotic production. Inorganic salts are generally not considered to be good nitrogen sources. Some amino acids, while not economical for industrial use, have been reported to be effective. However, aromatic amino acids, particularly tryptophan, phenylalanine and tyrosine, inhibit the production of aromatic polyene macrolides.

Temperature and pH

Fermentation temperature and pH values must also be controlled carefully. While temperatures of up to 120°C for exposure times of less than one hour do not render the antibiotic pimaricin inactive, fermentations are generally conducted at a temperature of 28 °C. At the extremes of the pH ranges, this antibiotic is inactivated since it is normally stable at pH values between 5.0 and 9.0 (with an isoelectric point of pH 6.5). Bacitracin production is also

inhibited by the drop in pH which takes place when the culture contains high levels of glucose. Another source of inhibition of pimaricin production is exposure to UV light with wavelengths of 300 – 350 nm (Mc Cabe, 1990).

Agitation and aeration

In submerged culture, the polyene antibiotics are produced under aerobic conditions. Agitation and aeration of the bioreactor contents are, therefore, two very important process factors. Consumption of oxygen in complex media has been reported to be very fast during the growth phase and therefore high agitation rates are required. The use of baffles helps to increase the oxygen content in shake flasks. In fermenters, levels of dissolved oxygen should be maintained at 20% saturation (Martin, 1979) with most of the oxygen required for the growth phase of the developing microorganism rather than for the subsequent antibiotic production phase. Reducing the agitation rates and hence the dissolved oxygen levels during the latter stages of the fermentation, as opposed to maintaining high aeration rates throughout, are methods thought to be more advantageous in the production of the secondary metabolites (Martin, 1979).

It has been reported that oxygen limitation may induce or repress the production of antibiotics by actinomycetes. In a recent study, El-Enhasey *et al.* (2000) investigated the effect of medium volume, agitation speed and the addition of a biopolymer to the medium on antibiotic production levels in shake flasks. Results from a study using 250 mL shake flasks indicated that increasing the broth volume from 50 to 100 to 150 mL resulted in a reduction in pimaricin production, from 1.5 to 0.25 to 0.143 g/L, respectively. The decreasing productivity with increasing culture volume (corresponding to reduced surface area per unit volume) strongly indicates that oxygen supply influences antibiotic production.

Biomass levels and glucose utilisation rates were also reported to decrease with increasing medium volume. Levels reported by El-Enhasey *et al.* (2000) are in good agreement with results from similar volume studies with *S. natalensis* conducted by O' Shea (1998).

Increasing the agitation speed to a maximum of 250 rpm resulted in a corresponding increase in biomass (maximum of 5 g/L) and pimaricin production (maximum of 1.7 g/L) by *S. natalensis*. However, glucose utilisation rates were largely independent of the agitation speed.

Oxygen availability in the shake flasks was altered by the addition of various concentrations of a biopolymer (sodium alginate) to the medium (El-Enhasey *et al.*, 2000). Both glucose utilisation rates and pimaricin production levels were reported to be adversely affected by the presence of increasing concentrations of the biopolymer in the medium. No significant changes to the biomass levels were reported.

2.4.1 BIOSYNTHESIS OF THE POLYENE MACROLIDE ANTIBIOTICS

Biosynthesis of polyene (and non-polyene) antibiotics is by the 'polyketide pathway', which involves a head-to-tail condensation of active two- and three- carbon units to form the macrolide ring. Very little is known about the biosynthesis of the aminosugars of polyene macrolides. The carbon skeleton of mycosamine appears to be derived from glucose. It is accepted that the aminosugars of the polyene macrolides are synthesized through the formation of nucleoside diphosphate sugar derivatives, due to the similarity of their biosynthesis to that of aminosugars of gram-negative bacteria.

Aparicio *et al.* (2000) cloned, sequenced and analysed the gene cluster responsible for the biosynthesis of pimaricin. Sixteen open reading frames (84 985 base pairs) were found to encode 13 homologous sets of enzyme activities of the polyketide synthase (PKS) which were distributed within five giant multienzyme proteins. Two of the genes, pimS0 and pimS1 have been fully sequenced by these workers. Disruption of the genes encoding the PKS was found to abolish pimaricin production by *S. natalensis*.

The synthesis of new derivatives of polymacrolide antibiotics has also been reported. Mendes *et al.* (2001), revealed the presence of the *pimD* gene (in pimaricin) whose product is very similar to cytochrome P450 monooxygenases. These oxidative enzymes are responsible for catalysing the site-specific oxidation of the precursors to many macrolide antibiotics. Mendes *et al*, demonstrated that the *pimD* gene was responsible for the conversion of 4,5-deepoxypimaricin to pimaricin in *Streptomyces natalensis*.

2.4.2 REGULATION OF BIOSYNTHESIS

A large number of polyene macrolides are affected by the presence of phosphate which depresses their synthesis at concentrations of 5 mM and above. As previously mentioned, carbon catabolite regulation also effects the production of antibiotics, namely, streptomycin,

penicillin, actinomycin and bacitrcin. However, slow feeding of the carbon source to the fermenter results in increased yields. Some of the polyene antibiotic producing strains are sensitive to their own antibiotic and accumulation of the antibiotic can lead to inhibition of production, a condition known as feedback regulation. For example, *Streptomyces noursei* synthesizes both cycloheximide and fungicidin. Addition of fungicidin to the culture inhibits the production of fungicidin but stimulates the production of cycloheximide (Martin, 1978).

2.4.3 PURIFICATION OF POLYENE MACROLIDE ANTIBIOTICS

The purity of most polyene antibiotics is dependent on several factors including the organism strain, the fermentation conditions used and the extraction procedures followed. Impurities might typically include an unwanted polyene antibiotic, a non-polyene antibiotic, inactive precursors and degradation products. These impurities could influence toxicity and interfere with assays performed on the required antibiotic. Several methods have been suggested for isolation of pure antibiotics. Discussed below are procedures which have been employed for pimaricin recovery and purification.

Bridger (1968), describes steps involving 'salting out' of the antibiotic from acidified solutions of the fermentation broth, recovering the precipatated antibiotic in a concentrated form, washing with bicarbonate solutions to purify the antibiotic, and then removing the salt by dissolving the antibiotic concentrate in a lower alkanol from which it is finally purified.

Alternatively, the active fluid (antibiotic) can be removed from the cells by increasing the broth pH to 10.0 and filtering off the cells. The fluid can then be extracted using an alcohol, the extract being concentrated by azeotropic distillation. Purification of the active antibiotic can then be achieved by precipitation from, for example, glacial acetic acid (Struyk and Waisvisz, 1975).

Millis *et al.* (1992), described another recovery and purification procedure for pimaricin, in which methanol was added to the fermentation broth and the pH was adjusted to 4.5 to dissolve the precipitated antibiotic. The suspended solids were then removed and the pH was increased to 6.0 to 9.0 to precipitate the pure pimaricin. A flowsheet for this process is provided in Figure 2.3.

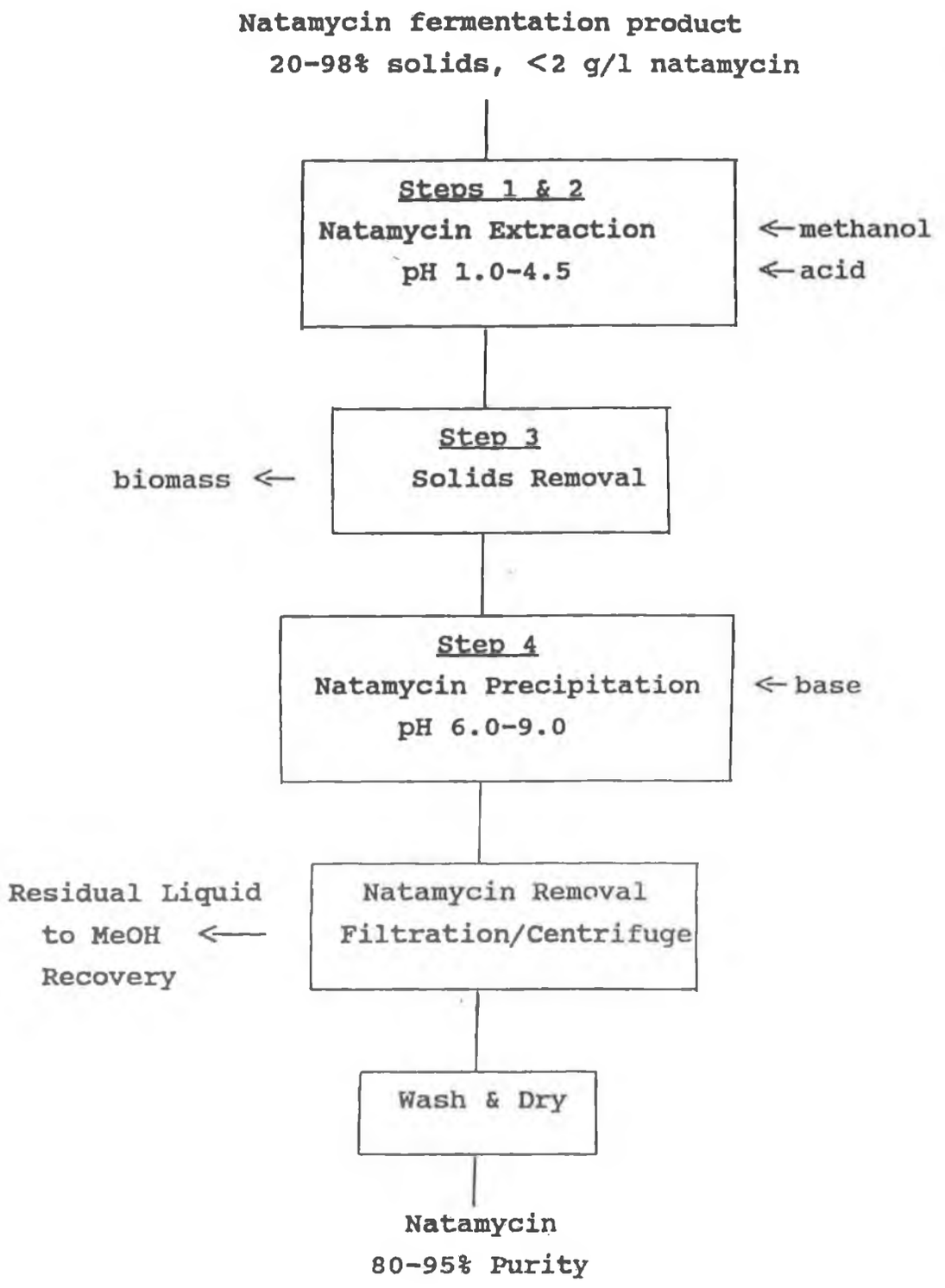

Figure 2.3 Process flowsheet for pimaricin recovery (*from* Millis, 1992).

In 1995, Borden *et al.* described a similar procedure to that used by Millis *et al.*, (1992). However, upon addition of alcohol to the fermentation broth the pH was, in this case, increased to a value higher than pH 10.0 and to precipitate the pure pimaricin the pH was subsequently lowered.

2.4.4 ASSAYS FOR THE IDENTIFICATION OF PIMARICIN

Various methods/assays have been used to establish the identity and purity of polyene antibiotics. Chemical assays include paper and thin-layer chromatography, column and high performance liquid chromatography. Also included are titrimetric, colorimetric and spectrophotometric methods. Capitan-Valley *et al.*, (2000) successfully determined the quantity of pimaricin in lactoserum matrix using UV spectrophotometry and liquid chromatography. Both methods were rapid and simple to perform involving protein precipitation with methanol, followed by centrifugation. Applicable pimaricin concentrations for both methods ranged from 2 to 500 mg/L.

Fletouris *et al.*, (1995) also used a rapid spectrophotometric method to analyse pimaricin in cheese and cheese rind. The antibiotic was directly quantitated on the basis of the characteristic third derivative trough at 322.6 nm. The applicable range, in this case, was 0.5-20 mg/kg. An overall standard deviation of 1.4 % was recorded based on within-day and between-day variations.

Biological assays include methods based on diffusion and turbidimetric assays to determine the sample potency (Thomas, 1976).

2.4.5 THE β-LACTAM ANTIBIOTICS

The emphasis in this thesis is on an organism which produces pimaricin, a polyene macrolide. However, actinomycetes also produce β-lactams which are among the most well known antibiotics. Cephamycin C, clavulanic acid, penicillin N, deacetoxycephalosporin C and the Ocarbamoyl derivative of deacetylcephalosporin C, β-lactam antibiotics, are antibacterial antibiotics produced by another member of the Streptomyces, *S. clavuligerus*, (Nabais *et al.*, 1995). Production of cephamycin C and clavulanic acid are discussed here in detail.

Extensive research has been carried out on the β-lactam nucleus and its derivatives and in 1962 a report was written describing the production of penicillin N (also known as

cephalosporin N or synnematin B) by a Streptomycete (Crandall and Hamill, 1986). With the exception of this description of penicillin N production from a Streptomycete, for 30 years after the penicillin structure was determined, it was thought that the β-lactam ring was solely associated with fungal metabolites, *e.g.* Penicillin and Cephalosporin. The 1970s brought the introduction of three new β-lactam antibiotics produced by different Streptomyces species: 7-methoxycephalosporin C (produced by *S. lipmanni*), cephamycin C and A16886A (both produced by *S. clavuligerus)*. Cefoxitin, a semisynthetic cephamycin, is a clinically useful antibiotic used in treatment against gram-positive and gram-negative organisms (with the exception of *Pseudomonas*).

Clavulanic acid production

Clavulanic acid (Figure 2.4) is a member of the clavam group of β-lactams and was the first antibiotic of this group to be isolated from a culture of *S. clavuligerus*. It contains the 1-oxadethiapenam ring system, common to all members of the clavam group. The antibiotic is most effective as an inhibitor of β-lactamases but does exhibit modest antibacterial activity (Crandall and Hamill, 1986).

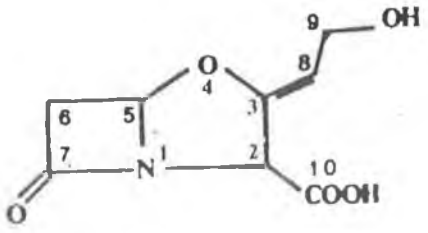

Figure 2.4 Structure of clavulanic acid (*from* Belmar-Campero, 1989).

Abraham (1978) reported that a number of related enzymes are involved in peptidoglycan crosslinking in the cell membrane of bacteria. There are also a number of binding proteins present. It has become evident that the effect of a β-lactam antibiotic on a bacterial membrane depends on its ability to react with these enzymes involved in cell wall synthesis.

2.4.6 REGULATION OF ANTIBIOTIC PRODUCTION

Chemically defined media have been used more frequently than complex media for the production of antibiotics by Streptomyces species. Such media, containing a variety of carbon, nitrogen and phosphate sources, allow for a thorough examination of the influence these components have on antibiotic production (Rollins, 1989; Nabais *et al.*, 1995). Production is

normally higher in media where the availability of substrate limits the growth rate of the microorganism. Lebrihi *et al.* (1988) carried out batch and continuous fermentations of *S.clavuligerus* and showed, for all substrates investigated, that cephamycin C production was highest when the bacteria developed slowly, with no production at rapid growth.

Phosphate

Farid *et al.* (2000) have reported on the effect of phosphate concentration on pimaricin production by *S. natalensis*. An 8% increase in antibiotic production levels was observed when phosphate, at a concentration of 0.05 g/L, was added to the medium. However, increasing the concentration of phosphate above this level significantly reduced production.

In *S. clavuligerus* (Lebrihi *et al.*, 1988), the presence of phosphate at growth limiting concentrations was found to be more significant in batch (at 2 mM) than in continuous culture (at 0.05 mM).

Lebrihi *et al.* (1987), investigated phosphate repression of cephamycin and clavulanic acid production by *S.clavuligerus*. It was found that production was reduced by 50% and 80% when the concentration of phosphate in the fermentation medium was 50 mM and 100 mM, respectively. It was also observed, at these concentrations, that phosphate repressed the biosynthesis of cephamycin synthetase an enzyme in the pathway involved in the production of cephamycin C. Below 10mM phosphate, repression was not observed as expandase was not limiting in this case (Lebrihi *et al.*, 1987).

Lubbe *et al.* (1985) demonstrated the negative effect of phosphate on antibiotic production. Inhibition and/or repression of the enzymes required for antibiotic synthesis was studied. Cyclase and expandase, two of these enzymes, are inhibited by phosphate, but inhibition is stronger for the latter.

Nitrogen

Cyclase, expandase and epimerase, the three enzymes of the β-lactam antibiotic pathway, are also subject to nitrogen source repression (Brana *et al.*, 1986). The presence of NH_4^+ in the medium results in inhibition of the formation of cyclase and expandase but not epimerase. The epimerase had been found to be insensitive to ammonium and nitrogen control in *S. clavuligerus*.

Brana *et al.* (1986), also found that some amino acids, namely, glutamine, glutamate and alanine, inhibited antibiotic production when they were added to resting cell systems. Inhibition caused by glutamate is thought to be due to its transport or metabolism rather than to the glutamate itself. Lysine and α-aminoadipate have been found to be stimulatory to antibiotic production (Fang *et al.*, 1996). The α-aminoadipate is a precusor of the β-lactam antibiotics and lysine is converted to α-aminoadipate in Streptomycetes.

Carbon

Carbon is another source of negative regulation of antibiotic synthesis, (Brana *et al.*, 1983). Research has shown that production of cepham antibiotics by resting cells of *S. clavuligerus* is disturbed by the presence of glycerol and other carbon sources and was found to be related to aeration conditions. Only at low cell densities or increased aeration rates, was the rate of antibiotic production independent of the carbon source.

Oxygen and Iron

The effect of oxygen on production was studied by Rollins *et al.* (1989), who also investigated the effects of iron in the medium. Iron is well established as an important metal for secondary metabolite production in bacteria, including the Actinomycetes. Rollins *et al.* (1988) demonstrated that, in batch fermentations of *S. clavuligerus,* grown in complex medium, an increase in the amount of dissolved oxygen to saturation levels subsequently led to an increase in antibiotic production. However, they subsequently showed that, when grown on glycerol-asparagine medium, higher dissolved oxygen levels had a negative effect on cephamycin formation. From this, they concluded that the composition of the fermentation medium itself can regulate the effect of oxygen on antibiotic production, by preventing oxygen transfer to the cells, thus slowing down the growth rate and hence increasing production of secondary metabolite. Iron added to fermentation medium without oxygen supplementation was found to have very little effect on the production of penicillin N (the intermediate in the pathway to cephamycin C biosynthesis). However, increased levels of cephamycin C were observed, indicating that the complete pathway benefited from the presence of iron in the medium.

Optimisation of antibiotic production can only be achieved if the fermentation conditions are optimised. As already illustrated, oxygen plays a very important role in antibiotic production by *S. clavuligerus*. This is reflected in the abundance of literature produced on this subject.

Belmar-Campero and Thomas (1988) studied the effects of stirrer speed on the morphology and production of clavulanic acid by *S.clavuligerus*. They discovered that there was no direct link between growth and production and stirrer speed. However, morphology was affected by changes in stirrer speed, *i.e.* increasing the speed resulted in fragmentation of long filaments to shorter, less-branched fragments.

The effect of oxygen fluctuations in the fermenter on growth and antibiotic production by *S. clavuligerus* was studied by Yegneswaran *et al.* (1991). Cycling of aeration to the fermenter reduced the growth rate during the exponential growth phase. However, the maximum biomass level was unaffected and reduced oxygen levels reduced the expression and stability of key biosynthetic enzymes, such as δ-(L-α-aminoadipyl)-L-cysteinyl-D-valine (ACV) synthetase (Rollins *et al.*, 1991). This enzyme catalyses the first step in the biosynthetic pathway of cephamycin C.

2.5 IMAGE ANALYSIS

2.5.1 INTRODUCTION

Early use of microscopes to view microorganisms restricted morphological studies to qualitative analysis. Quantitative analysis, first established through the use of instruments such as the digitising table (Metz *et al.*, 1981), provided a more detailed analysis but had many disadvantages. Use of these instruments was both time consuming and subject to human error. However, the advent of semi-automated and fully automated image analysers have provided for rapid and accurate morphological characterisation of fermentation organisms.

Numerous applications of image analysis have been reported. In medicine, it has been used to automatically assess the quality of magnetic resonance imaging (MRI) equipment (Bowel *et al.*, 1999) and to interpret the images produced from these instruments. Such interpretation has been shown to support the diagnosis of cardiac disease (Santarelli *et al.*, 2000). In agriculture, it has been applied to variety testing of mushrooms (Vandevooren, 1991) and has also shown potential in classifying lamb carcasses in terms of prediction of saleable meat yield (Stanford *et al.*, 1998). It has proven useful in the field of bioremediation (Tsutsumi *et al.*, 2000), microbial enumeration, milk and chocolate powder sizing, analysis of tea-bag perforations and raw materials analysis in food technology (Dziezak, 1988), to quantify chlorophyll content in leaves and to observe leaf morphology (Mc Gowan, 1998). In microbiology, it has been used

in antibiotic detection (bioassays) (Gavaille *et al.*, 1994) and as a rapid screening procedure for bacterial infection in the food industry (Singh *et al.*, 1997). Comparative studies of DNA fingerprints have become faster and more accurate through the introduction of image analysis to the field of genetics (Palti *et al.*, 1997).

2.5.2 ANALYSIS OF FILAMENTOUS MICROORGANISMS

Many microbiological applications of image analysis have been reported but its application with particular reference to filamentous microorganisms will be discussed here. In submerged culture, filamentous microorganisms exhibit two distinct forms of morphology *i.e.* pellets and free filamentous form. In industrial scale production of secondary metabolites using these microorganisms, it is the latter form which is more commonly used. However, there are disadvantages associated with this form, in that highly viscous broths may result, reducing heat and mass transfer in the fermenter and subsequently affecting secondary metabolite yields. Characterisation of the morphology of the microorganism through the use of image analysis is, therefore, very important (Packar and Thomas, 1990).

2.5.2.1 DEVELOPMENT OF IMAGE ANALYSIS TECHNIQUES

Early techniques to characterise the morphology employed visual observations. Phase contrast microscopes were used by Vitalis *et al.* (1963), to compare the morphology of streptomycin-producing and non-producing strains of *S. griseus* on a visual basis. Chater (1972) also used phase contrast microscopy to classify mutants of *S. coelicolor* into six types, based on the presence of spores.

Early attempts at obtaining morphological measurements were made using an electronic digitising table (Metz et al., 1981). Many disadvantages were associated with this technique; it was labour intensive, time consuming and subject to human error, as well as difficult to automate, but it was, for its time, highly innovative. Using this technique, the total hyphal length, length and number of hyphal branches and hyphal growth unit (length of hyphae per growth tip) could be determined and recorded by a computer.

Adams and Thomas (1988) describe the morphological characterisation of *S. clavuligerus* (ATCC 27064) using both a semi-automatic image analysis system and a digitising table. The image analysis system yielded lengths, on average, 6% greater than the digitising method. This

apparent discrepancy was because the digitising table measured a series of chord lengths (rather than the longer arc lengths used by the image analysis system). However, it was also uncertain that true length measurements were made with the image analysis system due to the effects of image processing prior to measurements. It was concluded that this method was both more precise and convenient when compared to the digitising method. The development of a fully automated system allowed more rapid morphological characterisation of microorganisms.

Packar and Thomas (1990) described, in detail, the principle stages involved in automated image analysis. The method involved the use of application-specific software to further study the morphology of *S. clavuligerus*. This replaced the general purpose programs previously used and allowed for calibration factors and image analysis parameters (specific for a particular fermentation) to be preset, omitting the need to return to these initial settings each time a new slide/sample was viewed. The image was digitised, the resulting binary image was processed and measurements were made on the microorganism within the measuring frame. Data was then sent to a file for subsequent statistical analysis. With work on one field of view completed, another field was analysed and more microorganisms measured. In this study, morphological characterisation of *S. clavuligerus* by this automated method was further compared to the use of both the digitising table and a manual image analysis method which required the user to manually move the microscopic stage and edit the binary image. A total of 100 microorganisms were analysed in the study and no significant differences between the morphological parameters determined using the three methods were detected. However, the automated method was the fastest method and this advantage would be the most relevant when analysing larger samples. Full morphological analysis of 1000 microorganisms, took only 90 minutes.

Tucker *et al.* (1992) continued the work of Packer and Thomas, using a more advanced program to morphologically characterise *S. clavuligerus*. In addition to hyphal-based measurements, a more detailed description of the freely dispersed form (*i.e.* the clumps) was undertaken. The percentage of mycelia in the clumps was determined, as well as clump area and perimeter. The circularity factor, (defined as $\frac{(perimeter)^2}{4\pi * (Area)}$) was also determined. This parameter gives an indication of the roughness of a clump. The clump compactness was determined by calculating the ratio of the area of the hyphae in the clump to the total area

enclosed by its actual perimeter. These extra parameters help to give the user a more complete description of the morphology of the organism and it should also be noted that the time required for this more detailed analysis of 100 microorganisms was only 16 minutes.

Fungal spores are used in the laboratory for culture maintenance and to provide inocula for fermentations and, as such, culture morphology and productivity can be greatly influenced by the condition of the spores. Previously, spore viability was determined using a plate count technique, but problems such as lack of reproducibility, long incubation times and an underestimation of percentage viabilities can be associated with this technique.

Paul *et al.* (1993) developed a means of assessing the viability and germination of fungal spores (*P. chrysogenum*) in submerged culture using a fully automatic image analysis system (Quantimet 570 image analyser). Structural variations during germination, including spore swelling, germ tube formation and elongation, were measured in terms of distributions of spore and germ tube volumes and germ tube length. This method provided many advantages over the colony counting and photomicroscopic techniques previously employed. It was more rapid, more accurate (due largely to the ability to remove debris through the use of a manual editing stage) and more consistent. It could be applied to different fungal preparations to provide reliable information on the inoculum quality and condition and it could also be used to investigate the relationship between incubation time and percentage germination under different cultivation conditions.

Recently, Agger *et al.* (1998) used a double staining method and fluorescent probes to further improve descriptions of growth and product development in fermentation organisms. The method involved the use of a fluorescent dye 3,3'-dihexyloxocarbocyanin ($DiOC_6$) to stain hyphal organelles and Calcoflour White (CFW- a substance which binds to chitin and β-glucan) to stain the cell walls. The use of the CFW significantly improves the detection of the total hyphal area, while both stains help in the study of cellular differentiation in filamentous fungi.

A flow-through cell, similar to that described by Treskatis *et al.* (1997) was also used by Spohr *et al.* (1998) to measure the growth kinetics of *Aspergillus oryzae*. The development of a single spore to branched hyphae could be followed continuously, independent of factors such as agitation and sparging. The removal of such factors allows the independent study of the relationship between growth kinetics and morphology. Monod-type kinetics were used to

describe the correlation between the depletion of nutrients and the morphology. It was discovered that the ratio between the total hyphal length and the number of tips (*i.e.* the hyphal growth unit) does not change with nutrient depletion. Spohr *et al.* (1997) also reported an increase in α-amylase production from a more densely branched recombinant of the organism.

2.5.2.2 IMAGE ANALYSIS-BASED MORPHOLOGICAL STUDIES

Morphological studies of filamentous organisms (fungi and bacteria) generally involve classification in terms of hyphae, clumps or pellets. However, with the increased knowledge and use of the automated image analysis researchers have begun to explore possible relationships between morphology and physiological events.

2.5.2.2.1 HYPHAL MORPHOLOGICAL STUDIES

Image analysis has been used (Paul *et al.*, 1994) to examine morphology and vacuolation in *Penicillium chyrsogenum* from fed-batch fermentations. The occurance of mycelial fragmentation, reflected in the decrease in mean hyphal length, was not only attributed to shear (in the reactor) but was also affected by the high proportion of vacuoles. It was found that fragmentation was greater during times of nutrient limitation (*i.e.* the onset of the production phase) when the hyphae became more heavily vacuolated. This study highlights the potential of manipulating hyphal fragmentation by inducing or awaiting favorable physiological conditions, *i.e.* less viscous cultures, resulting in increased oxygen transfer.

Effects of varying agitation rates and hence variable oxygen transfer rates have been studied by Lejeune *et al.* (1995). As the use of image analysis to morphologically characterise microorganisms was becoming more familiar, researchers turned their attention to modelling the growth kinetics of these organisms. Lejeune *et al.* set up a simple model to describe the growth of a single mycelium of *Trichoderma reesei* (QM9414). Tip extension in individual branches of the mycelium were described using saturation type kinetics and a frequency distribution was used to describe random branching. The model was used to simulate a population of mycelia and in tandem with experimental data model parameters such as number of tips and hyphal lengths were found.

Satisfied that mechanical agitation rates had an effect on fungal growth kinetics, Lejeune and Baron (1995) searched for a method to quantify fungal growth. Previous methods had

involved simply determining the dry cell weight concentration. However, morphological parameters such as total hyphal length could also be proportional to dry weight concentration if factors such as constant density of biomass, constant mean hyphal diameter and non-occurrence of hyphal fragmentation were satisfied. This was the approach adopted by Gonzales-Blanco *et al.* (1993) in their method for determining fungal specific growth rate using image processing. In this work the specific growth rate was found to be proportional to the ratio between the average tip extension rate and the mean hyphal length. This observation was subsequently confirmed by Lejeune and Baron (1995).

2.5.2.2.2 CLUMP MORPHOLOGICAL STUDIES

Most antibiotics are produced as secondary metabolites by actinomycetes and fungi. Their production is often the result of a nutrient limitation or the introduction of an autoregulator (a chemical known to induce antibiotic production) to the submerged culture. Antibiotic production is also characteristically accompanied by a change in the morphology of a microorganism and Yang *et al.* (1996) investigated the possibility of a relationship between antibiotic production and morphological change in *Streptomyces virginiae.* Virginiamycin production commenced after the growth phase, during which glycerol was slowly consumed by the organism. The onset of antibiotic production also coincided with a noticeable drop in nutrient levels (indicated by the sharp decrease in carbon dioxide concentration in the exhaust gas) and with autoregulator synthesis by the batch culture. The morphology of the organism at this stage was investigated by preparing suitable dilutions of the culture and staining slides with methylene blue. A Spectrum II image analyser confirmed a morphological change from free filamentous form to highly entangled filaments. The parameter employed to describe the changing morphology of this organism was the oval major axis length. Three classifications were determined: 100-225 μm (free filaments), 225-400 μm (entangled filaments) and 400-500 μm (pellets). The results from this work indicated that both morphological changes and autoregulator synthesis by the cells are influenced by the depletion in nutrients. However, once the morphological changes occur there is no further correlation between morphology and antibiotic production.

Further investigations into this possible correlation between morphology and secondary metabolite production were performed by Treskatis *et al.* (1997), who concentrated on the development of an improved method for morphologically analysing samples. A batch culture

of *Streptomyces tendae* (Tu 901/8c) was cultivated. An algorithm to measure eight different morphological parameters, including shape factors, circularity factors, object area and perimeter, was developed. This significant improvement in the algorithm in terms of parameter numbers/types helped to further classify an organism into five separate categories, giving it a more detailed morphological description. Treskatis *et al.* also introduced the use of a measuring chamber which could house culture samples taken directly from the fermenter. Without any deformation caused by sample drying or the use of cover slips. These could then be analysed in real time, without the need for dilution or staining (previously required for image analysis). All of these contributions have helped researchers to develop a greater understanding of the morphological and physiological changes taking place in a fermentation in a continuous way. The drawback is that a dedicated and inherently expensive system is required.

Christiansen *et al.* (1999) continued the work of Spohr *et al.* (1998), using a small flow-through cell to investigate the growth of a single hyphal strand within a mass of hyphal elements, in terms of tip extension rates and the hyphal branching patterns. Saturation type kinetics were used to describe tip extension rate with respect to hyphal length. Once the hypha reaches a certain minimum length (found to be independent of prevailing glucose concentration), it was found that the number of tips formed was proportional to the length of the hypha. Branching intensity appeared to increase with increasing glucose concentration. Simulation of the hyphal growth pattern showed an exponential increase in both tip number and hyphal length and these trends were verified experimentally.

2.5.2.2.3 PELLET MORPHOLOGICAL STUDIES

Effects of pellet morphology on productivity and composition of secondary metabolites are relatively unexplored (Braun and Vecht-Lifshitz, 1991). Ryoo (1999) used fractals to study the complex mycelial morphology of *A. niger*. The morphology was quantified by a fractal value which was then related to various physiological conditions. It was found that the fractal value of mycelial mycelium was inversely related to the average mycelial growth unit and decreased with an increase in the inoculum level. Increasing sucrose levels resulted in a decrease in both the average diameter of the pellets and in the fractal value of the mycelium; increasing phosphate levels had the opposite effect. It was determined that the fractal value could be used successfully as a morphological parameter of fungal mycelium.

In submerged culture, pellets have been classified into three different groups: 1) fluffy pellets (having rough edges), 2) smooth pellets (limited lateral growth) and 3) hollow pellets. However, the distinction between pellets and highly entangled clumps is still subjective and system specific. Attempts have been made by numerous researchers to distinguish between the two, one being on the basis of differences in mean grey values on an interactively pre-established limit. Pellets were recognised by their low mean grey value corresponding to their high biomass and further characterised by the mean object area and shape and the percentage present in a given sample. This method is inherently very time consuming as it requires numerous images to be analysed (Reichl *et al.*, 1992). Paul and Thomas (1997) also attempted to distinguish between pellets and clumps. They defined a pellet as an entity which had a central 'core' region *i.e.* absence of holes. Rough and smooth pellets could be distinguished from one another by a fullness factor (approximately equal to one for the smooth pellet). Further distinctions were made between clumps and hyphae. Entities which incorporated three or more hyphal loops were defined as clumps, whereas those fewer than three were defined as hyphae. Durant *et al.* (1994) proposed a very interesting technique involving a simple staining procedure. The stain, when applied to a sample of pellets, clumps and hyphae (entangled biomass) will remain attached to the pellets (which, as a result, become coloured) but will leave the entangled biomass colourless when washed out of the sample. This contrast in colour between the various morphological forms allows each to be identified simply by image analysis. The method has been used to observe the effect of agitation speed on the morphology of a strain of *Schizophyllum commune*. At lower agitation speeds of 120-200 rpm, the pellet form mostly predominated. As the agitation speed was increased to speeds of up to 500 rpm, the representation of the pellet form decreased sharply and the more entangled filamentous form was predominant. This staining procedure reduces the image processing time and has been viewed as a method to describe the 'diffusional' properties of biomass *i.e.* how readily an agent can access parts of the biomass. However, experimental factors such as the decolouration time and indeed the stain type must be optimised for each organism.

CHAPTER 3
MATERIALS AND METHODS

3.1 THE ORGANISM

The organism used for all studies was *Streptomyces natalensis*, NCIMB number 10038 (NCIMB Ltd., UK). This organism is also listed as ATCC 27448 (American Type Culture Collection, USA), CBS 700.57 (Central Bureau Voor Schimellcultures, Holland) and NRRL 2651 (Northern Research Laboratory, USA). The organism was obtained as a freeze-dried culture and was resuspended in liquid medium. The resuspended organism was used to produce both plate and liquid cultures.

3.2 MEDIA

3.2.1 MAINTENANCE MEDIA

The organism was maintained on both Tomato Paste Based Oatmeal (TBO) and YEPD agar plates. The composition of both solid media types are shown in Table 3.1. It was also routinely stored in a solution of 30 % glycerol and 25 μL of Triton X-100.

Table 3.1 Solid media composition

	Manufacturer	**Conc. (g/L)**
Tomato paste agar		
Oatmeal (food grade)	Flahavans & Sons (Ireland)	20
Tomato paste	Rolli (Leon, Spain)	20
Technical agar No. 3	Oxoid (Basingstoke, UK)	25
YEPD agar		
Yeast extract	Oxoid	10
Bacteriological peptone	Oxoid	20
Glucose monohydrate	BDH (Poole, UK)	20
Technical agar No. 3	Oxoid	10

3.2.2 INOCULUM PREPARATION MEDIUM

To ensure adequate biomass for inoculation into fermentation media, the organism was cultivated in liquid culture medium (Table 3.2) prior to inoculation into the fermentation media. In the case of the YEME medium, both the glucose and the $MgCl_2.6H_2O$ were autoclaved separately. In the case of the SPG, YED and YEME medium, the pH was adjusted to pH 6.4.

Table 3.2 Inoculum preparation media

	Manufacturer	**Concentration (g/L)**
YEME medium		
Glucose monohydrate	BDH	10
Sucrose	BDH	340
Bacteriological Peptone	Oxoid	5
Malt Extract	Oxoid	3
Yeast Extract	LabM (England)	3
$MgCl_2.6H_2O$ (2.5 M)	BDH	2 mL/L
YED medium		
Glucose monohydrate	BDH	10
Bacto-yeast extract	Oxoid	10
SPG medium		
Glucose monohydrate	BDH	20
Neutralised soyapeptone	Oxoid	25
$ZnSO_4.7H_2O$	M&B (England)	0.5mM

3.3 FERMENTATION MEDIA

3.3.1 YEME AND SPG LIQUID MEDIA

The components and concentrations used in the formulation of these media are as described in Table 3.2.

3.3.2 PHOPHATE-LIMITED MEDIUM

The components of the phosphate-limited medium are shown in Table 3.3. This medium was previously used by Martin and Mc Daniel (1976).

Table 3.3. Phosphate-limited medium

Component	Manufacturer	Concentration (g/L)
Glucose monohydrate	BDH	50
L-asparagine		10
$ZnSO_4.7H_2O$	M&B Ltd.	0.02
$MgSO_4.7H_2O$	M&B Ltd.	0.2
$FeSO_4.7H_2O$	Reidel-de Haen	0.02
$CuSO_4.7H_2O$	Reidel-de Haen	0.02

3.4 CULTIVATION OF THE ORGANISM

3.4.1 CULTIVATION ON SOLID MEDIA

The organism was cultivated on both YEPD and Tomato paste Based Oatmeal (TBO) agar plates. Subculturing was performed on a fortnightly basis to ensure viable vegetative cultures. The organism was routinely maintained on TBO plates. It was cultured on YEPD to indicate that the fermentation was uncontaminated.

3.4.1.1 TOMATO PASTE BASED OATMEAL AGAR

Two protocols were used for maintaining the organism on TBO plates. The first involved taking a lawn of the organism, from a TBO maintenance plate, and suspending it in a 3 mL aliquot of sterile Ringers solution. 1 mL of this suspension was then used to inoculate a fresh plate. The second protocol involved inoculating a fresh plate with a 40 μL aliquot of spores suspended in a glycerol solution. In both cases, these plates were incubated at 30°C for 14 days to allow spore formation to occur. A characteristic grey colour indicates the presence of spores. The plates were then stored at 4°C. All plate work was performed in a (horizontal) laminar air flow cabinet.

3.4.1.2 YEPD AGAR

A loop full of cells was taken from a stock plate and aseptically streaked onto a fresh YEPD plate. These plates were then incubated at 30°C for 4 days and stored at 4°C.

3.4.2 CULTIVATION IN LIQUID MEDIA

3.4.2.1 GLYCEROL STOCK SOLUTIONS

The organism was also maintained in a solution of 30 % glycerol and 25 μL of Triton X-100. Sterile glass beads (2.5-3 mm diameter), covering approximately one quarter of the plate, were used to remove spores from the surface of a day 14 TBO plate. A 9 mL aliquot of sterile Triton X-100 solution (25 μL Triton X in 100 mL deionised water) was used to resuspend the spores. Mycelia, which may be present, were removed from the spore suspension by centrifugation at 1000 rpm for 2 minutes. Further centrifugation, at 3500 rpm for 10 minutes, resulted in the formation of a pellet of spores. These spores were resuspended in 6 mL of the glycerol solution. 1 mL aliquots of the resuspended spores were then transferred to sterile eppendorfs for long term storage at -20 °C.

3.4.2.2 SHAKE FLASK CULTURES

All shake flask cultures were grown in 250 mL Erlenmeyer flasks (with or without wire-baffles), containing either 50 or 100 mL of medium, as indicated below. Cotton wool and foam bungs were used to close the flasks and to prevent contamination, while still allowing an adequate oxygen supply to the organism.

3.4.2.2.1 INOCULUM SHAKE FLASK CULTURES

For the inoculum cultures in Part One of the optimisation study, 50 mL aliquots of inoculum preparation medium were placed in 250 mL Erlenmeyer flasks (unbaffled) and inoculated with 1 mL of suspended culture from a day 14 TBO maintenance plate. For the second part of the optimisation study, 50 mL aliquots of YEME inoculum medium were placed into 250 mL Erlenmeyer flasks (wire-baffled) and were inoculated directly with a 40 µL spore suspension (from glycerol stocks). All flasks were incubated at 30°C and 200 rpm in an orbital incubator shaker (Gallenkamp), for periods of between 12 and 50 hours, as specified below.

3.4.2.2.2 SHAKE FLASK FERMENTATIONS

For all fermentations in Part One of the study, 100 mL aliquots of a fermentation medium were placed in 250 mL Erlenmeyer flasks (unbaffled) and each inoculated with either 10 % (volume/volume) or ~5 g/L of an inoculum culture. The flasks were then incubated for up to 8 days at 30°C on an orbital shaker (200 rpm).

For Part Two of the study, 50 mL aliqouts of the YEME fermentation medium were placed in 250 mL Erlenmeyer flasks (wire-baffled) and each inoculated either directly with a 40 µL spore suspension or a 10 %, 24 hour YEME inoculum. The flasks were then incubated for up to 72 hours at 30°C on an orbital shaker (200 rpm).

3.5 MEASUREMENT OF FERMENTATION PARAMETERS

3.5.1 DETERMINATION OF BIOMASS CONCENTRATION

100 mL of deionised water was passed through a sheet of Whatman No. 1 filter paper (70 mm diameter) in a Buchner funnel apparatus. The filter paper had previously been pre-dried overnight at 105 °C. The weight of the paper both before and after water addition was determined using an analytical balance (Mettler Toledo, Model B154). A predetermined volume of culture was then passed through the filter paper, to separate the biomass from the rest of the culture fluid. To ensure that all cellular material had been removed, the supernatant was passed through the filter for a second time. The filter cake was then washed with a further 100 mL of deionised water (to remove excess extracellular material) and was reweighed. The sample wet weight (g/L) was determined by calculating the increase in the weight of the filter paper.

Placing the wet sample in an incubator (105 °C) for 24 hours, and then re-weighing the filter paper, allowed the sample dry weight (g/L) to be determined.

3.5.2 DETERMINATION OF SUGAR CONCENTRATION

An RQflex reflectometer (Merck & Co., Inc., New Jersey, U.S.A) was used to determine the concentration of glucose present in a sample. The technique is enzymatically-based, involving reaction of the sample (broth) with glucose oxidase and peroxidase which are present on a reaction strip. After reaction, the reflectometer uses a photometric technique to determine glucose concentration on the basis of relative reflectance of the reaction zone on the strip, with reference to the results obtained using standards of known glucose concentration. The strips are temperature sensitive and must be stored in the fridge at 4°C. Samples of the supernatant are diluted 1:100 with de-ionised water and the instructions provided with the instrument are then followed carefully in order to obtain accurate measurements. Samples were analysed in duplicate and the mean of representative results for a series of glucose standards are presented in Figure 3.1.

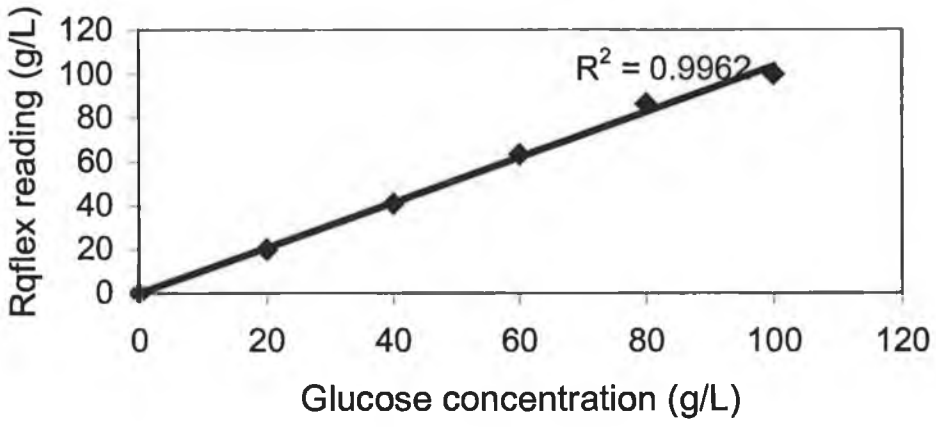

Figure 3.1 Representative glucose standard curve for RQflex Reflectometer

3.5.3 DETERMINATION OF pH

The broth (supernatant) pH was determined using a WTW Microprocessor Precision-pH/mV-Meter (WTW Measurement Systems, Inc., Florida 33916).

3.5.4 DETERMINATION OF PIMARICIN CONCENTRATION

A modification of the bioassay, developed by Raab (1972), was employed to determine pimaricin levels. An overnight culture of *Saccharomyces cerevisiae*, listed as ATCC number 9763, was prepared. Its optical density determined using a spectrophotometer at 600 nm. In some cases, it was necessary to dilute the samples so that the O.D. could be read. YED, with 2 % agar, was prepared and dispensed into sterile petri dishes (Sterilin) - exactly 20 mL per plate - and these were allowed to set. Using a flame-sterilised 3mm cork borer, a well was made in the centre of each plate. A 100µL aliquot of either supernatant sample (4000 rpm, 5 minutes) or pimaricin standard was placed in the well. The plates were then covered and allowed to stand at 4 °C for 2 hours, to permit sample diffusion to take place. They were then placed into the laminar flow cabinet where an overlay of YED and *S. cerevisiae* (1 % agar) was added to each plate. The overlay was allowed to set and plates were incubated at 30°C for 24 hours. After incubation, a light box was used to highlight clear zones on the plates. These indicated the presence of pimaricin and could be compared to a range of standards.

The pimaricin standards used for this assay were in the range 5 μg/mL to 400 μg/mL. The pimaricin was diluted in a 65:35 mixture of methanol and distilled water. Samples were analysed in duplicate and the mean of the results was calculated.

Figure 3.2 shows a standard curve for this bioassay, while Figure 3.3 demonstrates the distinction between positive and negative results.

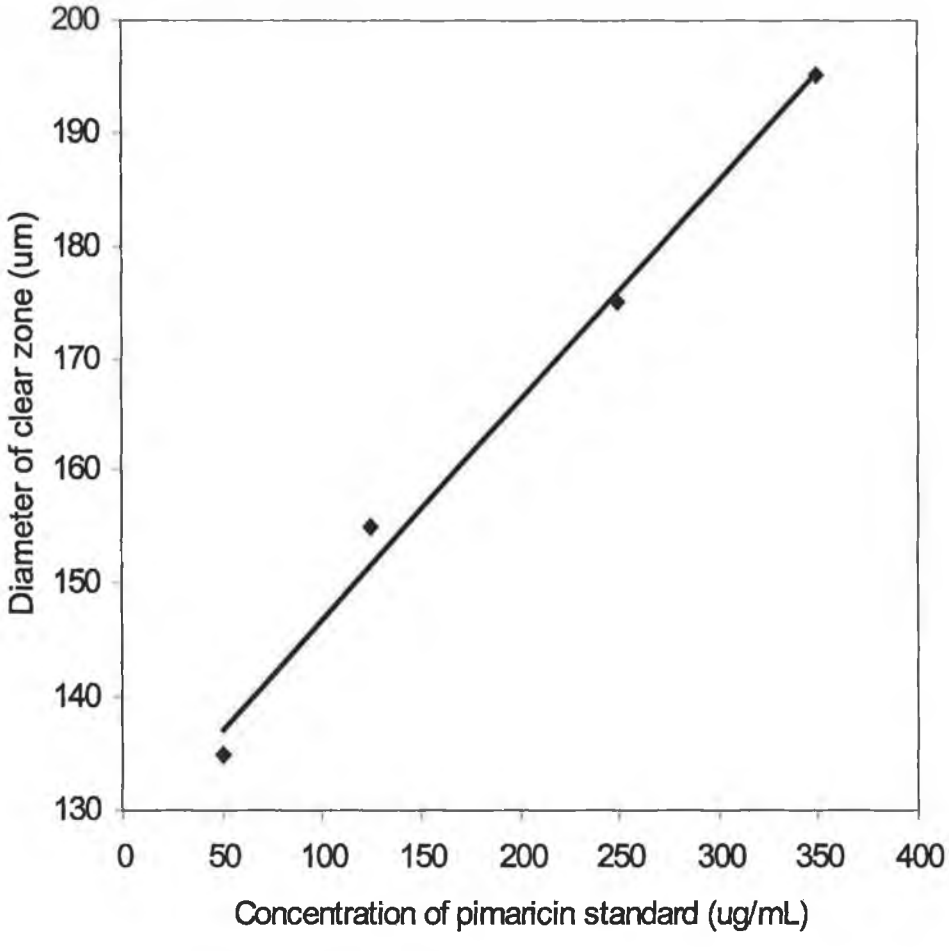

Figure 3.2 Representative standard curve for pimaricin bioassay

(a)

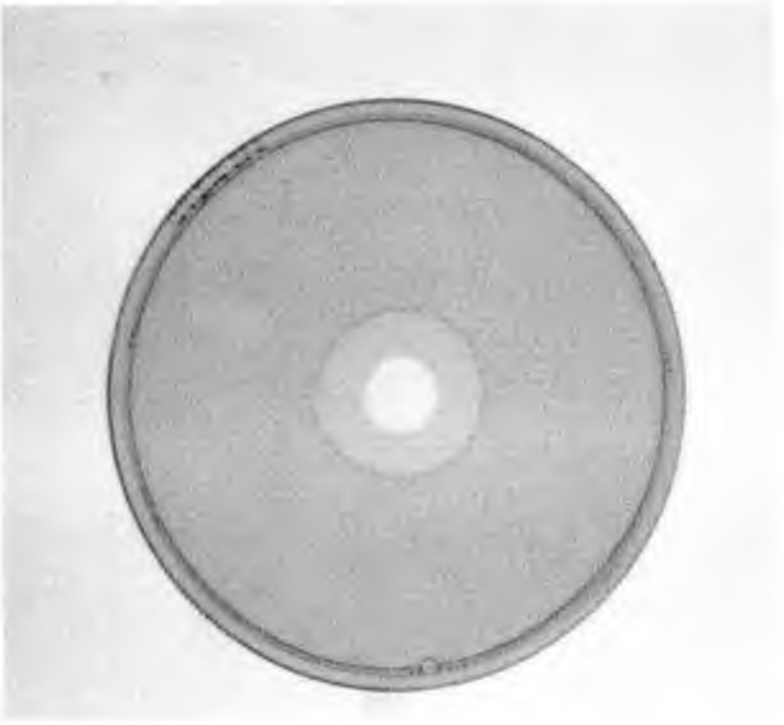

(b)

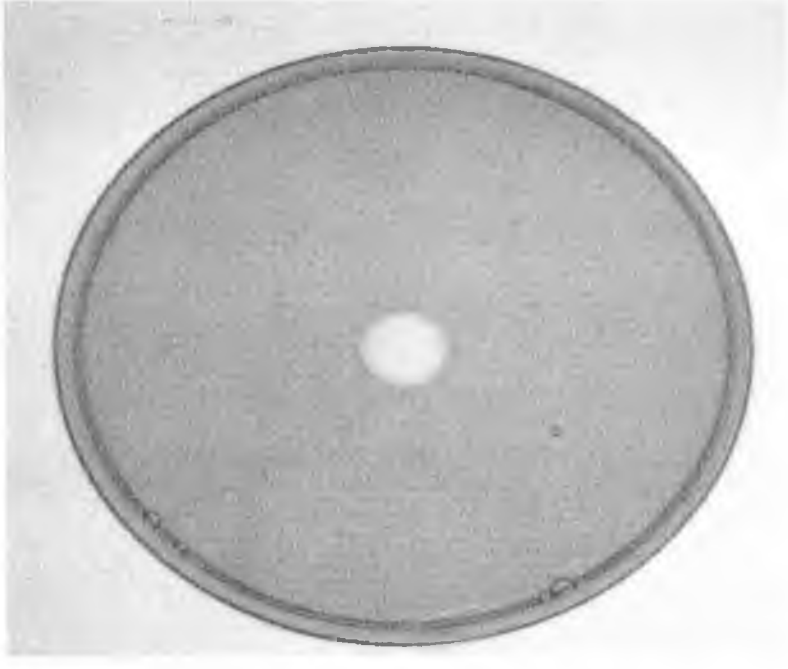

Figure 3.3 Representative (a) positive and (b) negative results for pimaricin bioassay (Pimaricin concentration of 250 μg/mL)

3.5.5 DETERMINATION OF MORPHOLOGICAL PARAMETER OF CHORD LENGTH USING LASENTEC® FBRM PROBE

A Lasentec® FBRM probe (Lasentec Inc., USA) was used to morphologically characterise the organism. Undiluted broth samples, taken directly from shake flasks, were placed into 200 mL beakers and the probe was inserted into the medium. A laser beam was projected through a sapphire window of the probe. This beam is highly focused just outside the window surface, traveling at very high speeds (2 m/s to 6 m/s) and following a path around the circumference of the window. At these speeds, motion of the entities is insignificant to their measurement. As they pass by the window surface, the beam intersects the edge of an individual entity. Laser light is backscattered by the entity until the beam reaches its opposite edge. The FBRM optics gather the backscatter and convert it into an electronic signal. Distance traveled by the beam, and hence the chord length of an entity, is determined by multiplying the time period of backscatter and the speed at which the beam is traveling. No particle shape is assumed by the probe and the chord length distribution is essentially unique for any given entity size and shape distribution. Also, chord length distributions are solely a function of the change in entity dimensions and number, assuming that the shape is constant over millions of entities. Data was recorded every 30 seconds and the results were exported to a software package that accompanies the probe, Lasentec® FBRM Control Interfaces, version 6.0 (Lasentec Inc., USA), for further analysis.

CHAPTER 4
IMAGE ANALYSIS

4.1 IMAGE ANALYSIS HARDWARE

The three main components of the image analysis hardware employed in this study were a personal computer equipped with a framegrabber and image analysis software, a video camera and a microscope.

Computer

The computer supporting the image processing and analysis software contained an Intel Pentium II microprocessor. The system contained an IC-PCI framegrabber board (Imaging Technologies, Inc., MO 63336), which was used to obtain live and 'frozen' (video-based) images. The monitor used was an 02128-TCO colour monitor (Nokia Display Products Oy Salorankatu 5-7).

Camera

The camera used was a JVC KY-F55B colour video camera (Victor Company of Japan, Ltd., Japan). This was attached to the microscope using a C-type lens mount.

Microscope

The microscope used was an Olympus BX40 brightfield microscope (Olympus Optical Company, Japan). The magnification used for all studies was 10X, under which conditions each image pixel corresponded to 0.632 μm. Constant settings for both the lighting and condenser position were employed to ensure that uniform and reproducible images were obtained.

4.2 IMAGE ANALYSIS

The software which was used was a Windows-based package, Optimas 6 (Media Cybernetics Inc., Iowa). The main stages involved in all image analysis work are:

- Obtaining a grey/colour image which may be stored
- Processing the grey/colour image
- Isolation of objects of interest, to yield a binary image
- Manual or automatic processing of the binary image
- Measurement of selected objects of interest
- Data output and statistical analysis

Used in conjunction with the camera and microscope, Optimas 6 facilitated all of these tasks. Optimas also has its own high-level interpreted programming language, ALI (Analytical Language for Images), which allows macros (complex series of steps which are frequently repeated) to be written. Therefore, identical sequences of image processing can be performed on images from numerous samples, permitting a high degree of automation and significantly reducing processing time.

4.2.1 SLIDE PREPARATION

Preparation of the sample is very important as it affects image quality and contrast. The morphology of microorganisms is often difficult to observe in wet, unstained preparations. For filamentous organisms, in particular, the use of staining procedures has proved beneficial in image analysis. A 50 μL aliquot of a suitably diluted sample was applied to a 1.2 mm thick Blue Star glass slide (Chance Propper Ltd., Warley, England). The dilution factor was chosen so that when viewed under the relevant magnification, approximately 10-15 % of field of view is occupied by the entities of interest. At this level of dilution the spatial arrangement of the entities of interest lends itself to more detailed analysis and, hence, to more accurate representations of the morphological forms present to be produced. The slide was allowed to air-dry for 24 hours. The surface of the

slide was then flooded with a solution of crystal violet (1 g/L) and allowed to stand for 5 minutes. Surplus dye was removed by washing with distilled water. Slides were allowed to air-dry for a further 24 hours before image analysis.

4.2.2 IMAGE ACQUISITION AND STORAGE

The camera of the image analysis system converts an optical image from a light microscope (or other source) into an electronic (video) signal suitable for processing. It does this using a CCD (light sensitive target). The video signal varies with screen illumination, with darker regions generating lower voltages than brighter regions and this original converted to digital form by an analogue-to-digital converter (ADC). The resulting digitised image contains 768 x 572 pixels. Each pixel is assigned a grey value ranging between 0 (representing black) and 255 (representing white) in the case of black and white images, or a series of numbers representing the colour or intensity of a pixel in the case of colour images. The lighting and focus of the original live image are adjusted to produce an image of suitable quality (determined by visual inspection) which can then be 'frozen' (acquired).

4.2.3 PROCESSING THE GREY IMAGE

The acquired grey image is often not suitable for immediate analysis. Images are, therefore, often enhanced using filters, to distinguish between wanted and unwanted regions. These unwanted regions may arise from inappropriate lighting settings, noise or the presence of dust/debris on the slide. Optimas used spatial filters to improve image quality. These fall into three catagories: noise reduction, edge enhancement and sharpening. Morphological transforms and pixel to pixel operations can also be used to improve the image quality.

4.2.4 ISOLATION OF OBJECTS OF INTEREST

Optimas sets up a threshold (set of intensity levels) to separate pixels of interest from the rest of the image. As a result, the image is segmented into a foreground (pixels of interest) and a background (all other pixels). Objects of interest can then be automatically identified and placed into a binary image for further processing.

4.2.5 MANUAL OR AUTOMATIC BINARY IMAGE PROCESSING

Manual or automatic processing of the binary image is necessary so that objects of interest can be more easily identified. Smoothing an uneven background (which may occur because of differences in lighting, sample thickness, staining and noise) and separation of touching objects (using erosion and dilation) are some of the methods provided by Optimas.

4.2.6 MEASUREMENT OF SELECTED OBJECTS OF INTEREST

Over 100 measurements are available in Optimas, ranging from shape and orientation measurements to size and texture measurements. Calibration (conversion of image pixels into actual measurements) is performed for each microscope objective employed, using a micrometer slide. The calibration process not only allows for application of real measurements but also corrects for errors which may arise in measurements due to certain physical conditions such as optical distortion and non-linear transmission of light through a sample.

4.2.7 DATA OUTPUT AND STATISTICAL ANALYSIS

Once measurements have been extracted, the data can be exported to Microsoft Excel for formatting and further analysis.

Automation of image analysis is highly desirable as it reduces human error and improves efficiency. Using Optimas, this can achieved through the simple process of recording macros. The possibility of running macros without manual intervention exists. The ability to input and output data and conditionally execute operations is also facilitated by these macros, resulting in a very flexible and user friendly system.

4.3 IMAGE ANALYSIS ALGORITHM FOR THE MORPHOLOGICAL CHARACTERISATION OF *S. natalensis*

An algorithm was developed for the morphological characterisation of *S. natalensis*. The purpose of this algorithm was to:

- Distinguish between the three morphological forms *i.e.* pellets, clumps and hyphae.
- Measure the properties of the above morphological forms, in terms of average entity area, core area (pellets), convex area (clumps), perimeter, convex perimeter, roughness and fullness; for hyphae, the length, number of tips, number of branches and the hyphal growth unit (defined as hyphal length/number of tips present were also measured).

The algorithm is schematically illustrated in Figure 4.1. The associated Optimas code and relevant definitions are provided in Appendix A1.

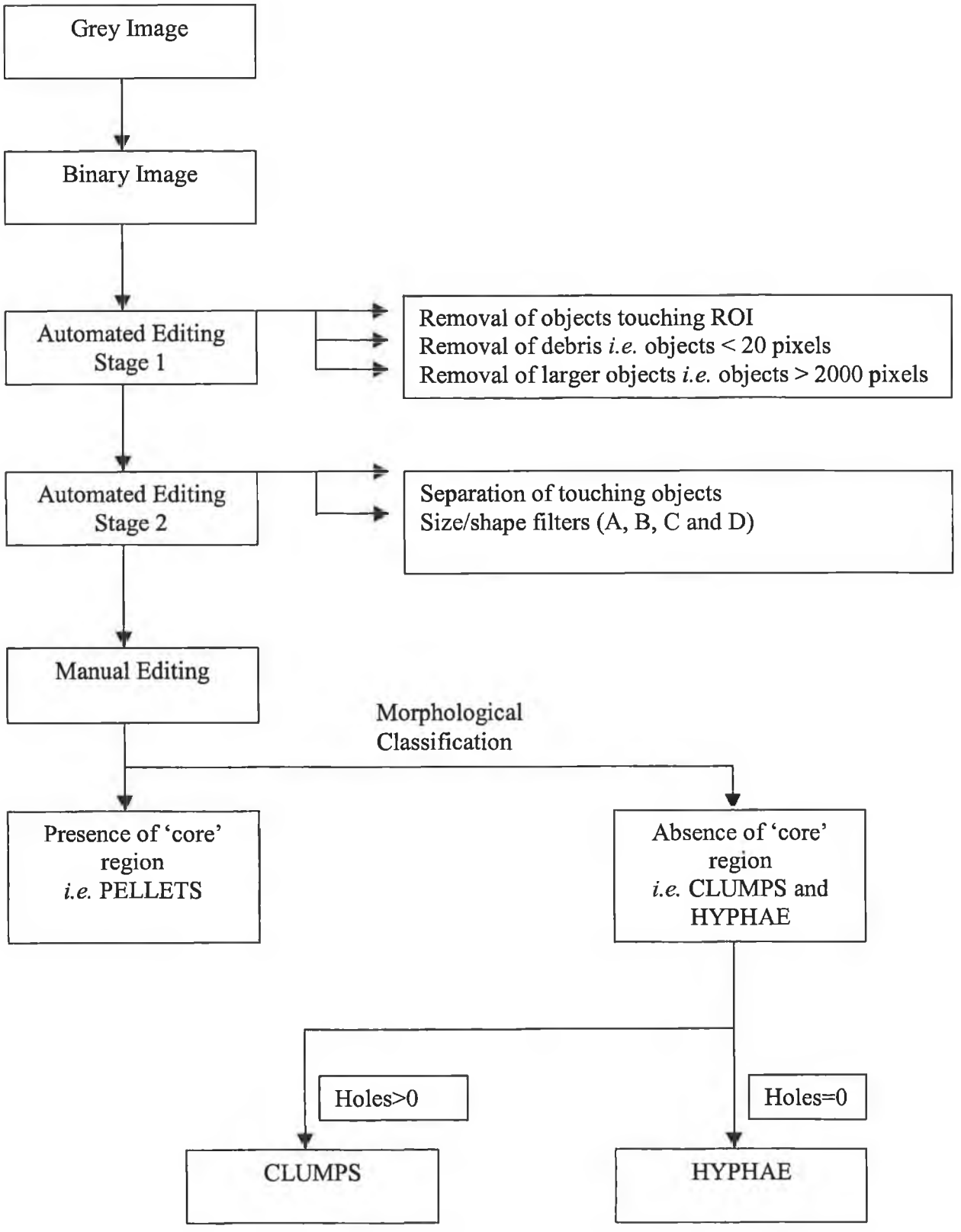

Figure 4.1 Image analysis algorithm

Initiation and Grey Image Acquisition

Before images were processed and analysed, the data relating to the sample type and analysis conditions were inputted. This information included:

- Experiment title
- Magnification
- Sample name
- Dilution factor

In order to provide a reference background, the operator was then required to move the microscopic stage so that a blank region on the slide was under investigation. The lighting was adjusted to a luminance value of 100%. As this process was repeated for each image it was assumed that the background grey levels were the same for all images. The user then viewed a region of interest on the slide and focussed the live image correctly, before acquiring the image (Figure 4.2).

Binary Image Processing, Automated Editing – Stage 1

The quality of the acquired image was enhanced by removing unwanted objects (Figure 4.3). This was achieved by setting a grey threshold of 165 (*i.e.* rejecting all paler 'background'). Size filters were then used to remove all objects consisting of 20 pixels or fewer (mainly debris) and those objects consisting of 2000 pixels or more (mainly insufficiently diluted biomass appearing as large aggregates).

Automated Editing – Stage 2

Problems arising due to objects touching one another (Figure 4.4) were solved by applying a number of binary operators to the image. Initially, the objects were eroded using an octagonal structuring element. This process separated the objects into individual entities whose size was reduced to a minimum of 500 pixels. Application of a series of

dilations on these modified objects (Figure 4.5), within the mask of the original image (Figure 4.6), allowed the objects to be slowly rebuilt to their original size, this time as individual objects which overlapped with adjacent objects. All subsequent measurements were made on these individual objects with no loss of significant data (Figures 4.7).

Before measurements were performed, each object was required to satisfy the three conditions (size/shape filters) listed in the Table 4.1. Application of these three conditions further separated debris from objects upon which measurements would be made. The limiting pixel and aspect ratio values were determined on the basis of prior analysis of an adequate number of objects from *S. natalensis* cultures. These values are system specific and application of this image analysis algorithm to another organism would necessitate prior determination of the appropriate values.

Filter Type	Filter Parameters
A	Area > 50pixels and fullness < 0.5 Or Area < = 50 pixels
B	Area < 250 pixels and aspect ratio > 1.25 Or Area > = 250 pixels
C	Area < 60 pixels and aspect ratio > 4 Or Area > 60 pixels
D	Area > 450 pixels

Table 4.1 Size/shape filters for analysis of *S. natalensis* samples.

Manual Editing

Following this automated binary editing stage, the operator may manually edit the enhanced binary image. Such manual editing may be required to remove debris which was mistakenly accepted as an object of interest. However, this occurance and subsequent manual editing was minimal.

Morphological Classification

Morphological classification of the accepted objects as pellets, clumps or hyphae can be achieved by separation of the objects into those which possess a defined 'core' region (pellets) and those which do not (clumps and hyphae). The measurement process initially requires the performance of a series of binary operations on all objects, which are subsequently checked for the presence of a 'core' region.

Identifying objects with a 'core' region was achieved by placing a copy of the accepted objects of interest into a separate binary image store and then identifying objects which are common to another binary image store, 'cores'. This latter binary image was produced by eroding the objects of interest, a total of 8 times, using a predetermined structuring element (Figure 4.8). This operation was sufficient to isolate those objects with a defined central 'core'. A copy of these objects, subsequently dilated 8 times using the same structuring element, was stored, ('cores'). All pellet measurements were then performed on objects in this grey image (Figure 4.9).

Clumps and hyphae are classified on the basis of the number of holes present within the object. Using image masking, the 'holes' are brought to the foreground of the image and the threshold is set between 0 and 125 levels of greyness. If holes are present (in the case of clumps) the number and area are measured and in the absence of holes the object is classified as a hyphal entity.

Objects which are classified as hyphae are placed into a newly created binary image store. These are skeletonised and accurate area and length measurements are obtained. By applying thinning filters to the image, the number of tips, number of branches and the hyphal growth unit (defined as hyphal length/number of tips present) are also obtained.

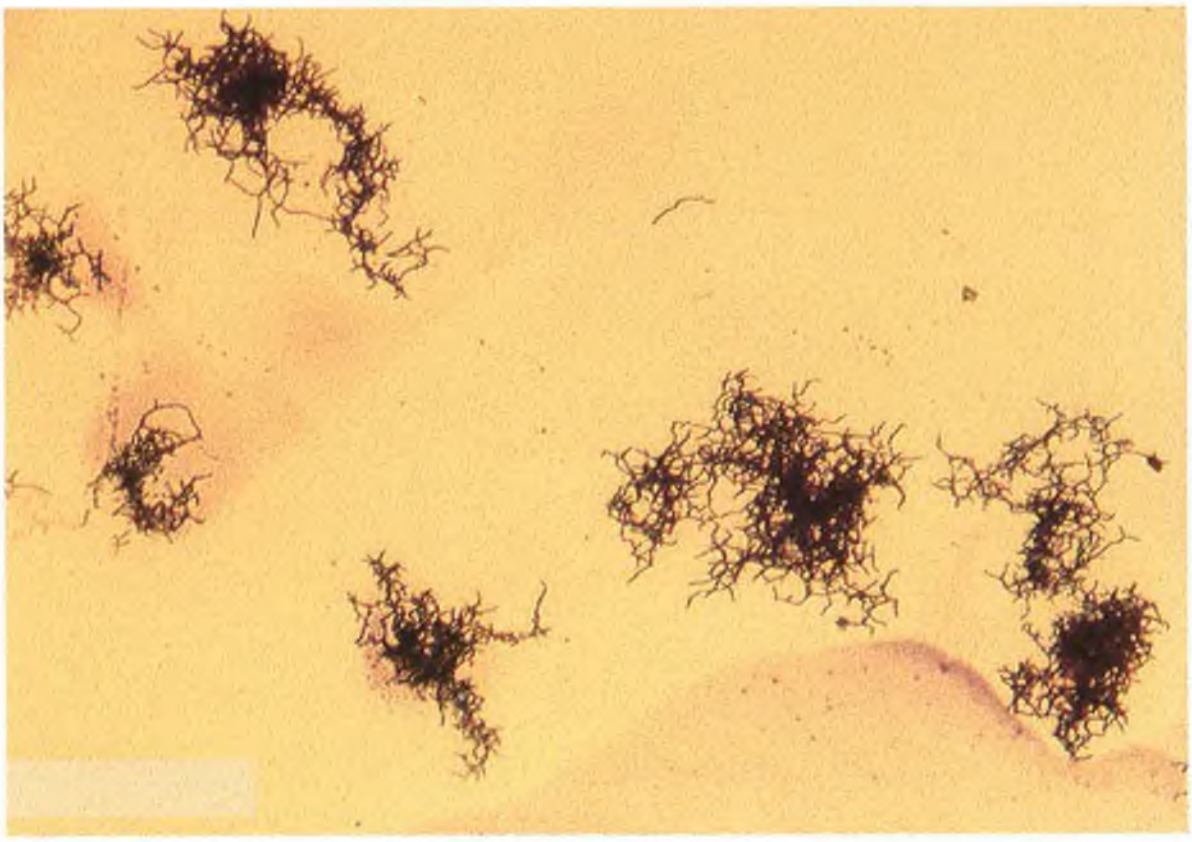

Figure 4.2 Acquired image.

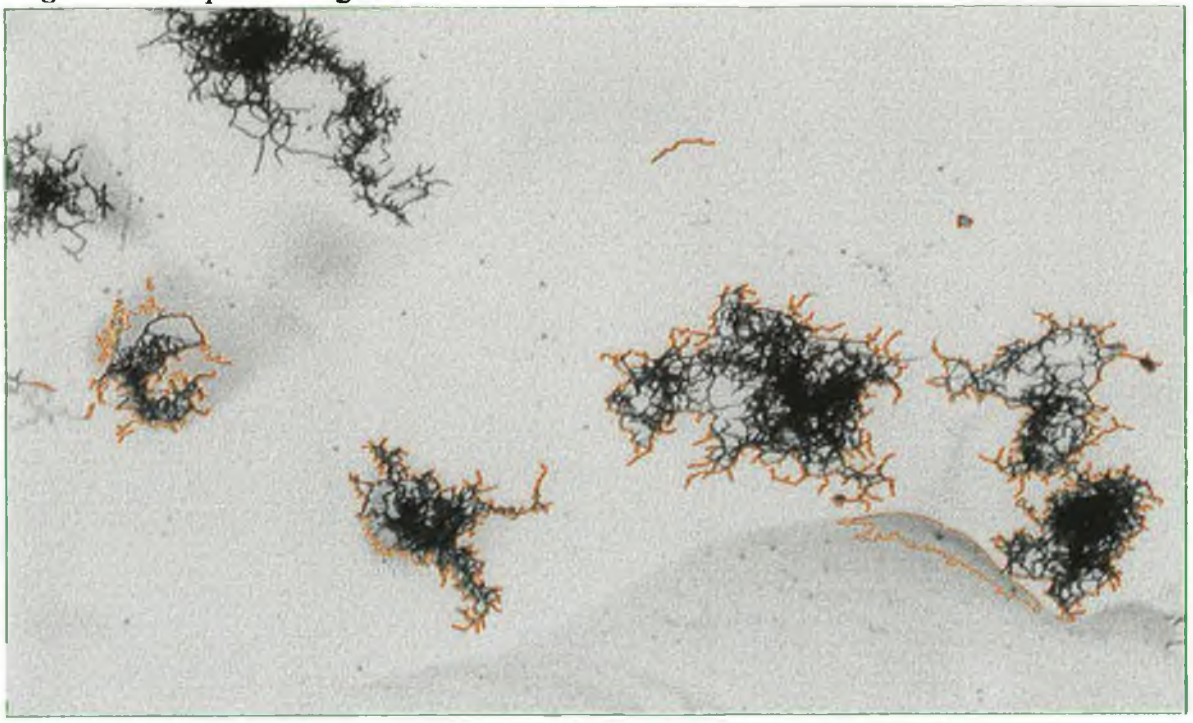

Figure 4.3 Removal of a) objects touching the region of interest (within green border) and b) debris. Areas to be considered indicated in orange.

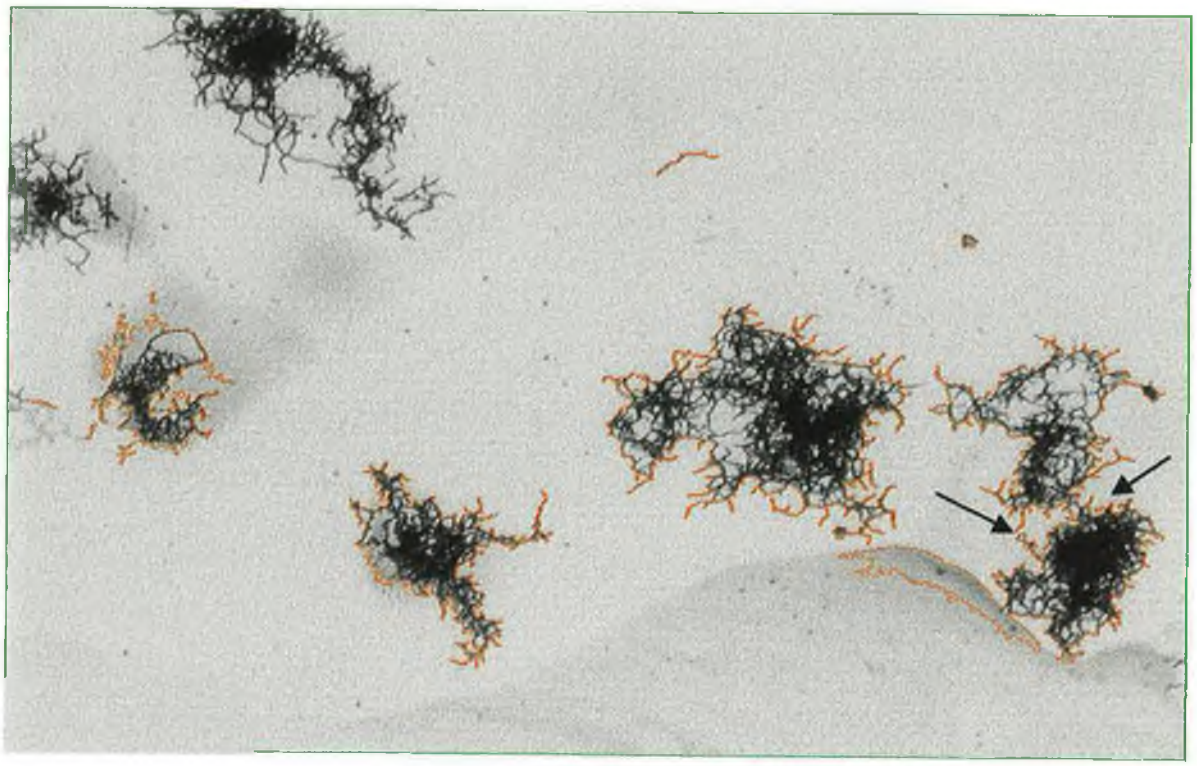

Figure 4.4 Separation of touching objects

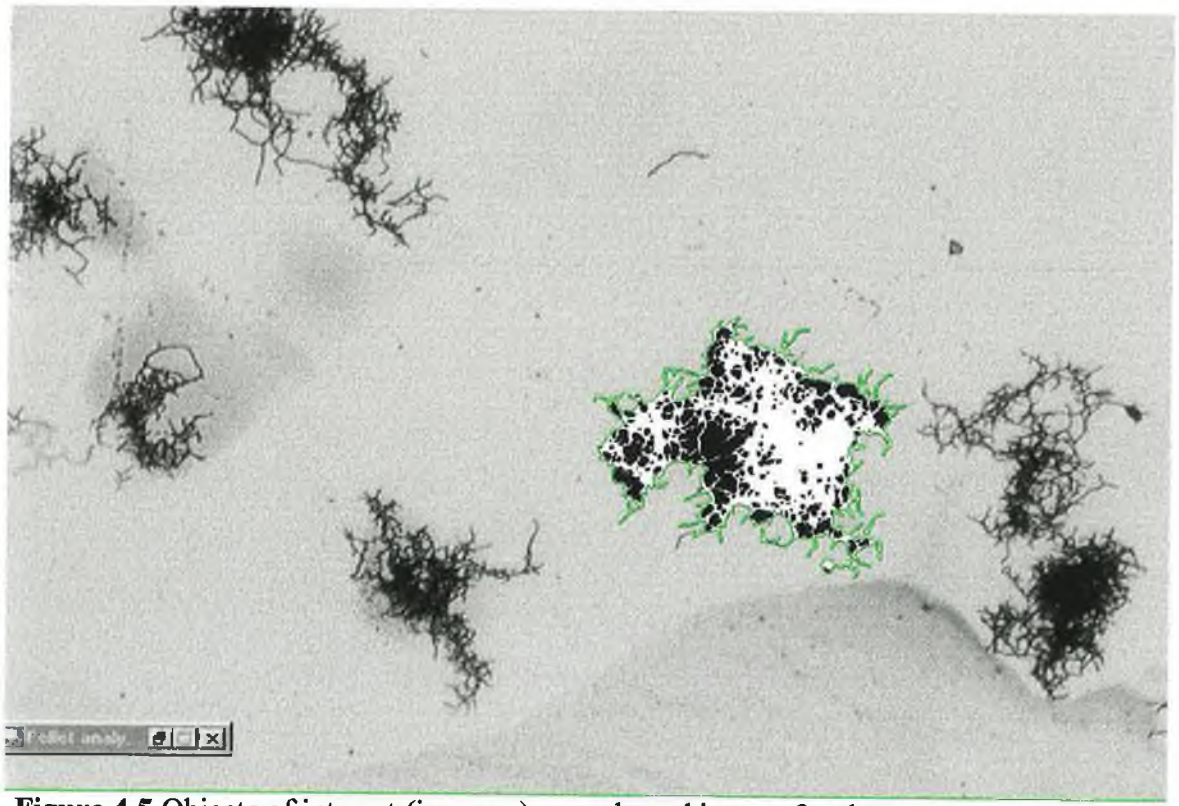

Figure 4.5 Objects of interest (in green) are selected in turn for the measurement process

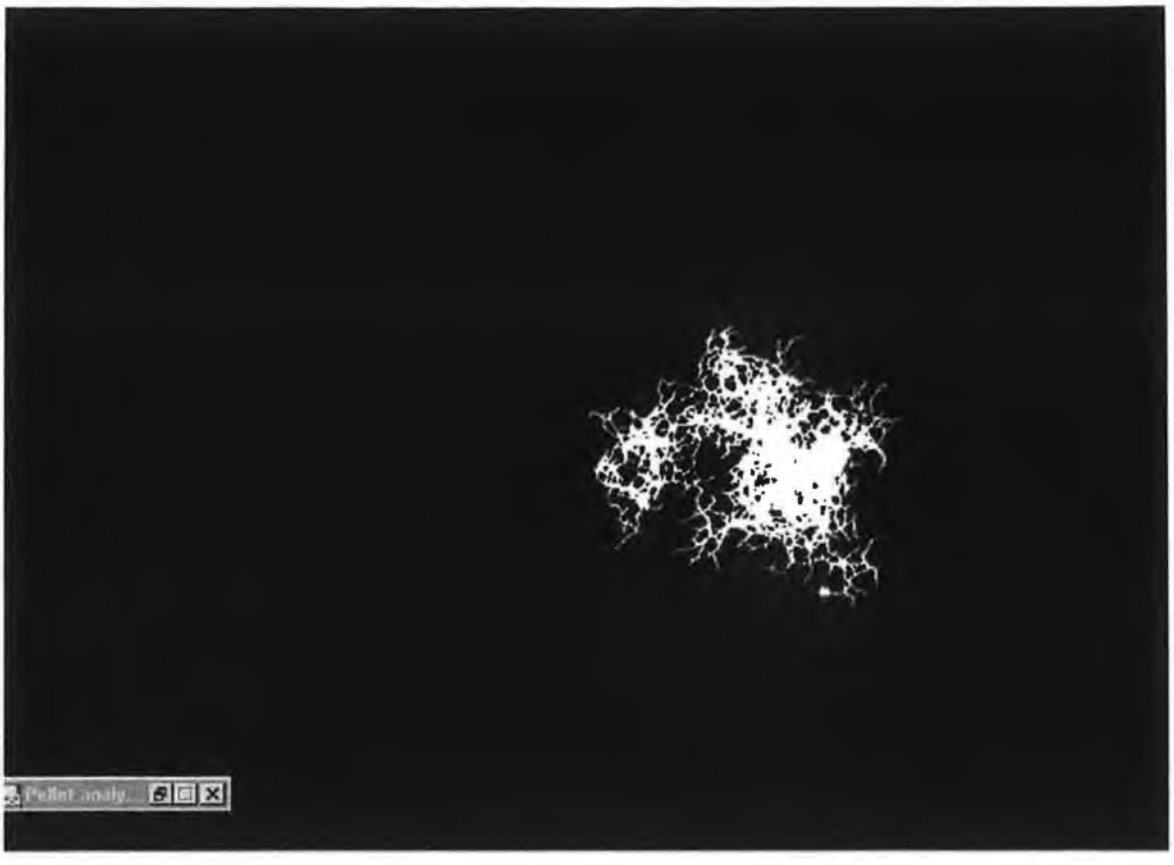

Figure 4.6 Inverted masking of image

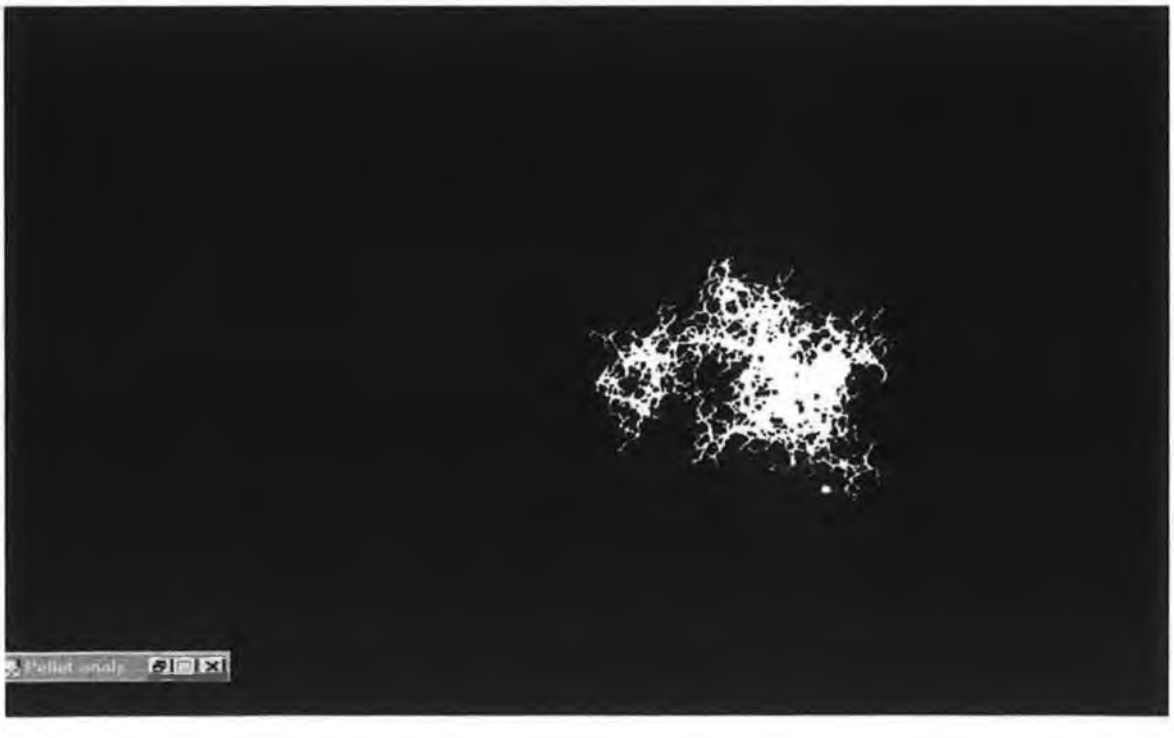

Figure 4.7 Reset to normal masking (item for measurement).

CHAPTER FIVE

RESULTS AND DISCUSSION – OPTIMISATION OF CULTIVATION STUDIES

5.1 MEDIUM OPTIMISATION FOR PIMARICIN PRODUCTION STUDIES

As outlined in the literature survey, despite its commercial significance, complete characterisation of *S. natalensis* during submerged cultivation has not been reported in the open literature. The series of medium/cultivation optimisation studies described in this chapter build directly on previous, related work undertaken by O' Shea (1998). The purpose of the current studies was to contribute, in a meaningful way, to the body of available knowledge about *S. natalensis*. A total of four studies were performed. 250 mL shake flasks each containing 50 mL of inoculum medium were inoculated with 1 mL of TBO plate suspension and incubated at 30°C for various periods of time. These flasks were subsequently used to inoculate 250 mL flasks each containing 100 mL of fermentation medium. This flask:broth volume ratio was chosen as a result of a series of volume studies previously performed by O'Shea (1998). Table 5.1 summarizes the experimental conditions employed in each of the four studies.

	Inoculum Medium	**Inoculum Age (h)**	**Inoculum Size** $\left(\frac{\text{inoculum volume}}{\text{total volume}}\right)*100$	**Fermentation Medium**
Study One	YED	12/18/24	10 %	SPG
Study Two	SPG	12/18/24	10 %	P-limited
Study Three	YED	50	0.5 g/L	P-limited
Study Four	YED	50	10 %	P-limited
	SPG	24	0.5 g/L	

Table 5.1 Summary of experimental conditions employed in Studies One-Four.

5.2 STUDY ONE

The primary aim of this first study was to investigate the potential of YED and SPG media for use during inoculum development and fermentation, respectively. A second objective was to determine the effect of inoculum age on culture performance using these media. In all cases, system response was evaluated in terms of biomass (dry weight) and pimaricin production and substrate (glucose) uptake. In Figure 5.2 and all subsequent figures, each data point represents the mean of duplicate samples taken from a single shake flask. Error bars have been omitted for clarity. However, a maximum standard error of 37.7 % was recorded.

1 mL TBO plate (Day 14) → 50 mL YED (200 rpm, 30°C, 12/18/24 h)

↓ 10 %

100 mL SPG medium (250 rpm, 30°C, 10 days)

Figure 5.1 Schematic representation of Study One

As illustrated in Figure 5.1, the organism was initially cultivated in YED medium using TBO plates which had been prepared as described in section 3.4.1.1.

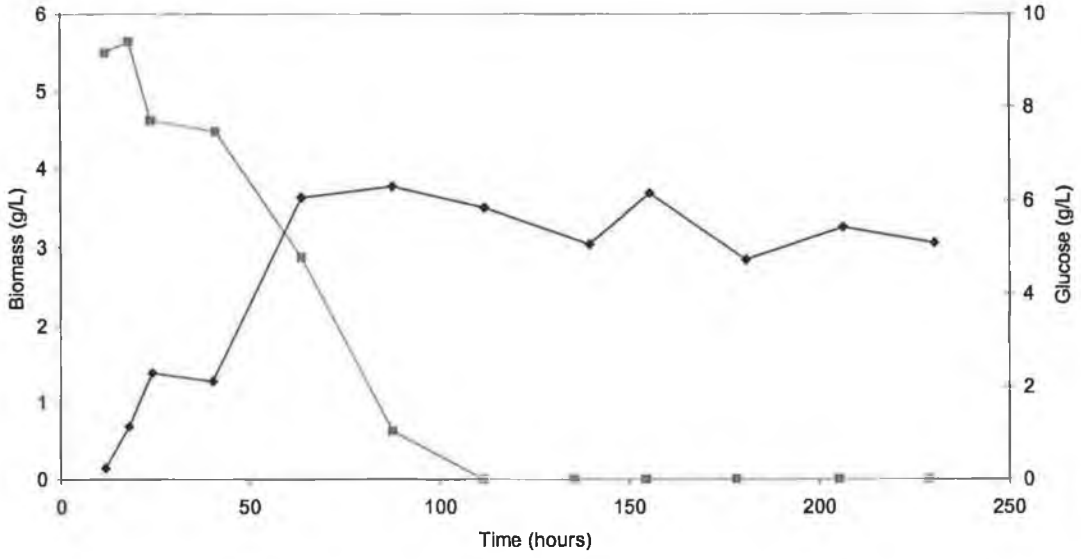

Figure 5.2 Biomass and glucose profile for *S. natalensis* grown in YED inoculum medium (◆ biomass; ■ glucose)

After approximately 88 hours cultivation in the YED medium, a maximum biomass level of 3.77 g/L is recorded. After this time, growth in the medium ceases, corresponding to glucose depletion in the medium. Media studies performed by O'Shea (1998) have shown that media containing yeast extract (namely, YEPD) have optimally supported the growth of *S. natalensis* with maximum biomass levels of up to 4.47 g/L reported after 140 hours. At this time, glucose levels in the medium were completely utilised by the organism. The results of the current investigation (Figure 5.2), although using a different yeast extract-based medium, support the earlier discovery of O'Shea. The positive effect of yeast extract on cell growth has recently been reconfirmed by Farid *et al.* (2000) who performed a series of experiments were performed to test the effect of various nitrogen sources (ammonium sulphate, ammonium chloride, sodium nitrate, urea and beef and yeast extract) on growth and antibiotic production levels of *S. natalensis*.

A 10 % 12, 18 and 24 hour YED inoculum was then used to inoculate flasks containing SPG, a phosphate-limited fermentation medium. Martin and Mc Daniel (1975) previously reported high biomass (~9g/L) and antibiotic production levels when *Streptomyces griseus* IMRU 3570 was grown in a phosphate limited medium using YED as the inoculum medium. Production of candicidin reached maximum levels of 1400 μg/mL when the organism was grown in SPG medium.

Figure 5.3 shows a) biomass, b) glucose and c) pimaricin profiles for study one. It is evident from the data presented that the age of the inoculum employed does not have a significant effect on the overall biomass or pimaricin yields or the glucose utilisation profile. While the biomass concentration in the 12, 18 and 24 hour inocula (at 0.0139, 0.0677 and 0.1389 g/L, respectively) varied significantly, the growth curves and maximum biomass levels (~ 5 g/L) produced in the SPG medium were almost identical for each of the three inoculum ages. El-Enhasey *et al.* (2000) also performed a series of similar experiments involving the cultivation of *S. natalensis* using 24, 48, 72 and 96 hour vegetative inocula. Data taken after 96 hours cultivation also confirmed that the biomass level recorded was almost identical, irrespective of inoculum age. Total nutrient utilisation occurs at approximately 250 hours. Pimaricin production begins, in all cases,

after approximately 53 hours cultivation but levels do not increase significantly until ~200 hours with levels of pimaricin as high as ~0.07 g/L recorded. It is difficult to say whether levels produced by the organism would have continued to increase and allowing the fermentation to proceed further may have proven informative in this regard. What is clear, however, is the fact that a medium limiting in phosphate, such as SPG, supports the production of pimaricin by *S.natalensis*, confirming the only other published discoveries of this by Aparicio *et al.* (1999) and Farid *et al.* (2000).

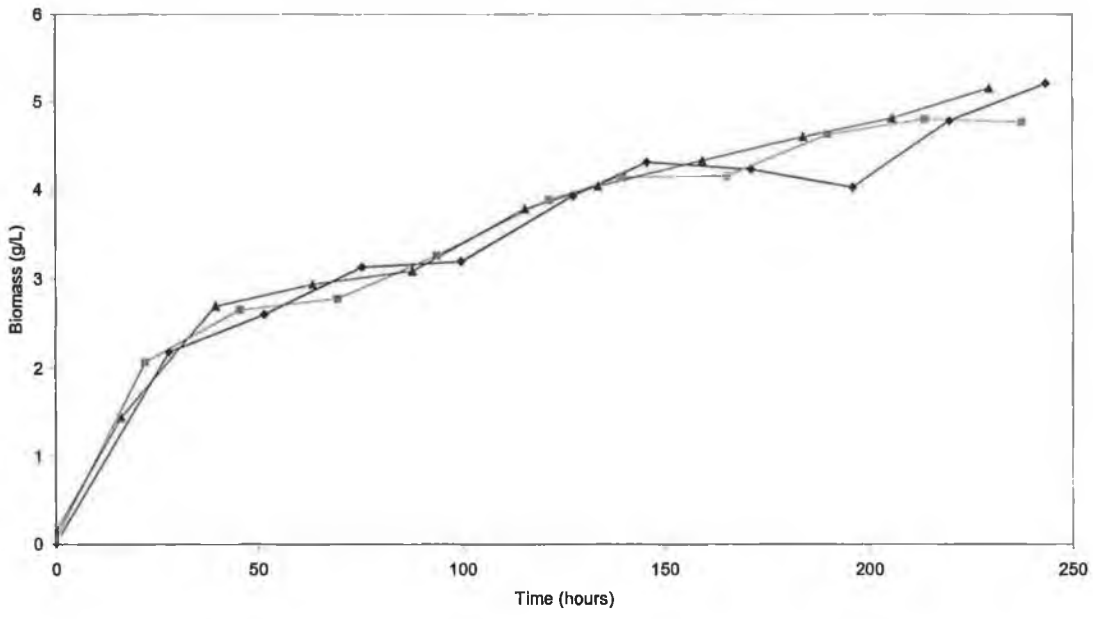

a)

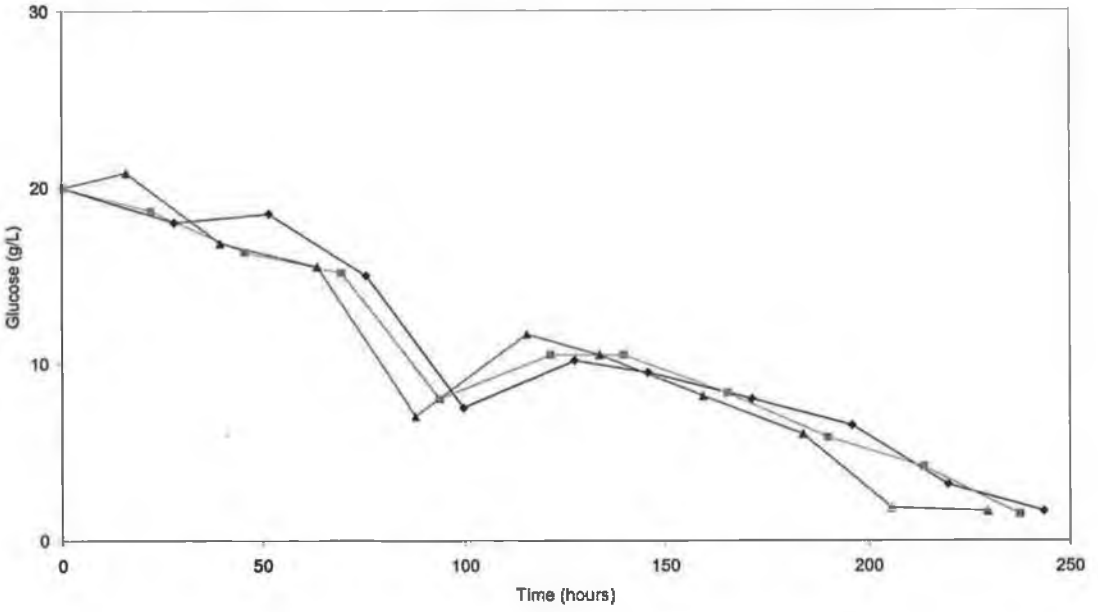

b)

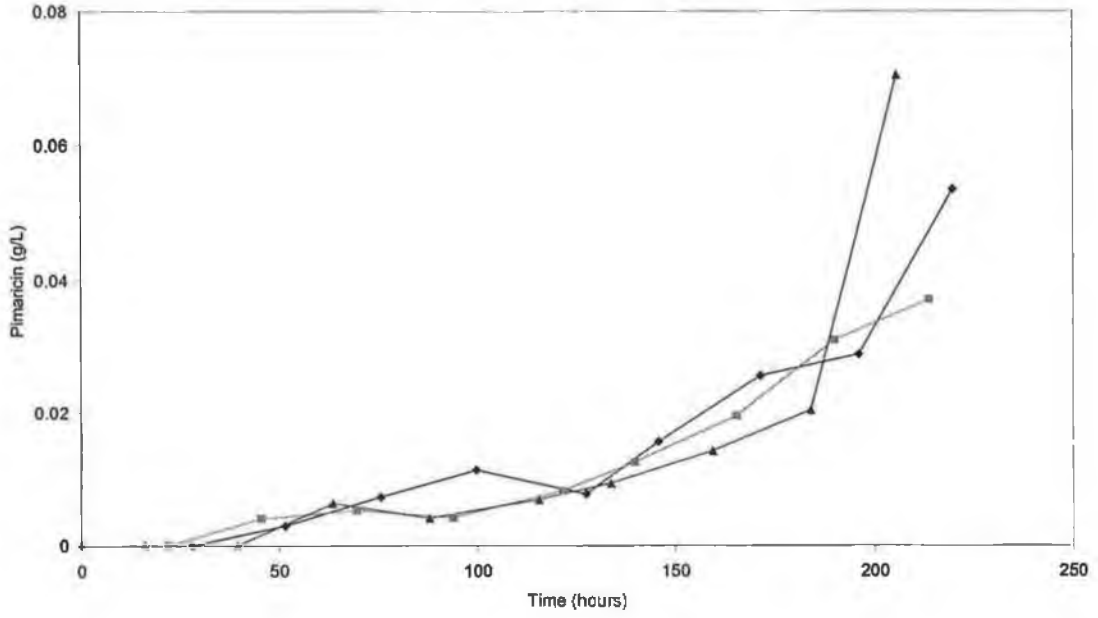

c)

Figure 5.3 a) Biomass b) Glucose and c) Pimaricin profiles for *S. natalensis* grown in SPG medium. ◆ 12 hour; ■ 18 hour; ▲ 24 hour inoculum)

Inoculum Age (hours)	Max. R_{vb} (g/L.h)	Max. $Y_{x/s}$ (g/g glucose)
12	0.077	1.726
18	0.093	1.501
24	0.088	0.807

Table 5.2 Growth characteristics of *S. natalensis* for Study One

It can be seen from Table 5.2 that the inoculum age also has no significant effect on the maximum specific biomass production rates, (R_{vb}), which occurred during the first 40 hours of each fermentation. The maximum biomass yields (per gram of glucose utilised), $Y_{x/s}$ also occur at this time, decreasing to values of approximately 0.025 g/g glucose after ~ 100 hours, which was maintained for the remainder of the fermentation in all cases. However, while both the 12 and 18 hour inocula show similar maximum biomass yields, there is a significant difference (~ 50 %) between these and the 24 hour inoculum. Differences in biomass levels, as previously mentioned, were not significant despite this apparent difference in $Y_{x/s}$ and it is therefore suggested that an alternative nutrient was utilised by the 24 hour inoculum for biomass production. This reduced usage of glucose for biomass production supports that theory that it is being used elsewhere by the organism, namely for secondary metabolite production. Indeed, after ~ 100 hours, specific pimaricin yields per gram of biomass present, $Y_{p/x}$, are higher for the 24 hour inoculum (Figure 5.4). This is also confirmed by the slightly higher specific antibiotic yields per gram of glucose utilised, $Y_{p/s}$, for this inoculum, (Figure 5.5).

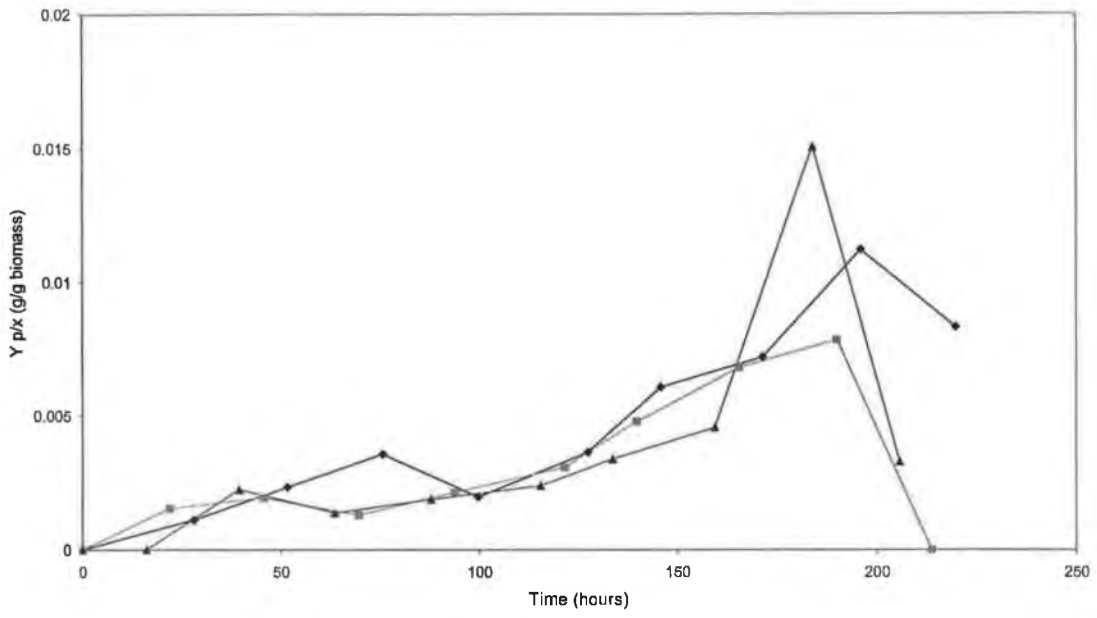

Figure 5.4 Pimaricin yield per gram of biomass present , ($Y_{p/x}$), in Study One.
(◆ 12 hour; ■ 18 hour; ▲ 24 hour inoculum)

In calculating values for the yield coefficients ($Y_{X/S}$, $Y_{P/S}$, $Y_{P/X}$), here and throughout the remainder of this chapter, it is necessary to take account of uncertainties in the primary data. For this analysis, on the basis of experimental observations of reproducibility, the uncertainties are estimated as follows: biomass – 0.5 g/L; glucose - 0.5 g/L; pimaricin - 0.005 g/L. At time *t*, the yield coefficient for biomass on glucose, $Y_{X/S}$, is calculated as follows:

$$Y_{X/S} = \frac{X_t - X_0}{S_0 - S_t} \tag{5.1}$$

where the subscript, 0, refers to the initial conditions. Equivalent expressions are employed for $Y_{P/S}$ and $Y_{P/X}$.

The fractional uncertainty in $Y_{X/S}$ is calculated as follows:

$$\frac{\omega_{Y_{X/S}}}{Y_{X/S}} = \left[\left(\frac{2\omega_X}{X_t - X_0} \right)^2 + \left(\frac{2\omega_S}{S_0 - S_t} \right)^2 \right]^{1/2} \tag{5.2}$$

where ω is to the uncertainty in any variable. The fractional uncertainties in $Y_{P/S}$ and $Y_{P/X}$ are calculated in a similar fashion. Representative calculations are performed using the biomass, glucose and pimaricin data for 18 hour inocula in Study One (presented in Tables A.2-A.4). At 213.75 hours, the fractional uncertainties are calculated as: $Y_{X/S}$ – 0.22; $Y_{P/S}$ – 0.28; $Y_{P/X}$ - 0.344. While uncertainties of between 22% and 34% are certainly significant, it is important to note that, in all cases, these values are likely to be overestimates. In the case of defined media, which have a specified initial glucose concentration, a value of 0.5 g/L overestimates the uncertainty in S_0. In the case of inoculum (t = 0 h) which has been produced under conditions which do not support pimaricin production, pimaricin concentrations are below detectable levels and are recorded as 0 g/L. Here, too, a value of 0.005 g/L overestimates the uncertainty. At earlier stages during the growth cycle, when pimaricin and biomass levels are lower and glucose concentrations higher, higher levels of uncertainty may be expected.

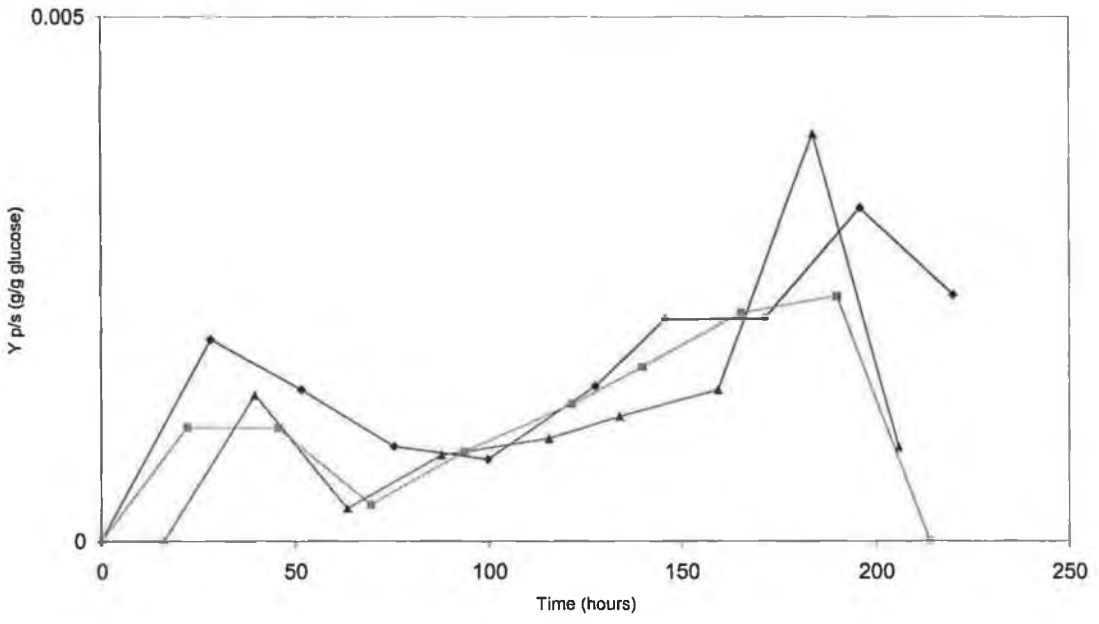

Figure 5.5 Pimaricin yield per gram of glucose utilised, $Y_{p/s}$, in Study One.
(◆ 12 hour; ■ 18 hour; ▲ 24 hour inoculum)

5.3 STUDY TWO

In an effort to improve antibiotic production and biomass levels both in the inoculum and in the fermentation medium, the organism was cultivated under phosphate limitation using alternative inoculum development and fermentation media. In this second study, SPG medium (which had resulted in maximum biomass levels of ~5 g/L in Study One, Figure 5.3 a) was used as the inoculum medium, with a more defined phosphate-limited medium as the alternative fermentation medium (Figure 5.6). The components of this latter medium are listed in Table 3.3. As before, the organism was initially cultivated in SPG medium using the TBO plates. The effect of the inoculum age on the culture performance was also investigated by using a 10 % inoculum (of 12, 18 or 24 hours) to inoculate flasks containing the defined phosphate-limited fermentation medium.

1 mL TBO plate (Day 14) → 50 mL SPG (200 rpm, 30°C, 12/18/24 h)

↓ 10 %

100 mL P-limited medium (250 rpm, 30°C, 10 days)

Figure 5.6 Schematic representation of Study Two

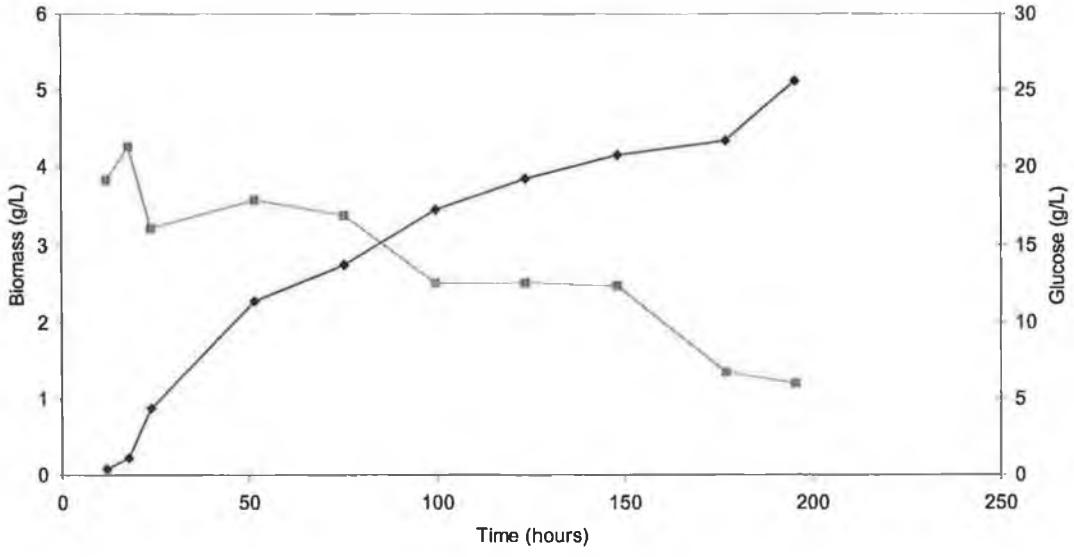

Figure 5.7 Biomass and glucose profile for *S. natalensis* grown in SPG inoculum medium (◆ biomass; ■ glucose)

Figure 5.7 shows the biomass and glucose profiles when the organism is grown in SPG medium. Data are only available for the first 200 hours of the cultivation. At this stage, it is unclear if the organism has reached the stationary phase of the growth cycle, as the biomass levels appear to be still increasing. The fact that approximately 6 g/L glucose remains unused by the organism also supports the suggestion that the organism has not finished growing. However, no data for other, potentially limiting nutrients are available.

Figure 5.8 shows (a) biomass and (b) glucose profiles for this second study. Here again, it is evident from the data presented that the age of the inoculum employed again does not have a significant effect on the overall biomass yield or glucose utilisation by the organism. Although, initial biomass concentrations in the 12, 18 and 24 hour inocula (at 0.0071, 0.021 and 0.088 g/L, respectively) varied, the growth curve and maximum biomass concentration of ~ 1.2 g/L produced in the phosphate-limited medium were almost identical for each of the three inocula. The organism, in each case, grows slowly, without achieving substantial biomass levels. It is again unclear if the organism has entered the stationary phase as biomass levels appear to be still increasing. Glucose utilisation profiles are similar for all three inocula. The substrate is consumed slowly over the course of the fermentation with levels as high as ~ 30 g/L still remaining unused at the end of the cultivation.

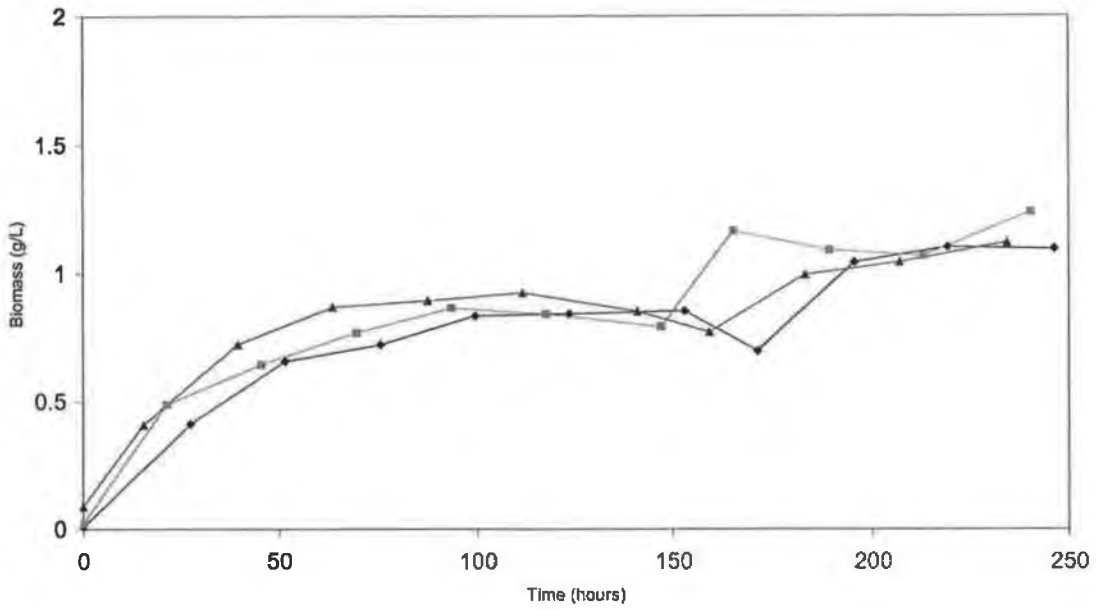

a)

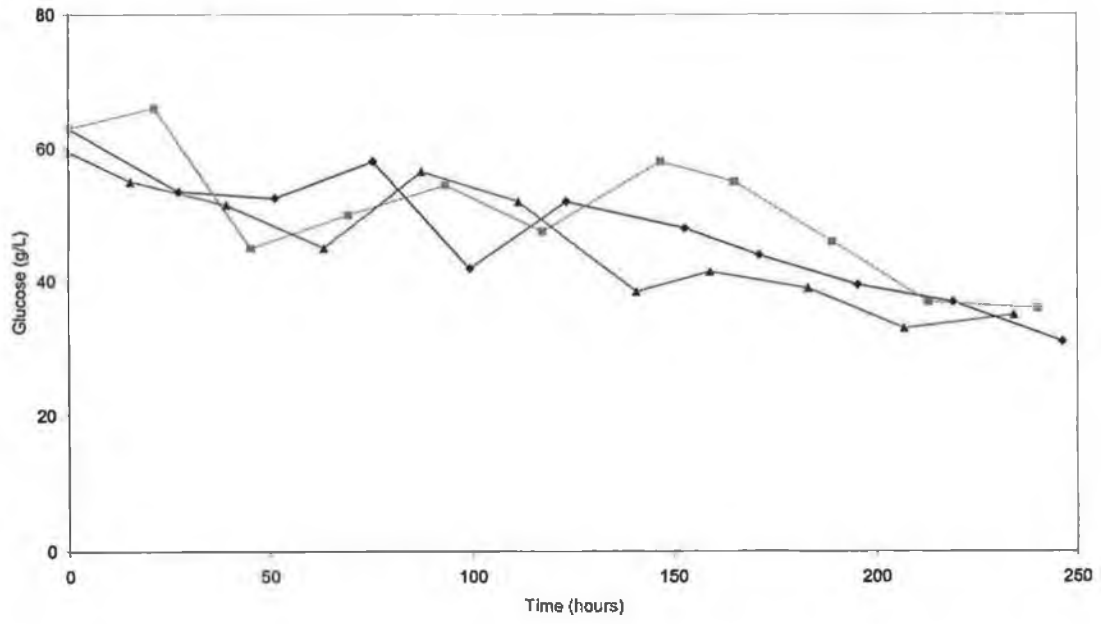

b)

Figure 5.8 (a) Biomass and (b) glucose profiles for *S. natalensis* grown in phosphate-limited medium.

(◆ 12 hour; ■ 18 hour; ▲ 24 hour inoculum)

As in Study One, for all three inocula, the maximum specific biomass production rates occur at the beginning of the fermentation. Production rates fall, thereafter, to reach a value of ~ 0.005 g/L.h (after ~ 100 hours of cultivation) which is maintained for the duration of the fermentation. (Table 5.3). Production rates and biomass yields per gram of glucose utilised are significantly lower than those observed in Study One, despite the fact that the initial glucose level is three times higher than in the SPG medium.

Inoculum Age (hours)	**Max. R_{vb} (g/L.h)**	**Max. $Y_{x/s}$ (g/g glucose)**
12	0.0149	0.1426
18	0.0226	0.1540
24	0.0262	0.2683

Table 5.3 Growth characteristics of *S. natalensis* for Study Two

The results from this study are in striking contrast to those observed in Study One. Given that initial biomass levels in all three inocula are significantly reduced in Study Two, one might expect this to be reflected in the fermentation medium in terms of reduced biomass levels. As can be clearly seen from the data in Figure 5.8 (a), maximum biomass levels did not exceed ~ 1.2 g/L. It is evident that the defined phosphate-limited medium does not support the growth of this organism. While this is a common characteristic of a medium designed for optimising secondary metabolite production and the medium has been reported to enhance antibiotic production levels, specifically, candicidin by *S.griseus* (Martin and Mc Daniel, 1976) it was anticipated that it would be beneficial for pimaricin production. However, analysis of broth samples from these trials indicated that no pimaricin had been produced. It was concluded that inoculum levels and subsequently biomass levels in the fermentation medium, were too low to allow any appreciable amounts of pimaricin to be detected by the bioassay method used to determine antibiotic production in these studies (section 3.5.4). An alternative theory to explain the reduced biomass levels and the apparent lack of pimaricin production was the presence of a 'glucose effect' due to the substantially higher levels of this nutrient in this medium.

5.4 STUDY THREE

Building from Studies One and Two, the aim of Study Three (Figure 5.9) was to investigate the use of an inoculum medium, more ideally suited to improved growth of this organism, with a view to enhancing biomass levels and hence overall antibiotic levels. YED medium was chosen as the inoculum medium, based on results from Study One, and the defined phosphate-limited medium was used as the fermentation medium. In a study of *S. griseus*, Martin and Mc Daniel (1976) identified an optimum inoculum biomass level of 5 g/L and a similar approach was adopted here. A 5 g/L inoculum (yielding an initial biomass level of 0.5 g/L in the fermentation shake flasks), produced by cultivating the organism for 50 hours in YED medium, was used instead of the 10 % (v/v) inoculum employed in all previous trials. The cultivation time of 50 hours (as opposed to 24 hours) was used in order to produce the necessary biomass. The results of the fermentation are presented in Figure 5.10.

1 mL TBO plate (Day 14) → 50 mL YED (200 rpm, 30°C, 50 h)
↓ ~ 5g/L
100 mL P-limited medium (250 rpm, 30°C, 10 days)

Figure 5.9 Schematic representation of Study Three

It is evident from the data presented in Figure 5.10 that biomass levels have indeed been enhanced significantly, reaching a maximum value of ~ 5g/L in the phosphate-limited medium. Growth is, again, quite slow (mean R_{vb} value of 0.036 g/L.h) with total utilisation of the glucose occuring by the end of the fermentation. At the beginning of the fermentation, a maximum biomass yield per gram of glucose of 0.345 g/g was recorded, decreasing to a steady value of 0.12 g/g glucose after 100 hours. At this stage, residual glucose was utilised for antibiotic production (max. $Y_{p/s}$ = 0.00159 g/g glucose).

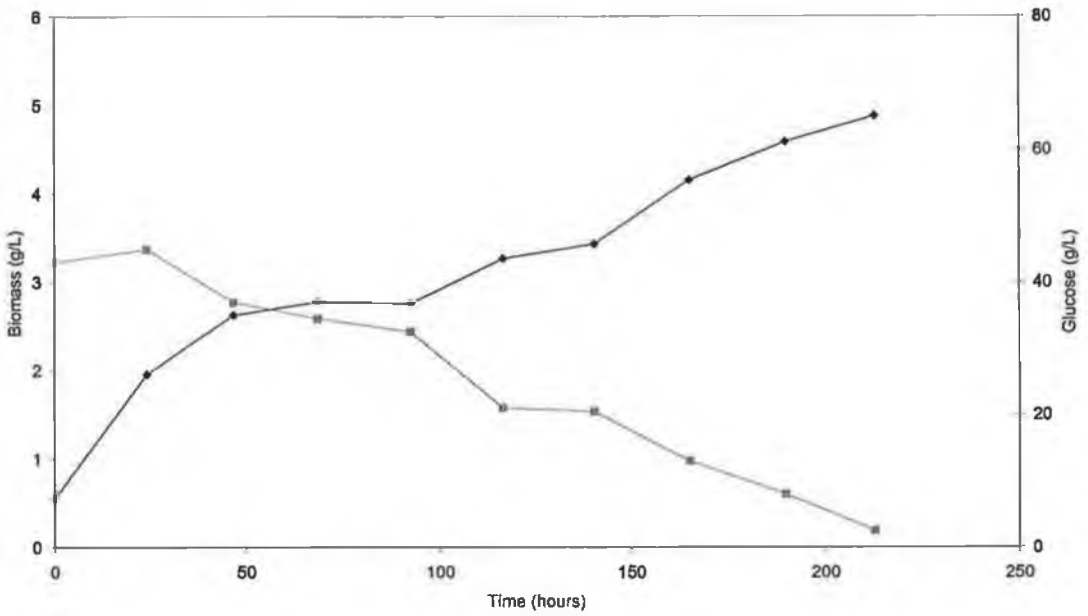

Figure 5.10 Biomass and glucose profile for *S. natalensis* grown in phosphate-limited medium (◆ biomass; ■ glucose)

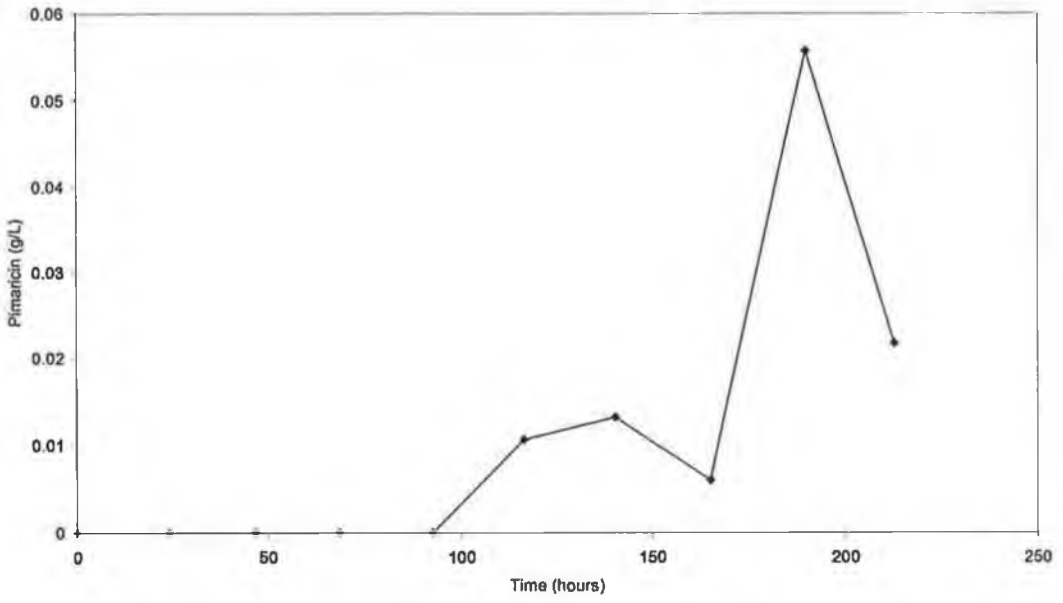

Figure 5.11 Pimaricin production profile for *S. natalensis* grown in phosphate-limited medium (◆ pimaricin)

Figure 5.11 shows that pimaricin production in the phosphate-limited medium begins after ~100 hours and continues to increase throughout the cultivation. A maximum level

of ~ 0.06 g/L is recorded. Similar maximum yields (0.0138 g/g biomass) to those observed in Study One were also observed in this study. The sudden decrease in pimaricin levels recorded after 200 hours is attributed to sample variability (with the recorded mean being affected by the absence of pimaricin in one of the trials). It is evident that the increased biomass concentrations in this medium allowed pimaricin production to be detected. Also that it was the inoculum used in this study which contributed to the subsequent increase in biomass and eventual production and detection of the antibiotic.

5.5 STUDY FOUR

Study Four (Figure 5.12) was essentially, a slight variation of the Martin and Mc Daniel (1976) method, employed here in Study Three. In this case, an intermediate step, involving cultivation in SPG medium, was employed between initial inoculum development in YED and subsequent cultivation for pimaricin production in phosphate limited medium. The SPG medium was inoculated with a 10 % inoculum from a 24 hour YED flask. The biomass produced in the SPG flask was then used to inoculate the phosphate-limited flasks, at an initial biomass concentration of 0.5 g/L. The results from the P-limited fermentation are presented in Figure 5.13.

1 mL TBO plate (Day 14) → 50 mL YED (200 rpm, 30°C, 24 h)
↓ 10 %
100 mL SPG (250 rpm, 30°C, 50 h)
↓ ~ 5g/L
100 mL P-limited medium (250 rpm, 30°C, 10 days)

Figure 5.12 Schematic representation of Study Four

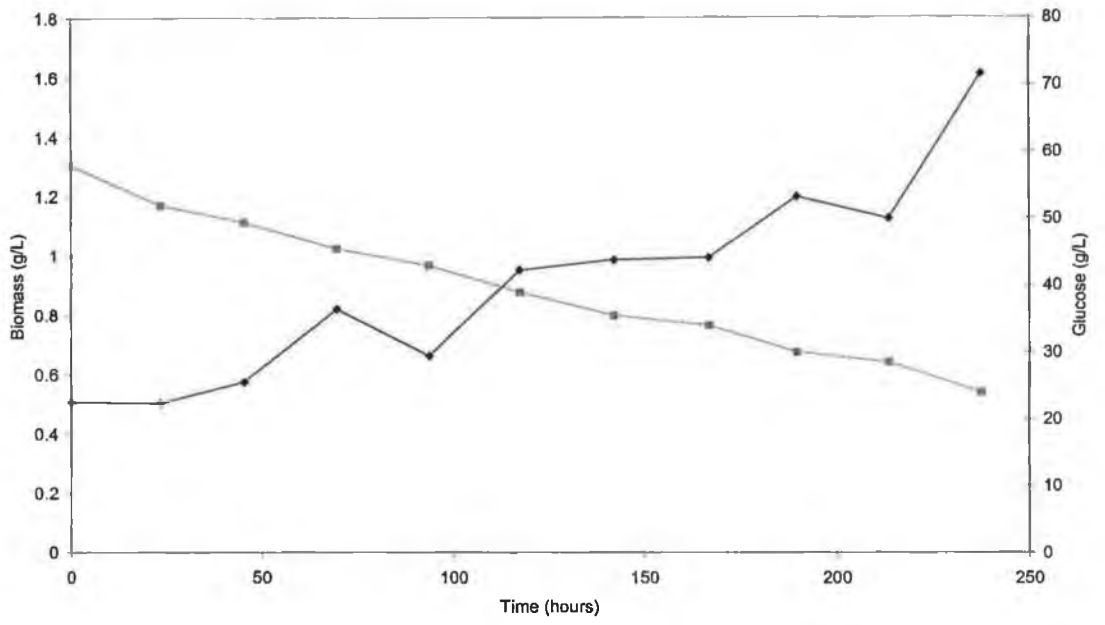

Figure 5.13 Biomass and glucose profile for *S. natalensis* grown in phosphate-limited medium (◆biomass; ■ glucose)

Despite the substantial level of biomass (~5 g/L)in the initial SPG inoculum, biomass levels in the phosphate-limited medium failed to reach levels higher than 1.62 g/L after approximately 250 hours of cultivation. Growth and utilisation of glucose in the latter medium was slow, with about 23 g/L glucose remaining unused at the end of sampling from this fermentation. It is unclear, from the limited data collected from this trial whether the organism had indeed entered the stationary phase of its growth cycle. The maintenance of the biomass production rate at a value of ~0.006 g/L.h from 100 hours cultivation onwards and the production of 0.01 g/L pimaricin detected in a single flask at 93.5 hours in this fermentation suggest that it had. Given that pimaricin was detected in only one flask and at such a low concentration, it is difficult to draw any conclusions from this study. However, while the introduction of an intermediate inoculum in the form of ~ 5 g/L SPG certainly proved beneficial for the production of candicidin by *S. griseus*, no enhancement of pimaricin production by *S. natalensis* was observed.

5.6 CONCLUSION

On the basis of the four studies described here, YED medium was identified as the preferred medium for inoculum cultivation, supporting high levels of biomass formation. In Studies One and Three, where this medium was used exclusively for inoculum production, biomass levels reached approximately 5g/L. Farid *et al.* (2000) have reported on the effect of varying the yeast extract concentration in their base medium on both growth and antibiotic production levels by *S. natalensis*. Increasing the concentration from 0-2 g/L resulted in a three-fold increase in pimaricin levels. Further, increasing the concentration led to a gradual decrease in levels. However, interestingly, increasing the concentration of yeast extract to values greater than 6 g/L (as in the YED medium employed in these studies) resulted in a marked increase in biomass levels (> 6 g/L). Similar biomass levels have been reported here. Although both types of phosphate-limited medium (SPG and defined phosphate-limited medium) supported pimaricin production, the levels recorded were very low and compared poorly with levels reported by other workers for this organism (Aparicio *et al.*, 1999).

CHAPTER SIX

RESULTS AND DISCUSSION – IMAGE ANALYSIS STUDIES

6.1 VALIDATION OF THE IMAGE ANALYSIS ALGORITHM

Biochemical engineers have a keen interest in quantifying the morphology of filamentous organisms in suspension culture, as this information is essential for the improvement of their understanding of the characteristics of both the fermentation organism and the fermentation broth. In general, the biomass must be considered as heterogeneous, consisting of different morphological groups whose relative proportions are continuously changing throughout the course of a fermentation. These morphological alterations may be variously attributed to mycelial breakage or changes in branching rates, caused by hydrodynamic shear or to changing environmental conditions (also influenced by hydrodynamic shear) which result in changes in cell physiology and, hence, in morphology. Development of a quantification system can permit visualisation of the morphological state of the culture. Development of such a system requires classification of the organism into various morphological groups, describing the broad range of morphologies exhibited by the organism.

In this research, *S. natalensis* was classified into the three different morphological groups: pellets, clumps and hyphae. The criteria for each of these groups are described in section 4.3. Figure 6.1 shows an example of 'typical' pellets, 'hairy' pellets and clumps and scattered hyphae. An image analysis algorithm was developed on this basis (Appendix 1). Three important validation steps were required before the algorithm could be used for sample analysis. These included determination of the correct a) the appropriate level of dilution of the broth sample, (b) the appropriate level of microscopic magnification and (c) the numbers of entities required for a statistically meaningful analysis of the organism sample.

a)

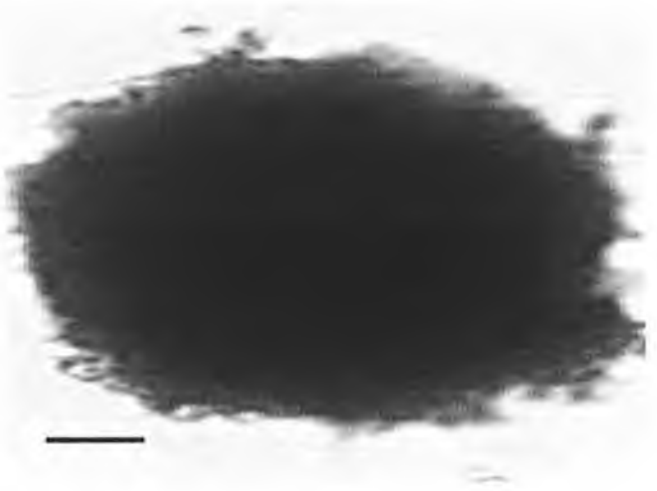

b)

c)

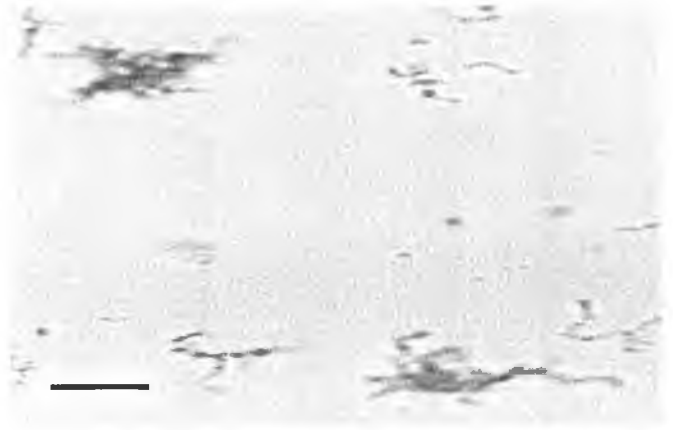

Figure 6.1. Example of *S. natalensis* morphology, a) typical pellets, b), hairy pellets and c) filamentous clumps and scattered hyphae. 100x, Bar = 50 μm.

6.1.1 VALIDATION OF SAMPLE DILUTION

In order to characterise the morphological state of an organism, good slide preparation of the sample is essential, in order to produce a high quality image for subsequent analysis. One of the factors important in this regard is the dilution of the sample. Treskatis *et al.* (1997) suggested that, for image analysis, the dilution factor should be chosen to ensure that, when viewed under the relevant magnification, approximately 10-15 % of field of view is occupied by the entities of interest. This level of slide coverage results in images in which the spatial arrangement of entities facilitates more detailed analysis and, hence, more accurate morphological representations of the forms present. To determine the required dilution factor a standard curve (Figure 6.2) was constructed, by cultivating *S. natalensis* in YEME medium and diluting the samples such that, when viewed under the microscope, approximately 10-15 % of the region of interest was occupied by entities. The dry weight of the samples was determined as described in Section 3.5.1. This standard curve was subsequently used to determine the necessary dilution factor in the analysis of all samples.

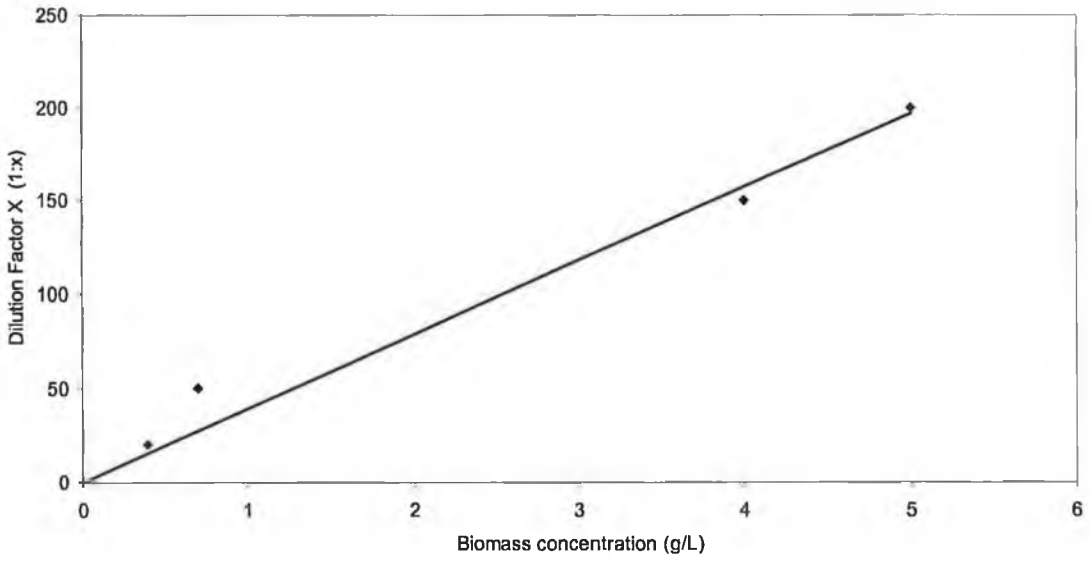

Figure 6.2 Standard curve for determination of dilution factor depending on sample biomass level (r^2 =0.9805).

6.1.2 DETERMINATION OF THE APPROPRIATE LEVEL OF MAGNIFICATION

Choice of an appropriate level of magnification for sample observation depends on a compromise between speed and accuracy. At lower levels of magnification, larger numbers of entities can be processed within a specified time period. However, the risk of false classification is higher, due to the lower level of resolution. Preliminary manual trials suggested that use of a x10 or x4 objective would be most appropriate for these samples. As the microscope head incorporates a second x10 objective, use of the x4 and x10 objectives corresponds to actual magnification factors of x40 and x100, respectively.

A sample from Study One of the media studies (organism grown in SPG medium, using a 24 hour YED inoculum) was viewed under both x10 and x4 magnification for image analysis purposes, in order to determine the better magnification factor. The algorithm was used to measure a total of 300 entities from the same slide and the results were exported to Microsoft Excel for statistical analysis.

Included in the exported parameters were average pellet, clump and hyphal areas (μm^2) and average hyphal length (μm). Individual equivalent diameters were calculated for all entities using the formula, $d=(4A/\pi)^{1/2}$, where A is the measured area of an entity. As the hyphal contribution to the data was considered negligible (section 6.1.3) only the pellet and clump data were statistically analysed. The frequency distribution of the data, on a number basis, was produced by sorting the data into a number of 'bins', (Figure 6.3). The minimum bin size was selected on the basis of the minimum measured entity size in each sample. Subsequent bins corresponded to a geometric progression from the initial value, using a factor of $2^{1/3}$, as is common in size analysis.

It is clear that, at both magnification levels, one distinct group of entities is present, represented by the single peak in each of the distributions. The peaks represent entities having equivalent diameters less than or equal to 14 μm and 18 μm, and constituting proportions of 0.25 and 0.28, when viewed under x4 and x10 magnification, respectively.

Further classification of the entities into distinct morphological forms is not possible using the data in this form. However, it can be suggested that, as the majority of the entities have equivalent diameters of 20 μm or less, a significant proportion of these entities are likely to be clumps and/or 'smaller' pellets.

It is evident from the results that there are distinct differences in the data collected depending on the level of magnification employed. Specifically, the distribution is shifted towards the left, *i.e.* towards smaller entities, when viewed under the lower level of magnification. At x10 magnification, larger entities, *i.e.* those with an equivalent diameter in excess of 45 μm, constitute 0.025 of the distribution; at x4 magnification, the corresponding fraction is 0.049. The relative number of smaller entities (<10 μm) detected at x10 magnification (0.01) is substantially smaller than at x4 magnification (0.196). These effects are also illustrated in the cumulative distributions of the data (Figure 6.4). Careful visual observation of the images during analysis revealed the cause of the shift of the distributions. At the lower magnification level, the lower level of resolution resulted in acceptance, as hyphae or clumps, of a large number of entities which when viewed at x10 magnification were correctly rejected as non-cellular matter or cellular debris. This classification was visually confirmed by inspection of the entities at x20 magnification.

As previously mentioned, in any given sample, a diverse range of morphologies may be present at any one time. These morphologies, are continuously changing during normal cultivation involving a vegetative inoculum. In addition to entity enlargement through hyphal extension, individual clumps may become entangled following collisions; larger entities may be disrupted, leading to smaller clumps and/or mycelial fragments. Hence their morphological distributions also change. The contribution of the larger entities to the total biomass present becomes apparent when the data are represented on a volume basis rather than on a number basis. Indirectly, then a morphological quantification of the culture also reflects describes the *amount* of biomass present in the sample. The contribution of each entity to the sample volume was estimated using the cube of the

equivalent diameter. Frequency distribution of the volume-based data was constructed (Figure 6.5).

It is clear that although significant numbers of 'smaller' entities were detected under x4, these did not contribute to the analysis on a volume basis. This is also reflected in the results obtained under x10. Figure 6.6 shows the cumulative volume-based distribution of the data. Approximately, 1 % of the total volume was accounted for by these smaller entities. Entities, having equivalent diameters greater than 45 μm in size, which were under-represented at x4 magnification on both a number and volume basis, were found to make a considerable (20 %) contribution when viewed under x10. The peak in the x4 volume-based frequency distribution at an equivalent diameter of approximately 22.6 μm represents the sensitivity of this form of representation to small variations in the number of entities in these larger bins. This, and similar, observations formed the basis for the subsequent sample size studies (Section 6.1.3).

On the basis of the results obtained from this limited study, it was concluded that analysis of samples under a magnification of x10 rather than x4 allowed a more representative morphological characterisation of the sample to be obtained.

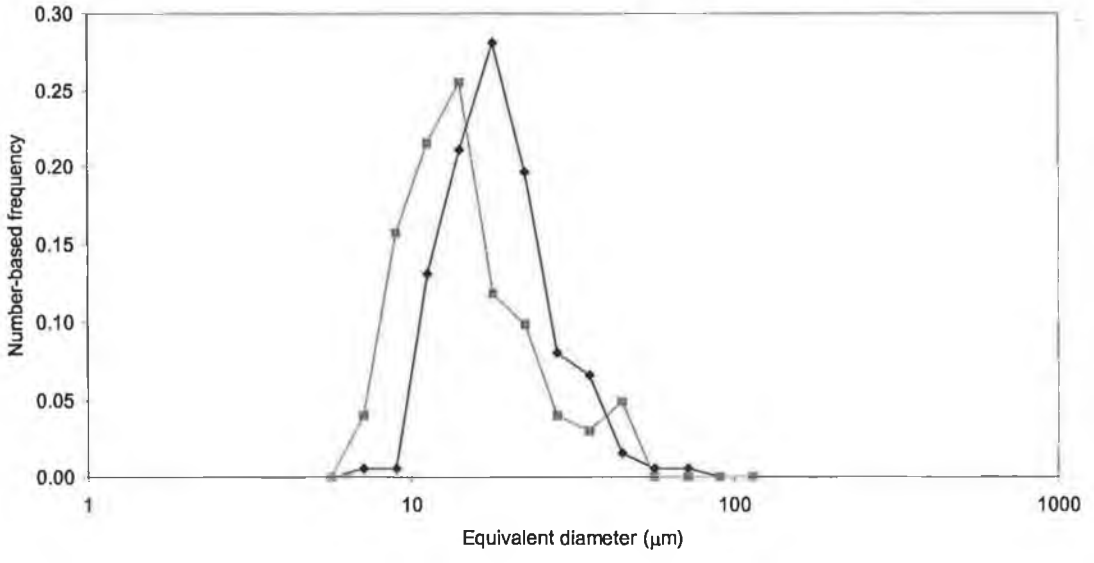

Figure 6.3 Development of a number-based frequency distribution for *S. natalensis* grown in YEME medium at x10 (◆) and x4 (■) magnification.

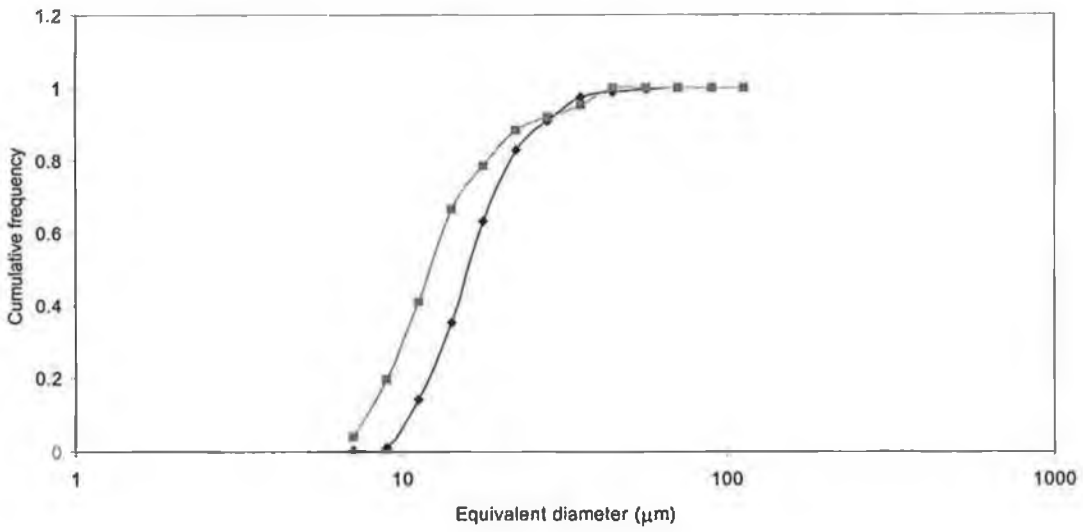

Figure 6.4 Development of a cumulative number-based frequency distribution for *S. natalensis* grown in YEME medium at x10 (◆) and x4 (■) magnification.

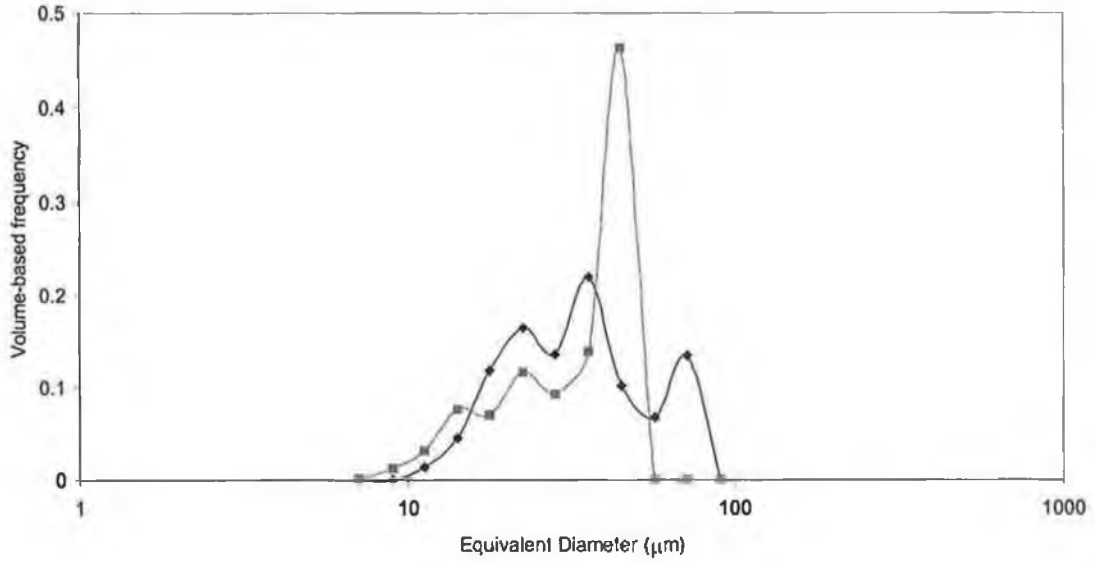

Figure 6.5 Development of a volume-based frequency distribution for *S. natalensis* grown in YEME medium at x10 (◆) and x4 (■) magnification.

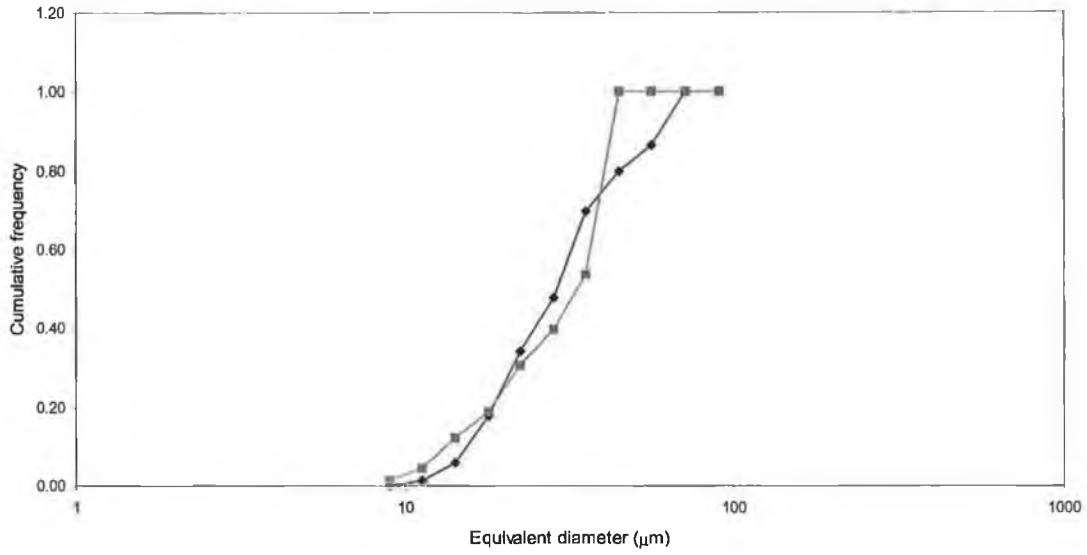

Figure 6.6 Development of a cumulative volume-based frequency distribution for *S. natalensis* grown in YEME medium at x10 (◆) and x4 (■) magnification

6.1.3 DETERMINATION OF AN APPROPRIATE SAMPLE SIZE FOR IMAGE ANALYSIS

A review of the literature relating to morphological characterisation of filamentous organisms reveals that the sample size for image analysis studies is based largely on associated time constraints, rather than statistical criteria. The number of entities measured is reported to vary from 50 (Mc Intyre *et al.*, 1998) to 1000 (Packer and Thomas, 1990). Processing time is a function of both the computing power of the image analyser and the morphological complexity and diversity of the sample. If image analysis is to be used as a tool for real-time process analysis and control then processing time must be short, relative to the doubling time of the organism and, ideally, of the order of minutes rather than hours. Processing times reported in the literature are of the order of 60-120 minutes for samples of approximately 200 entities. However, there is a paucity of studies in which the sample size is predetermined. The purpose of the work described here is to tackle this issue, with reference to *S. natalensis*.

In order to determine the minimum number of entities from a single sample that should be analysed to obtain a statistically valid morphological analysis of sample using the image analyser, a random sample from the YEME studies (Section 6.2) was chosen and prepared for analysis as outlined in Section 4.2.7. All appropriate manual interventions, such as magnification (x10) and lighting settings, required prior to analysis were also performed. The algorithm was used to measure a total of 1000 entities using slides prepared from a single fermentation broth and the data were exported to Microsoft Excel for subsequent statistical analysis. The data were then grouped into progressively larger sets of observations (increasing from 300 to 1000 in increments of 100) in order to investigate the sensitivity of the results to sample size.

Individual equivalent diameters from all three classification types (*i.e.* hyphae, clumps and pellets) were calculated, as before, using the formula, $d=(4A/\pi)^{1/2}$, where A is the measured area of an entity. A frequency distribution of the data, on a number basis, was produced (Figures 6.7 and 6.8).

Representing the data on linear scales, it is clear that two distinct groups of entities are present, highlighted by the two peaks in the distribution. The peaks represent 'smaller' entities, which have equivalent diameters less than or equal to 27 μm, and 'larger' entities, having equivalent diameters greater than 27 μm and less than 217 μm in size, respectively. Further classification of the entities into the three morphological forms is obviously not possible using the accumulated data in this form. However, analysis of the raw image analysis data (hyphae, clumps, pellets) indicates the hyphal entities constitute the vast majority of items with an equivalent diameter of 10 μm or less. The second peak (~60 μm) represents a combination of clumps and smaller pellets. The proportion of 'smaller' entities present in the sample is significantly higher than the proportion of largest entities *i.e.* those having equivalent diameters greater than 100 μm. These trends are illustrated in Figure 6.8, which shows the cumulative frequency distribution of the data. A significant proportion of the entities have equivalent diameters of less than 10 μm.

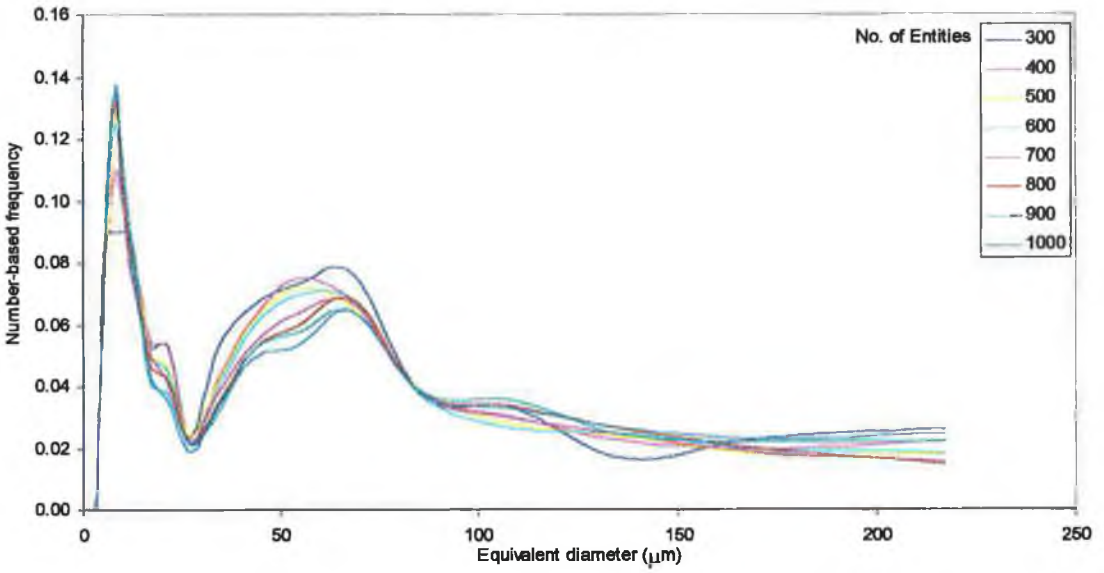

Figure 6.7 Development of a number-based frequency distribution for *S. natalensis* grown in YEME medium.

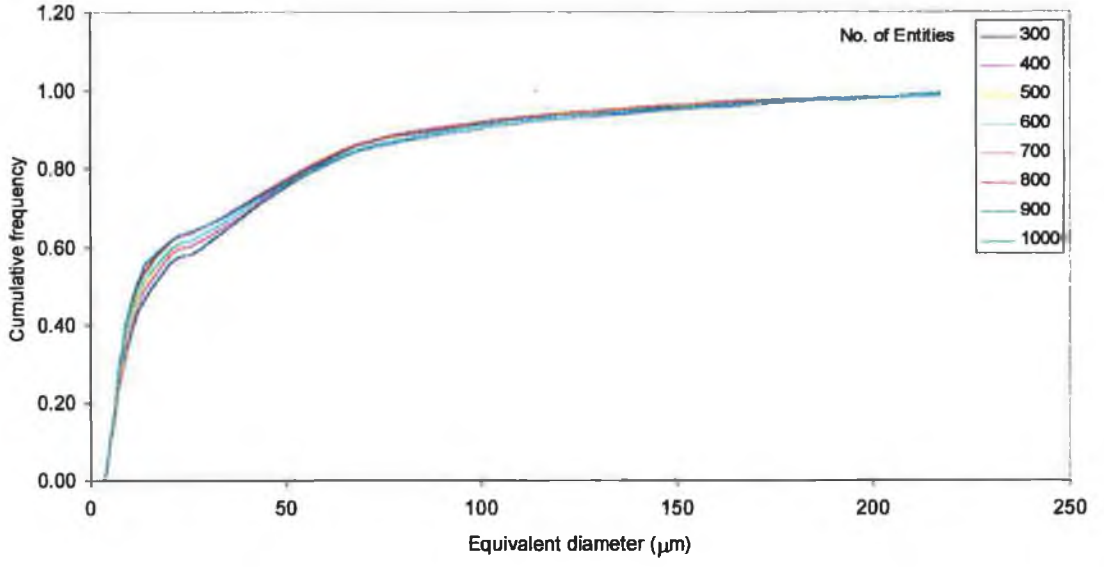

Figure 6.8 Development of a number-based cumulative frequency distribution for *S. natalensis* grown in YEME medium.

From a simple visual observation of Figures 6.7 and 6.8 it appears that, at least on a number basis, for samples of more than 600 entities, the morphological distributions are independent of sample size.

As previously outlined (Section 6.1.2), volume-based analysis of the data provides a more meaningful description of the morphological state of the organism than number-based analysis. Accordingly, this approach is, again, adopted here (Figures 6.9 and 6.10).

For all sample sizes investigated the 'smaller' entities contributed significantly to the frequency distribution on a number basis. However, it is clearly evident that their contribution on a volume basis is negligible. For a sample size of 600, entities with an equivalent diameter of greater than 108 μm account for approximately 7 % of the items analysed. On a volume-basis, these entities account for approximately 78 % of the total sample volume. Comparison between Figures 6.7 and 6.9 and Figures 6.8 and 6.10 reveals the higher dependency of the volume-based distributions on sample size than of the number-based distributions. However, in all cases, the trends are consistent with distributions converging as the sample sizes increase. For sample sizes greater than 600 the deviation between successive distributions is considered to be so small the associated increase in accuracy does not justify the extended processing time. Accordingly, for all subsequent work a minimum of 600 entities viewed under a x10 objective was proposed. Typically this required a total processing time of 300 minutes including image acquisition and analysis.

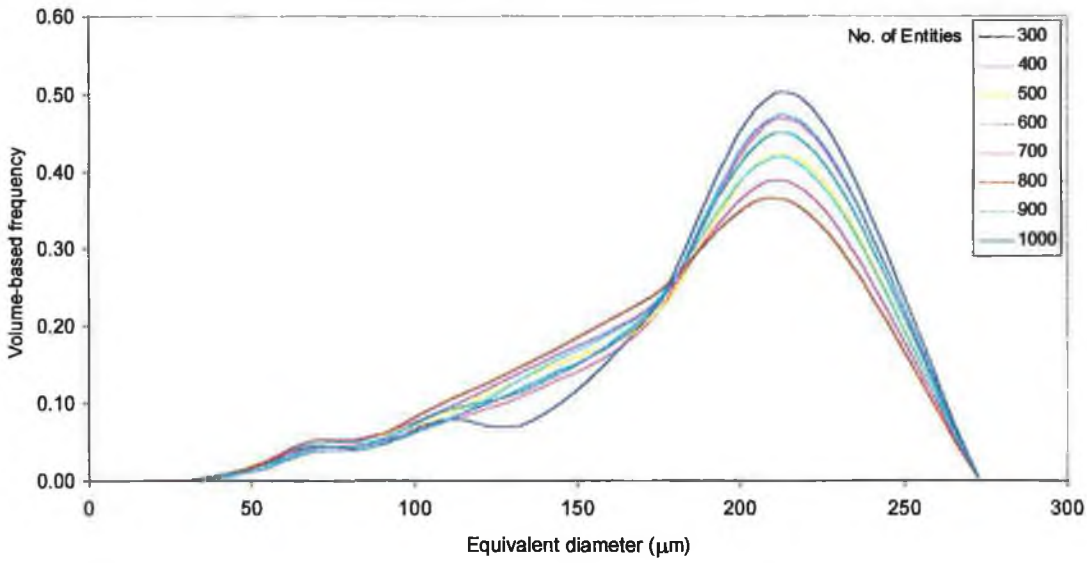

Figure 6.9 Development of a volume-based frequency distribution for *S. natalensis* grown in YEME medium.

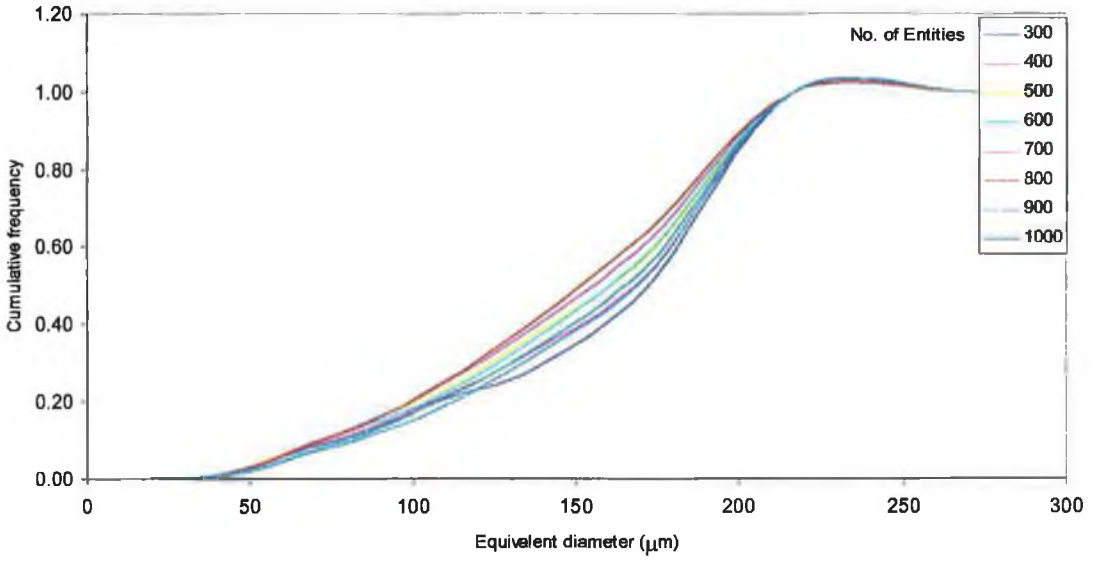

Figure 6.10 Development of a volume-based cumulative frequency distribution for *S. natalensis* grown in YEME medium.

A similar sample size was reported by Vigneau *et al.* (2000) as being appropriate for statistical analysis of image analysis data collected from a population of starch granules. In that case, a one-sample Kolmogorov-Smirnov statistic was proposed to determine the particle size distribution of starch granules by constructing a (1-α) confidence band for an observed cumulative distribution function, where α represents the significance level. This confidence band is based on the assumption that each particle contributes equally to the estimated cumulative distribution function and therefore, the Kolmogorov-Smirnov statistic is used for number- (as opposed to volume-) based size distributions. The width of the confidence band, $\Delta_{\alpha,n,}$ is determined using the formula

$$\Delta_{\alpha,n} = \left(\frac{-1}{2}\ln\frac{\alpha}{2}\right)^{\frac{1}{2}}$$

where n is the number of particles.

This relationship can be used to determine the number of particles which must be analysed in order to assess the particle size distribution with a specified confidence (Figure 6.11). On this basis, for the data employed by Vigneau *et al.* (2000) a sample size of 500 was determined to be appropriate.

Bowman (2001), applied the method reported by Vigneau *et al.*, (2000) to image analysis data collected for *S. natalensis* grown in submerged culture in a 10L Biostat fermenter. Based on recorded equivalent diameters, a sample size of 600 was reported as being appropriate for statistical analysis. This minimum sample size was also determined as being an appropriate number to analyse samples of *S. natalensis* in the current work.

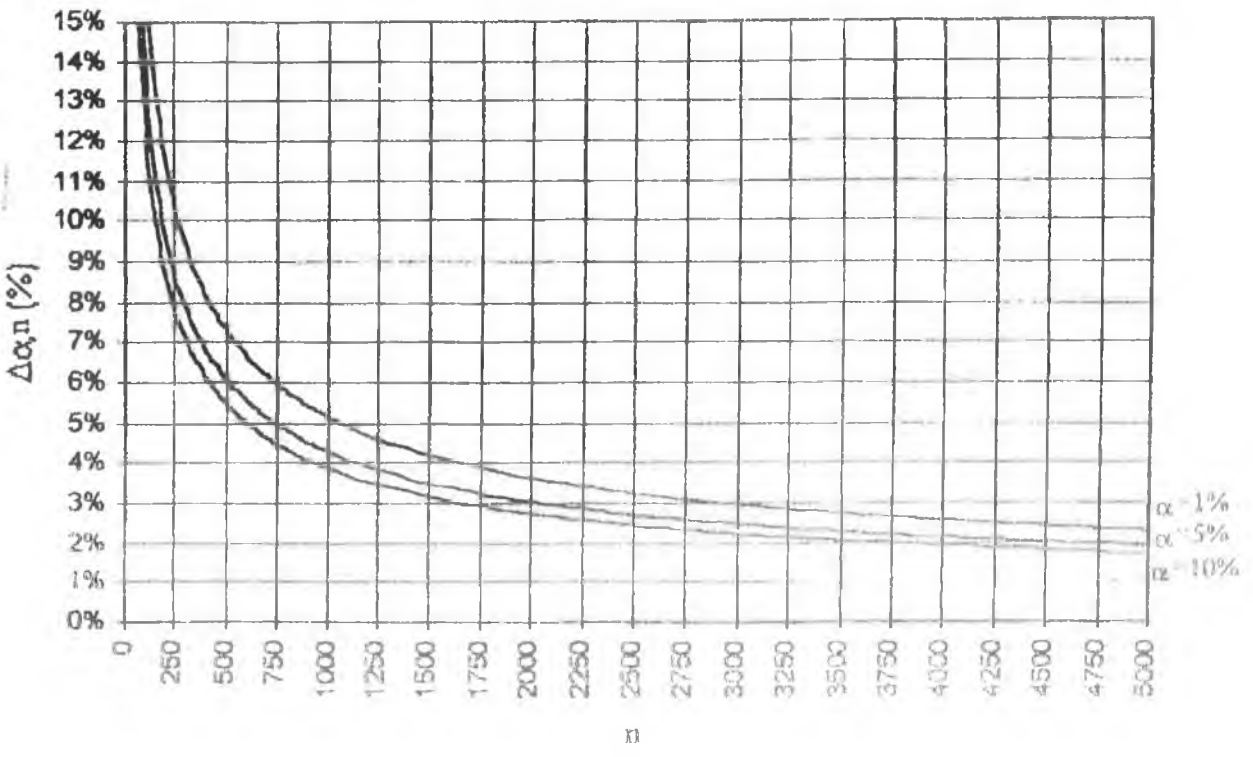

Figure 6.11 Evolution of the width of the Kolmogorov-Smirnov confidence band for a cumulative distribution.

6.2 MORPHOLOGICAL STUDIES

The following studies were performed in order to assess and make a comparison of the potential of both an Optimas image analyser and a Lasentec FBRM probe for meaningful morphological characterisation of *S. natalensis*. Broth samples originating from (a) spore inoculum and (b) a vegetative inoculum were analysed.

6.2.1 OPTIMAS IMAGE ANALYSER

The Optimas image analyser was used as previously described (Chapter 4 and Sections 6.1-6.2) to investigate the morphological development of the organism. The results are presented in Sections 6.2.1.1 (spore inoculum) and 6.2.1.2 (vegetative inoculum), respectively.

6.2.1.1 SPORE INOCULUM

The organism was cultivated in YEME medium, the components of which are described in Table 3.2, using a 40 μL spore inoculum (section 3.4.2.2.2). Samples were removed after 12, 18, 30 and 36 hours and prepared for morphological analysis. These samples were chosen, based on visual observations, as they were representative of the diverse range of morphological forms present throughout the fermentation. Biomass levels were also measured (section 3.5.1). The trial was performed in duplicate and results are presented in the form of two separate trials, 1 and 2.

Figure 6.12 shows the biomass profiles for this inoculum system. It is evident from the data presented, for both trials 1 and 2, that YEME medium supports the growth of *S. natalensis*. After a short lag period (18 hours), the organism grows in an exponential manner with a doubling time of approximately 6 hours reaching biomass levels of approximately 5 g/L, before entering the stationary phase.

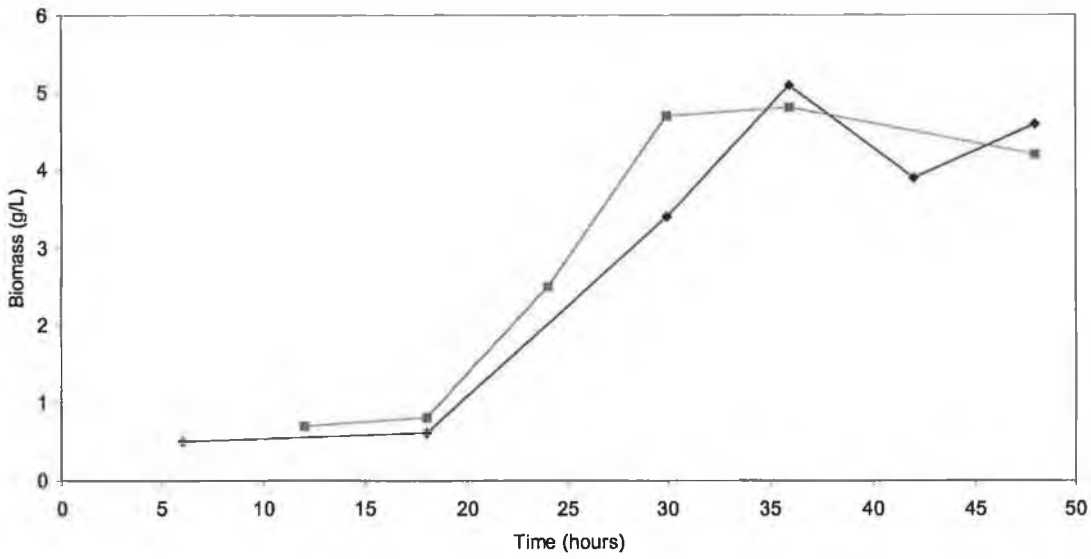

Figure 6.12 Biomass profiles for *S. natalensis* grown in YEME medium using a spore inoculum. (◆ trial 1, ■ trial 2)

For reasons previously outlined (Section 6.1), the image analysis algorithm was used to measure a total of 600 entities per sample. These entities occupied 10-15 % of the total area of the slide, were viewed at x10 magnification and the results were exported to Microsoft Excel for statistical analysis. Individual equivalent diameters from all three morphological categories were calculated and number-based frequency distributions were produced for trials 1 and 2 (Figures 6.13 a) and b), respectively).

Throughout the fermentation, based on the four samples analysed, for each trial, it is clear that two distinct groups of entities are present, highlighted by the two peaks in the frequency distributions. These peaks represent 'smaller' entities, having equivalent diameters ranging between 3.5 and 22 μm and 'larger' entities, ranging in size between 22 and 286 μm. For the 'smaller' entities, irrespective of the fermentation stage, entities having equivalent diameters of approximately 7 μm are most persistent. As the fermentation proceeds the relative frequency of these entities increases, from about 0.05 (at 12 h) to 0.14 (at 36 h). For the 'larger' entities, however, no single dominant entity size can be identified for all four stages of the fermentation. However, higher relative

frequencies are recorded for these 'larger' entities than for the 'smaller' entities. For example, on a number basis, entities with average diameters of between 57 μm and 90 μm account for approximately 46 % of all entities counted at 12 h in Trial 1; the corresponding figure for the range below 11 μm is approximately 14 %. Similar trends apply for all distributions shown for both trials. Moreover, there is obviously a high degree of consistency between the data for Trials 1 and 2. Considering the development of the distributions as the fermentations progress, a number of features are evident. Firstly, between 12 h and 18 h, there is a pronounced increase in the number and size of 'larger' entities present *i.e.* pellets and clumps. This is due to continuing growth during the exponential phase. It can, further, be postulated that collisions between the 'larger' entities (resulting in breakage) and cell death and lysis due to depletion of available nutrients and oxygen during the stationary phase both contribute to the observed reduction in number and size of the 'larger' entities and the corresponding increase in the number of 'smaller' entities from 18 h onwards. These trends are, again, mirrored in the cumulative frequency distributions (Figures 6.14 a) and b)). In particular, the appearance of large numbers of smaller entities in the latter stages of the fermentation is most pronounced.

Entities from all three morphological categories were considered simultaneously in the analysis of the data. It is clear that the 'smaller' entities which might be assumed to be hyphal elements, derived from larger clumps contributed significantly to the sample, accounting for up to 62 % of the total entities, in the case of the 36 hour samples. However, the contribution of hyphae alone to these 'smaller' entities is, at this point, unknown and therefore, their contribution, on a volume basis, is also unclear.

a)

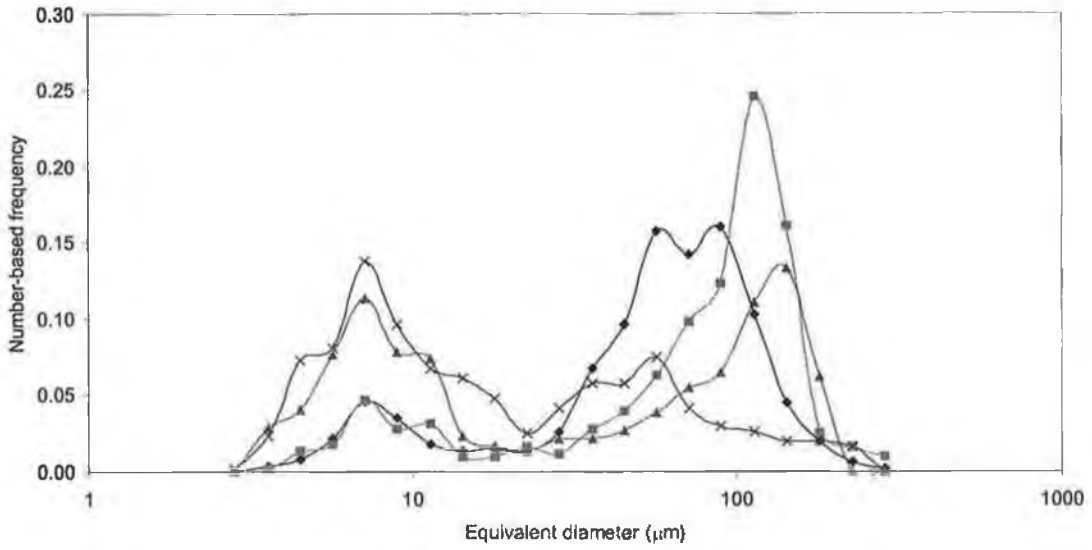

b)

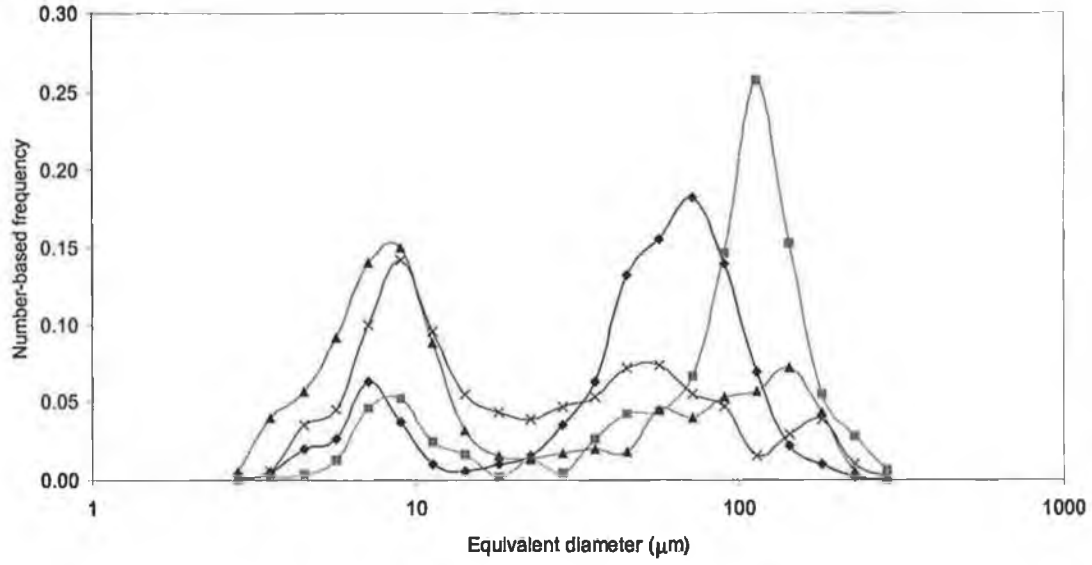

Figure 6.13 Development of a number-based frequency distribution (P+C+H) for *S. natalensis* grown in YEME medium from a spore inoculum a) trial 1, b) trial 2. (◆ 12 hour, ■ 18 hour, ▲ 30 hour, ✕ 36 hour)

a)

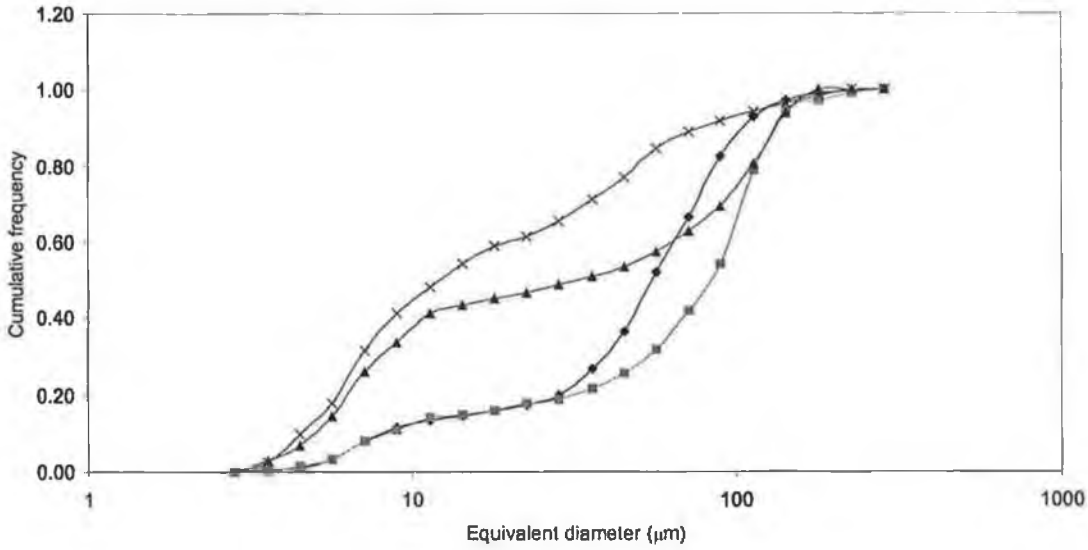

b)

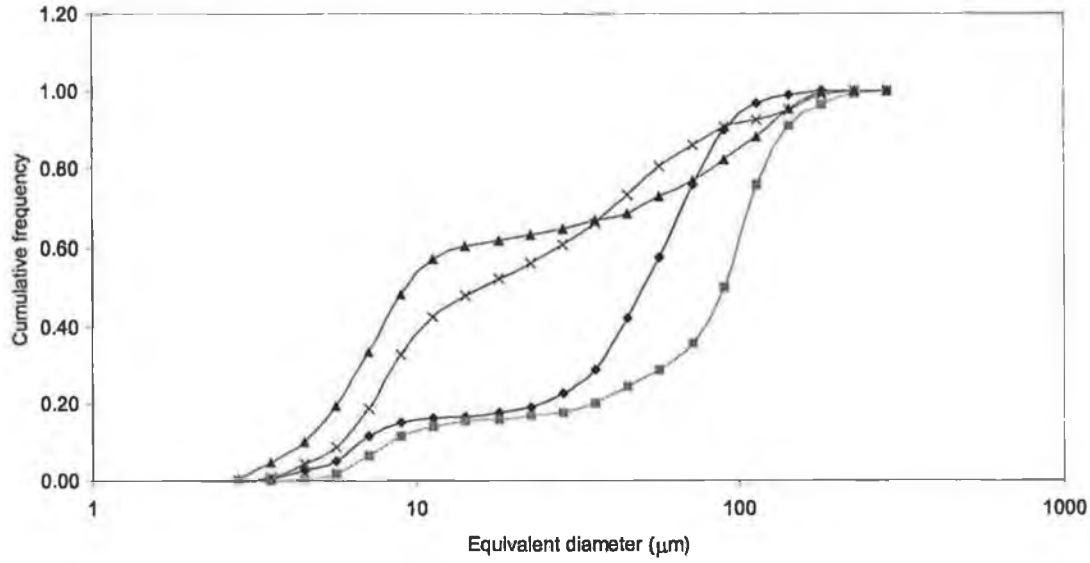

Figure 6.14 Development of a cumulative number-based frequency distribution (P+C+H) for *S. natalensis* grown in YEME medium from a spore inoculum a) trial 1, b) trial 2. (◆ 12 hour, ■ 18 hour, ▲ 30 hour, ✕ 36 hour)

Trial 1

Time (hours)	Contribution P + C (%)	Contribution H (%)
12	99.93	0.07
18	99.94	0.06
30	99.81	0.19
36	99.36	0.64

Table 6.1 Determination of the percentage contribution of Pellets and Clumps (P + C) and Hyphae (H) to the combined data, on a volume basis for trial 1.

As a representative example, the raw data from Trial 1 were assessed in terms of (a) combined pellets and clumps and (b) hyphae. The contribution of these redefined categories, on a volume basis, were calculated and the results are presented in Table 6.1. It is apparent that, although large in number, the total volume occupied by the hyphal entities is negligible. It was concluded, therefore, that only the pellets and clumps present in a sample would be considered in all other future analysis of the data to determine the overall morphological state of the organism.

The number-based frequency distributions (pellet and clump data only) for *S. natalensis* grown in YEME medium using spore inoculum for both trials 1 and 2 are shown in Figures 6.15 a) and b), respectively.

In both cases, the trends are broadly similar to those observed when considering all of the data simultaneously except, now, with the omission of the hyphal entities, the distributions are each characterised by just a single peak, representing 'larger' entities. In trial 1, the peaks move from approximately 64 μm (12 h) to 102 μm (18 h, 30 h) to 40 μm (36 h). For trial 2, the corresponding values are 54 μm (12 h), 85 μm (18 h), 108 μm (30 h) and 43 μm (36 h). The results for both trials are in good agreement with a maximum recorded difference in the most persistent entity size of less than 20 %. It is also interesting to track the frequency with which these most persistent entities occurred (Table 6.2). Although a comparatively crude basis for analysis, it provides a picture of the morphological development. For trial 1, the relative frequency of the most persistent entities (at the mean equivalent diameters quoted above) varied from 0.18 (12 h) to 0.27 (18 h) to 0.23 (30 h) to 0.15 (36 h). For trial 2, the corresponding values are 0.21 (12 h), 0.28 (18 h), 0.17 (30 h) and 0.14 (36 h). Again, the trends are in good agreement, with no more than 24 % variation between corresponding values.

It again appears that the steady increase in the number and size of the most persistent entities corresponds to continuing growth during the exponential phase. The subsequent decline in both number and size of these entities, coupled with the corresponding increase in the number of the 'smaller' entities present, is associated with clump/pellet fragmentation/disintegration during the stationary phase.

Figures 6.16 a) and b) shows the number-based cumulative distributions for trials 1 and 2, respectively, and the results obviously reflect those previously obtained by analysis of the frequency distributions. The course of the fermentation can be usefully tracked by considering the contribution of all entities with an equivalent diameter less than or equal to that of the most persistent entities (Table 6.2).

	Trial 1		Trial 2	
Time (hours)	**Frequency**	**Contribution (%)**	**Frequency**	**Contribution (%)**
12	0.18	71.20	0.21	66.30
18	0.27	88.10	0.28	64.50
30	0.23	79.50	0.17	83.30
36	0.15	56.60	0.14	59.10

Table 6.2 The number-based frequency of the most persistent entities to the data, and the % contribution of these and all smaller entities, trials 1and 2.

In trial 1, this percentage increased from 71.2 to 88.1 % during the early stages of the fermentation. A slight decrease, from 66.3 to 64.5 %, was recorded for trial 2. As the stationary phase begins, after 30 hours, for trial 1, a decrease from 79.5 % to 56.6 % is recorded. Percentages continue to increase to 83.3 % in trial 2 but do eventually decrease to 59.1 % after 36 hours cultivation.

Given that a volume-based analysis of the data may yield a more meaningful portrayal of the morphology of the organism, further analysis was performed.

a)

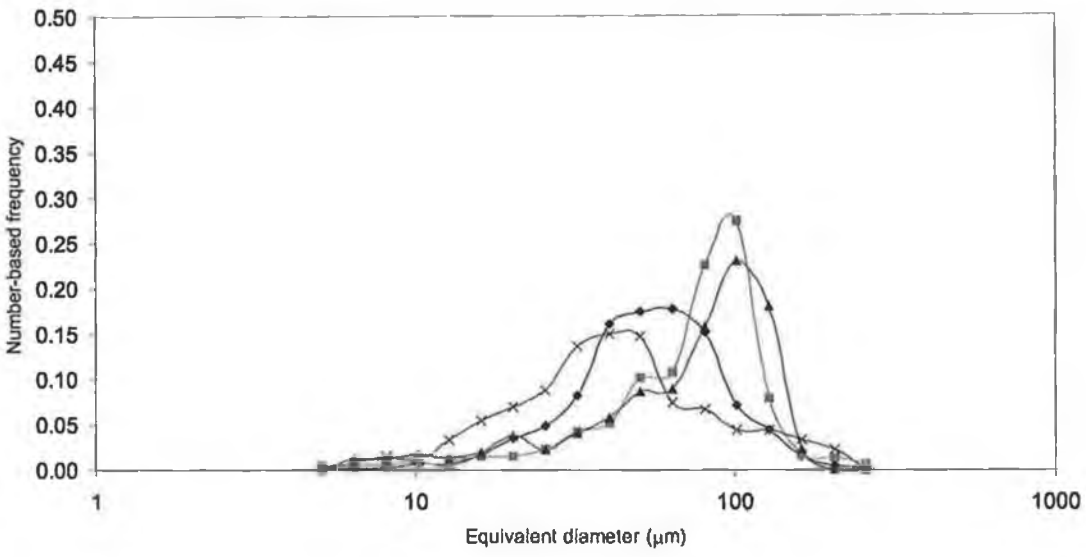

b)

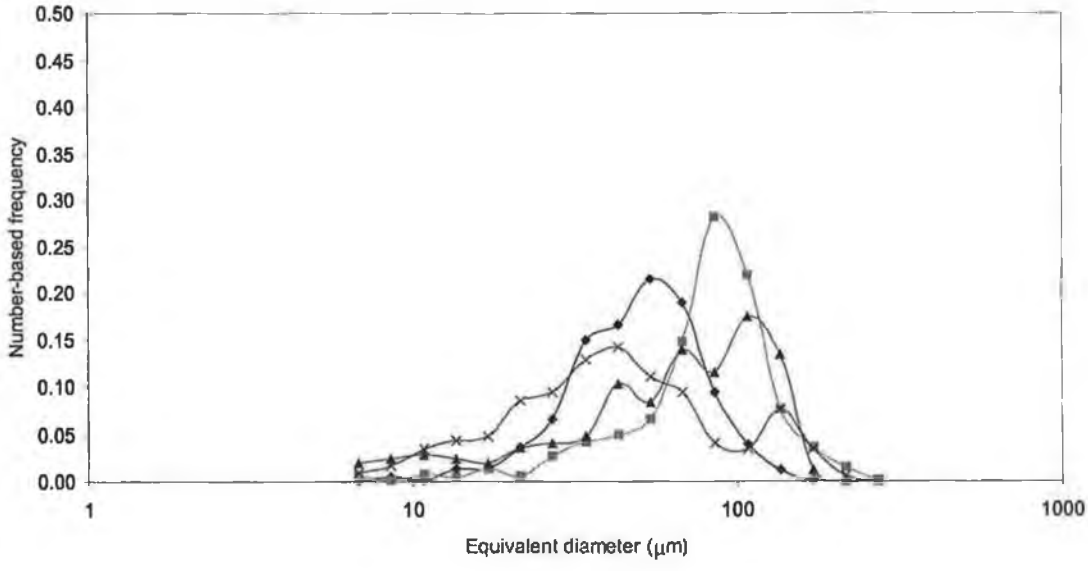

Figure 6.15 Development of a number-based frequency distribution (P+C) for *S. natalensis* grown in YEME medium from a spore inoculum a) trial 1, b) trial 2. (◆ 12 hour, ■ 18 hour, ▲ 30 hour, ✕ 36 hour)

a)

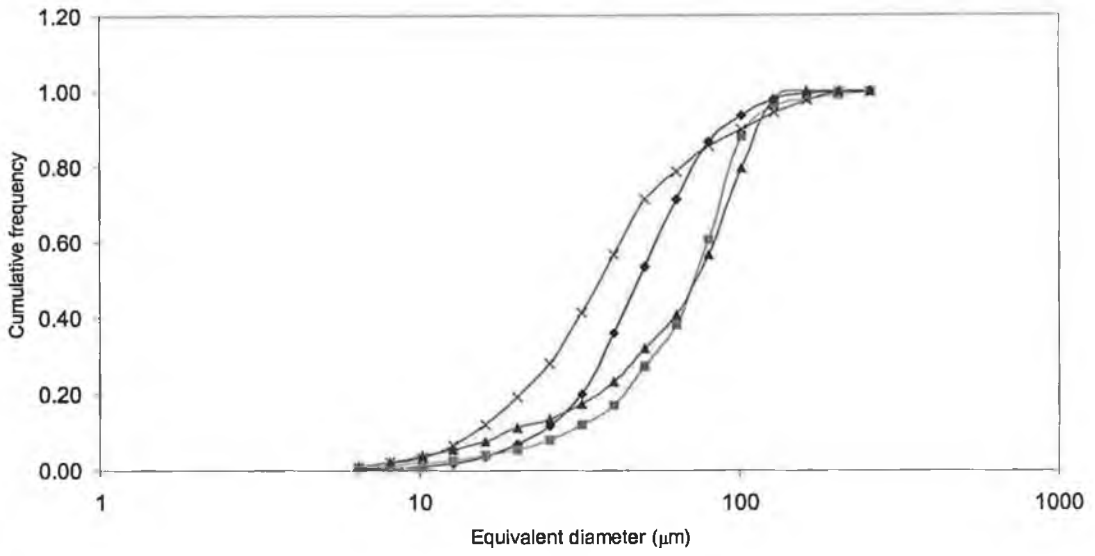

b)

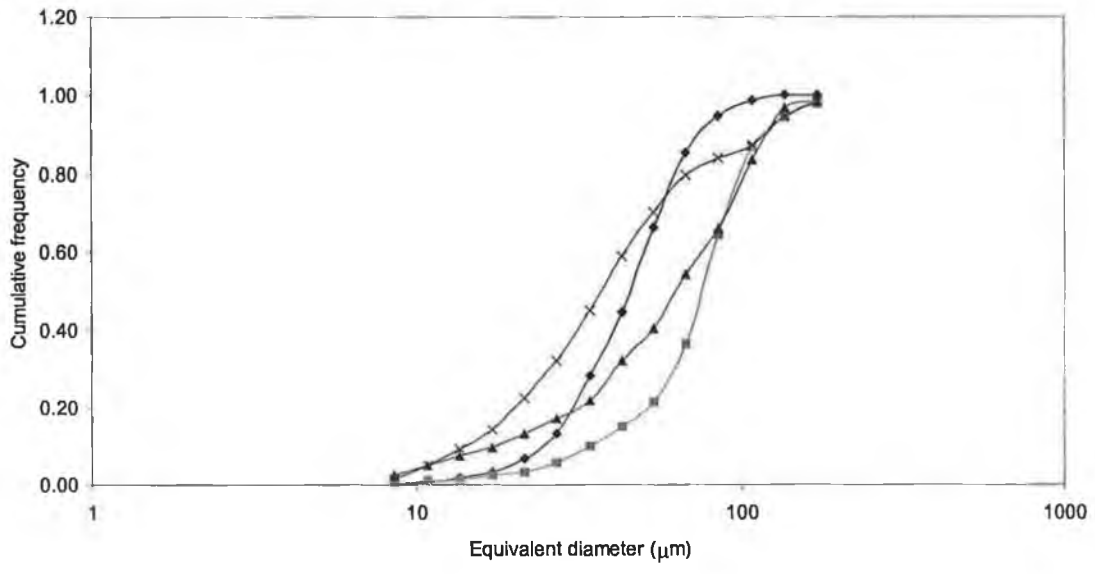

Figure 6.16 Development of a cumulative number-based frequency distribution (P+C) for *S. natalensis* grown in YEME medium from a spore inoculum a) trial 1, b) trial 2. (◆ 12 hour, ■ 18 hour, ▲ 30 hour, ✕ 36 hour)

Figures 6.17 a) and b) show the volume-based frequency distributions (pellet and clump data only) for *S. natalensis* grown in YEME medium using spore inoculum for both trials 1 and 2, respectively.

On a volume basis, for each of the four samples analysed, for both trends, the frequency distributions are unimodal. The dominant entities sizes, however, are different to those previously determined in the number-based analysis and, additionally, the time-based trends are different, with the dominant entity size increasing over the course of the fermentation, from 128.6 μm to 204 μm for trial 1 and from 68.2 μm to 136.2 μm for trial 2. The only deviation from this trend is a small reduction (from 128.6 μm to 102.1 μm) between 12 h and 18 h in trial 1. While the overall trends are very similar, the agreement between these distributions is poorer than for the number-based distributions (Figure 6.13).

So far, two 'most persistent entity sizes' have been identified – the first on a number basis, the second on a volume basis. What is particularly interesting here is the significant number-based reduction in the importance of the most persistent entities, when the data are re-evaluated on a volume basis. For example, in trial 1, at 12 h the most persistent entities on a number basis have an equivalent diameter of approximately 64 μm. Entities of this size, or smaller, account for 71 % of all entities counted. On a volume basis, these entities account for only 18 % of the population. Similar trends apply in all instances, as is evident from a comparison of the number-based (Figure 6.16) and volume-based (Figure 6.18) cumulative frequency distributions.

Considering the volume-based data, as the fermentation proceeds the frequency of the most persistent entities increased, approximately, from 0.20 to 0.31 to 0.451 as the fermentation progressed from 12 to 18 to 30 hours. However, values decreased to 0.33 for the 36 hour sample. This trend was also observed for trial 2. The frequency of these entities increased, approximately, from 0.23 to 0.31 to 0.45 as the fermentation progressed from 12 to 18 to 30 hours, finally decreasing to 0.38. The results obtained for both trials are in very good agreement. The maximum difference between recorded frequency values was less than 12 %. The frequency and the size of these most persistent entities, which contribute most significantly to the volume, increased steadily during the first 30 hours of the fermentation (with the exception of the 18 hour sample in trial 1).

This reflected the continuing growth and reproduction of the organism at this stage of the fermentation. Although their size continued to increase, the frequency on a volume basis decreased at 36 hours for both trials.

a)

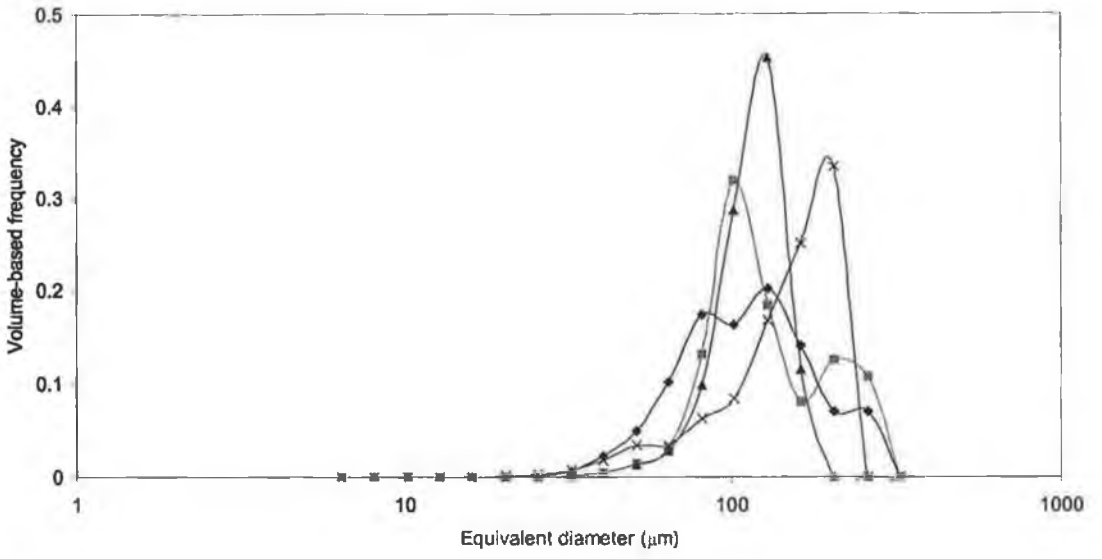

b)

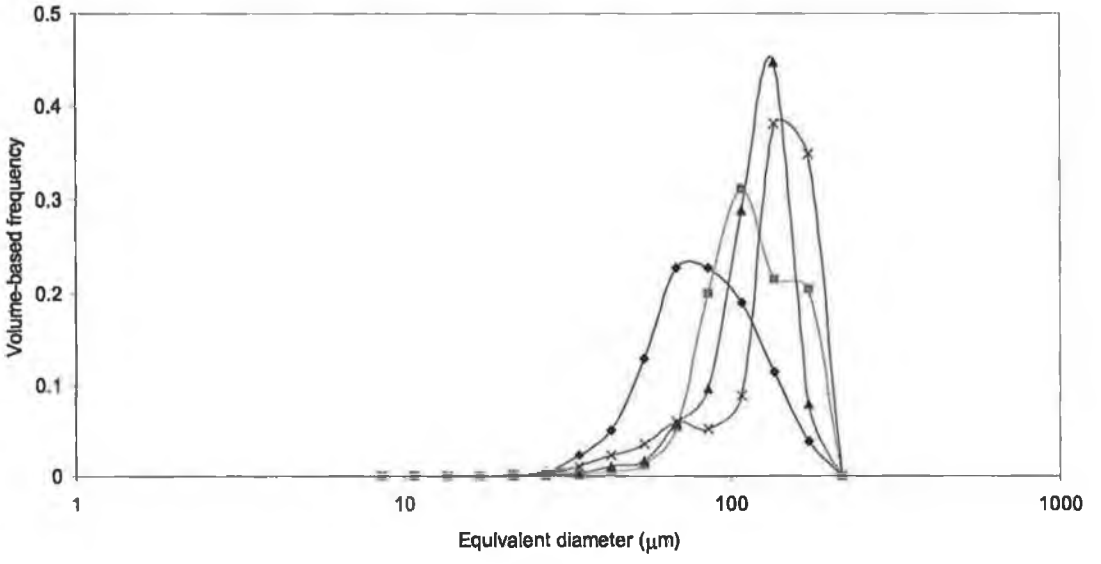

Figure 6.17 Development of a volume-based frequency distribution (P+C) for *S. natalensis* grown in YEME medium from a spore inoculum a) trial 1, b) trial 2. (◆ 12 hour, ■ 18 hour, ▲ 30 hour, ✕ 36 hour)

a)

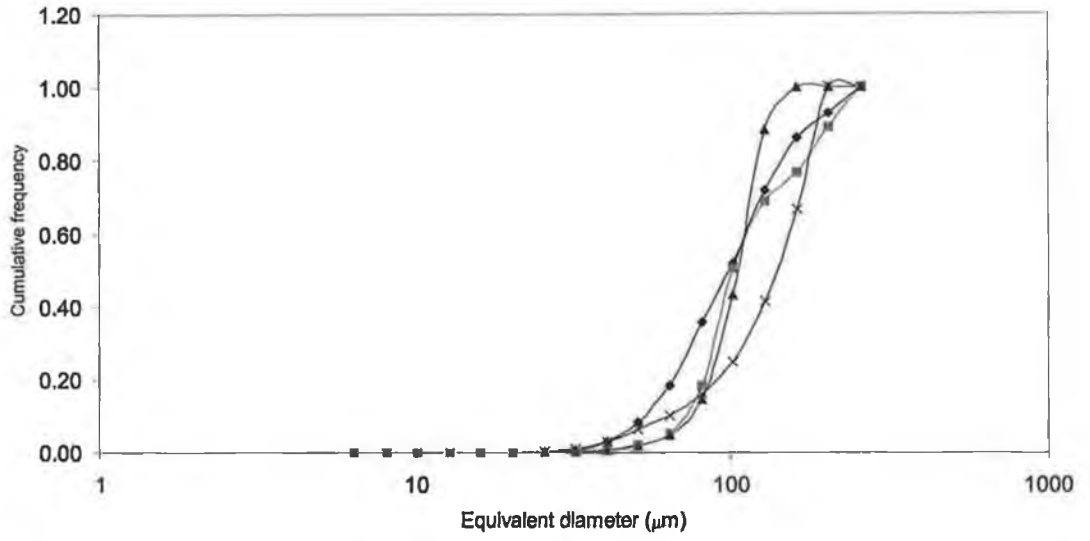

b)

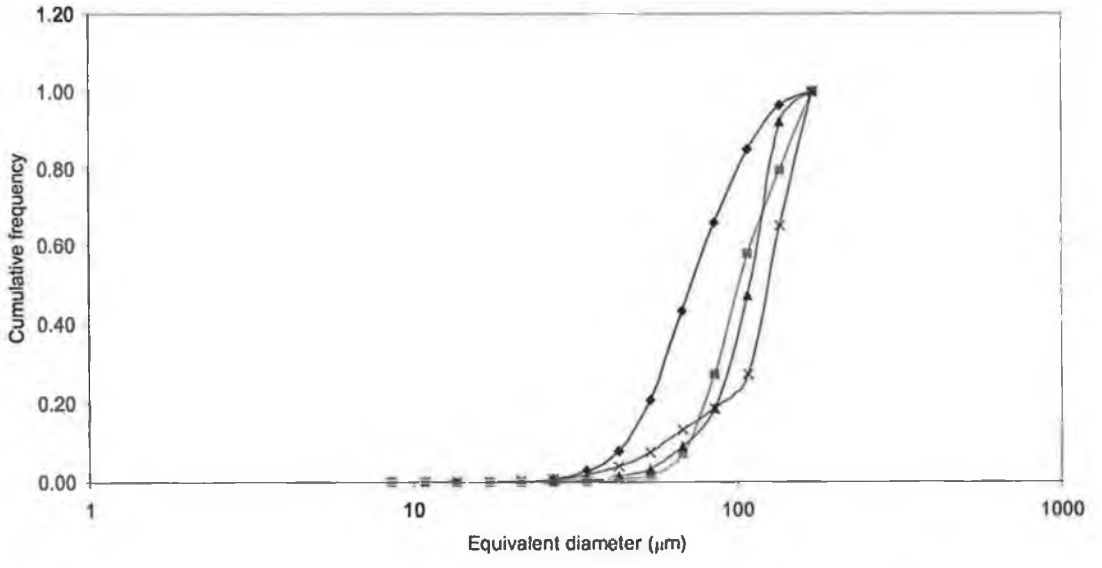

Figure 6.18 Development of a cumulative volume-based frequency distribution (P+C) for *S. natalensis* grown in YEME medium from a spore inoculum a) trial 1, b) trial 2. (◆ 12 hour, ■ 18 hour, ▲ 30 hour, ✕ 36 hour)

6.2.1.2 VEGETATIVE INOCULUM

For these studies, the organism was cultivated in YEME medium using a 10 %, 24 hour, vegetative inoculum (section 3.4.2.2.2). Samples were harvested 12, 20, 30 and 43 hours after inoculation and prepared for morphological analysis. Biomass content was also measured (section 3.5.1). As with the spore inoculum, the trial was performed in duplicate and results are presented in the form of two separate trials, 1 and 2.

Figure 6.19 shows the biomass profile for this system. It is evident from the data presented, in both trials 1 and 2, that the growth of *S. natalensis*, using this type of inoculum, was greatly reduced relative to the spore inoculum (Figure 6.12). Optimisation of this system is clearly required. In this chapter, however, these data are employed to permit direct morphological comparison between biomass produced from a vegetative inoculum (common in most industrial-scale processes) and biomass produced from a spore inoculum in the same medium. Substrate and secondary metabolite data (which are not available for this trial) might also provide useful information on the performance of this system.

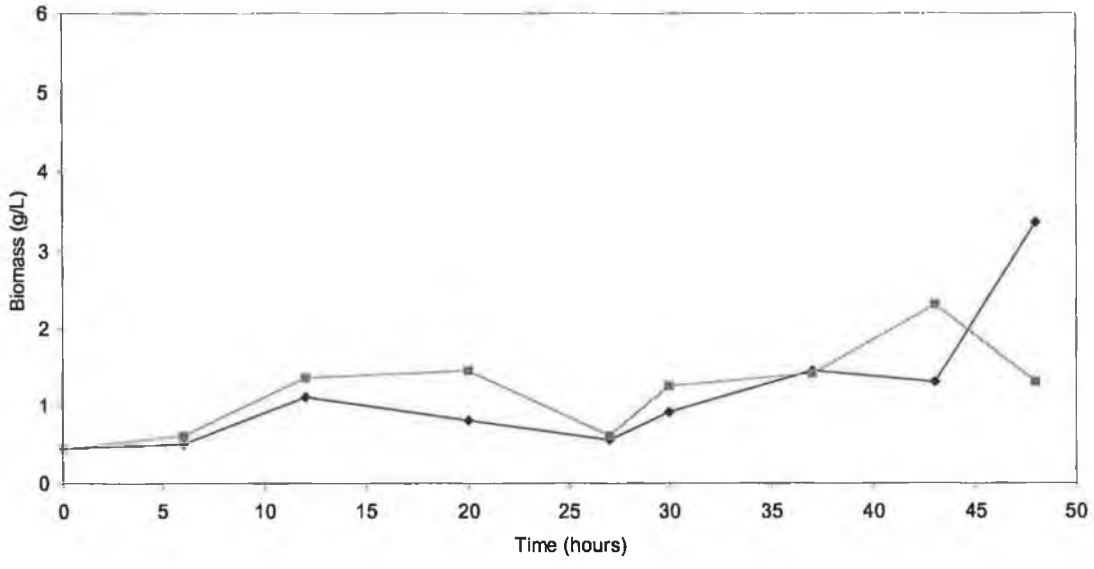

Figure 6.19 Biomass profiles for *S. natalensis* grown in YEME medium using a vegetative inoculum. (◆ trial 1, ■ trial 2)

Figures 6.20 a) and b), show the number-based frequency distributions (pellet and clump data only) for trials 1 and 2, respectively. Number-based cumulative distributions are shown in Figure 6.21.

Unlike the spore inoculum distributions (Figure 6.15) there are no single distinct peaks in the data. Instead, for each of the four samples analysed, a series of peaks representing various persistent entity sizes exist. Agreement between the distributions for trials 1 and 2 is good. The data show a distinct upward shift between 12 h and 18 h, reflecting growth and clump/pellet expansion. This is followed by a marked downward shift thereafter, suggestive of the onset of the stationary phase.

a)

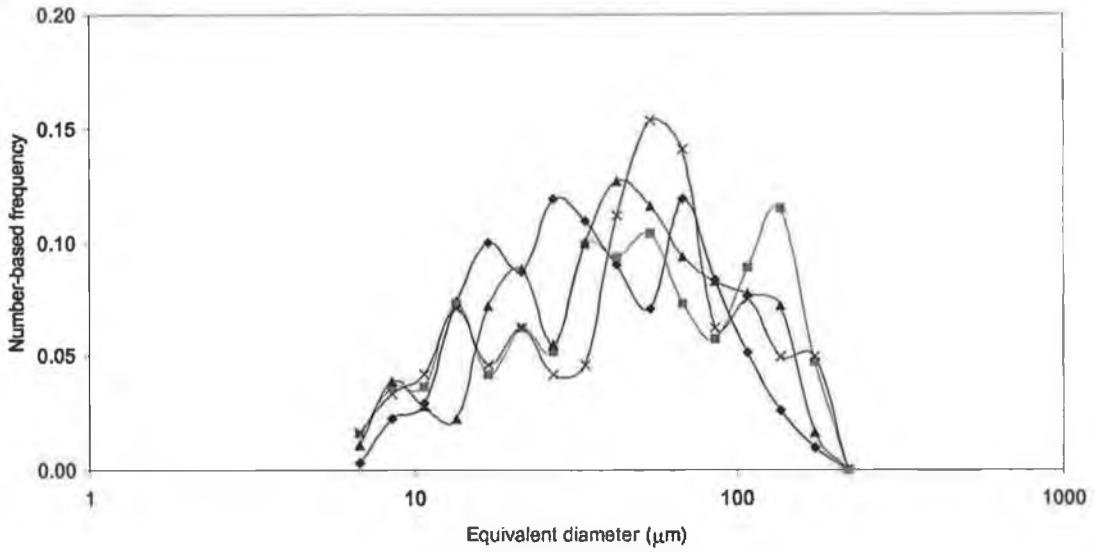

b)

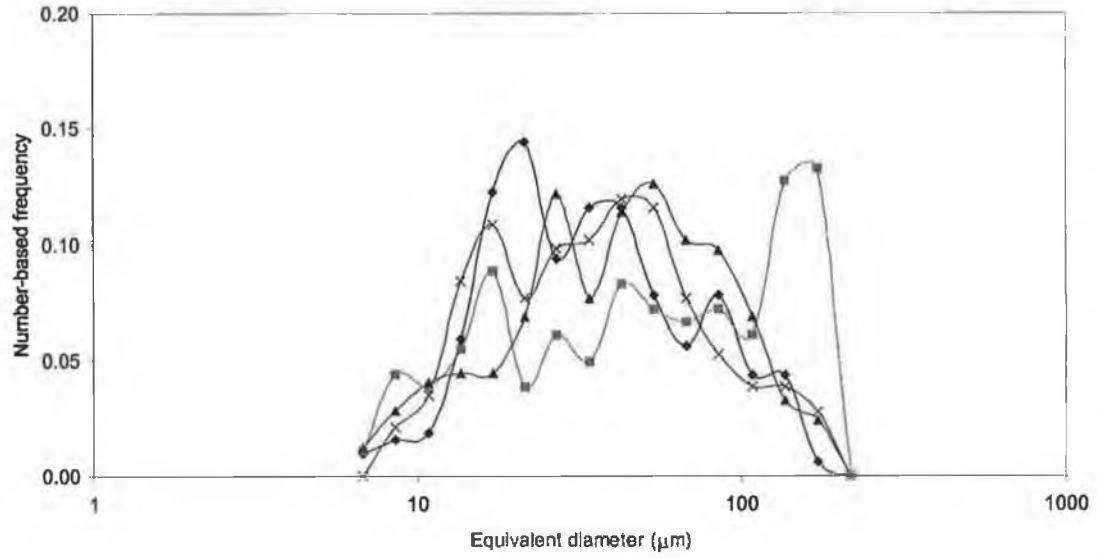

Figure 6.20 Development of a number-based frequency distribution (P+C) for *S. natalensis* grown in YEME medium from a vegetative inoculum a) trial 1, b) trial 2. (◆ 12 hour, ■ 18 hour, ▲ 30 hour, ✕ 36 hour)

a)

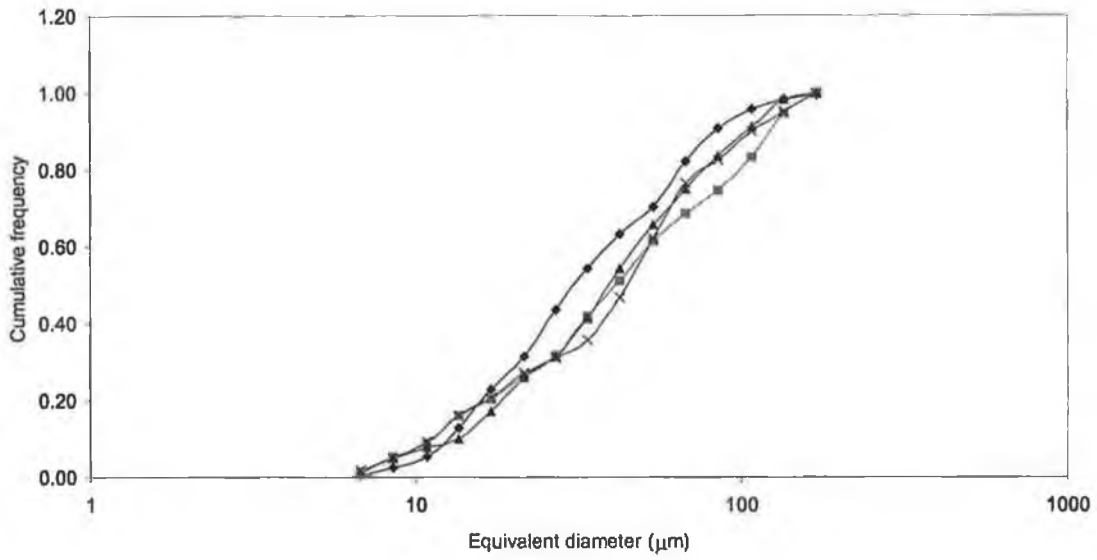

b)

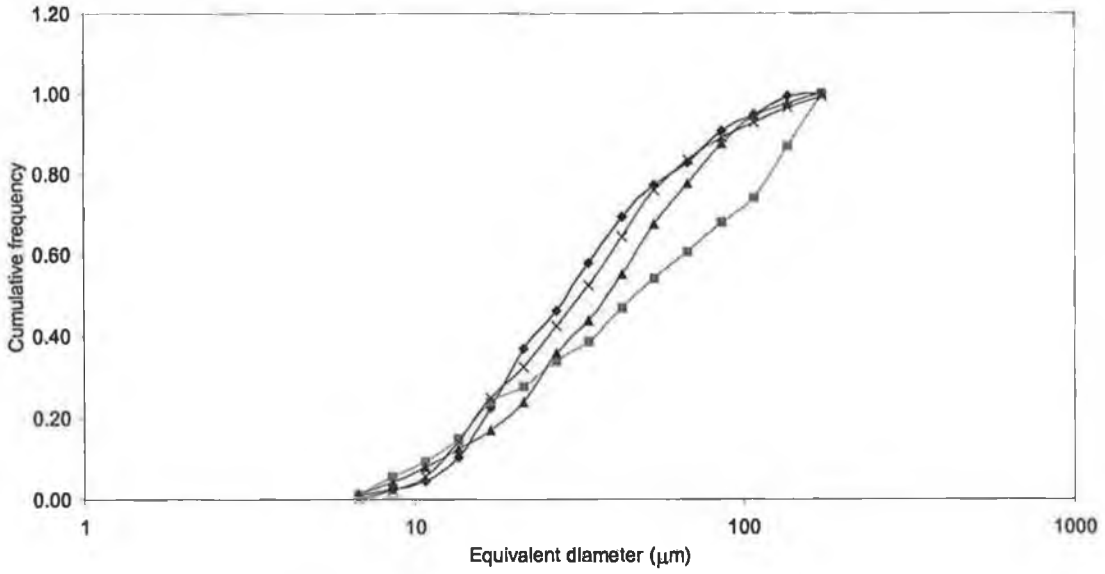

Figure 6.21 Development of a cumulative number-based frequency distribution (P+C) for *S. natalensis* grown in YEME medium from a vegetative inoculum a) trial 1, b) trial 2. (◆ 12 hour, ■ 18 hour, ▲30 hour, ✕ 36 hour)

Considering the volume-based frequency distributions (Figure 6.22) for each of the four samples analysed for both trials it is clear that one distinct group of entity size is most persistent. Further, the shift of these peaks, with time, is very similar to that observed for the samples originating from spore inoculum (Figure 6.17), although the position and magnitude of the peaks is different. For the samples generated from spore inocula, the dominant entity size, on a volume basis was 136 μm for Trial 2. For samples generated from a vegetative inocula, the corresponding value is 172 μm for both trials. Given the variability between the results of the spore inoculum trials, it is not possible to draw any firm conclusions about the influence of inoculum condition on the final morphological state of the organism.

a)

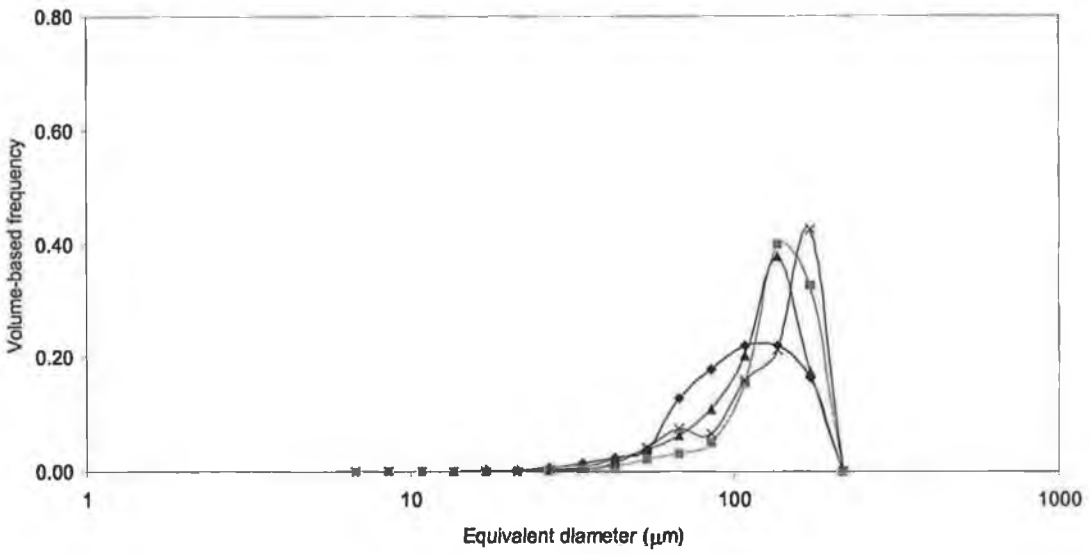

b)

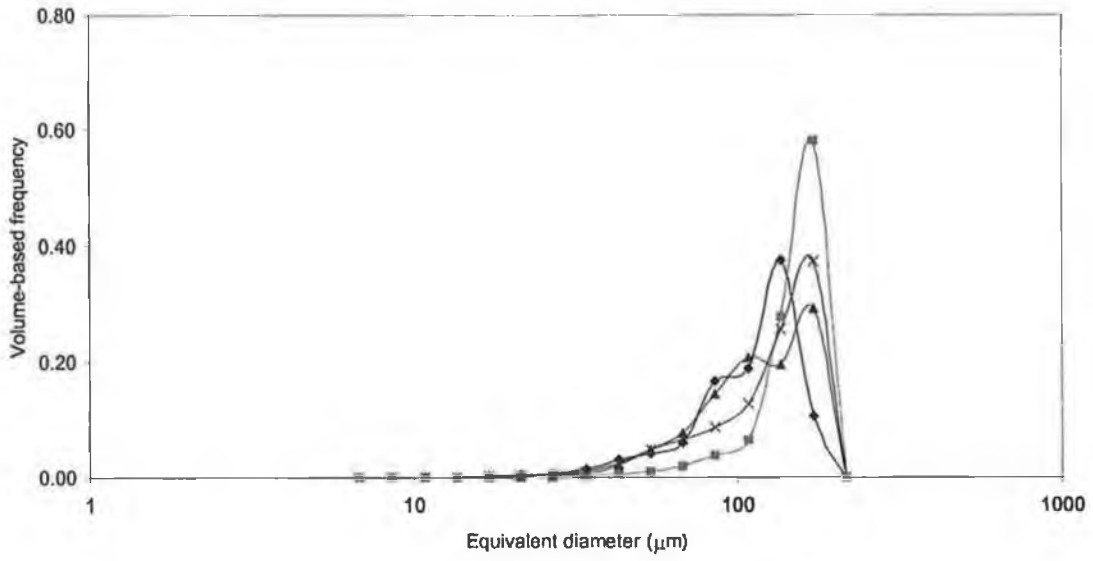

Figure 6.22 Development of a volume-based frequency distribution (P+C) for *S. natalensis* grown in YEME medium from a vegetative inoculum a) trial 1, b) trial 2. (◆ 12 hour, ■ 18 hour, ▲ 30 hour, ✕ 36 hour)

a)

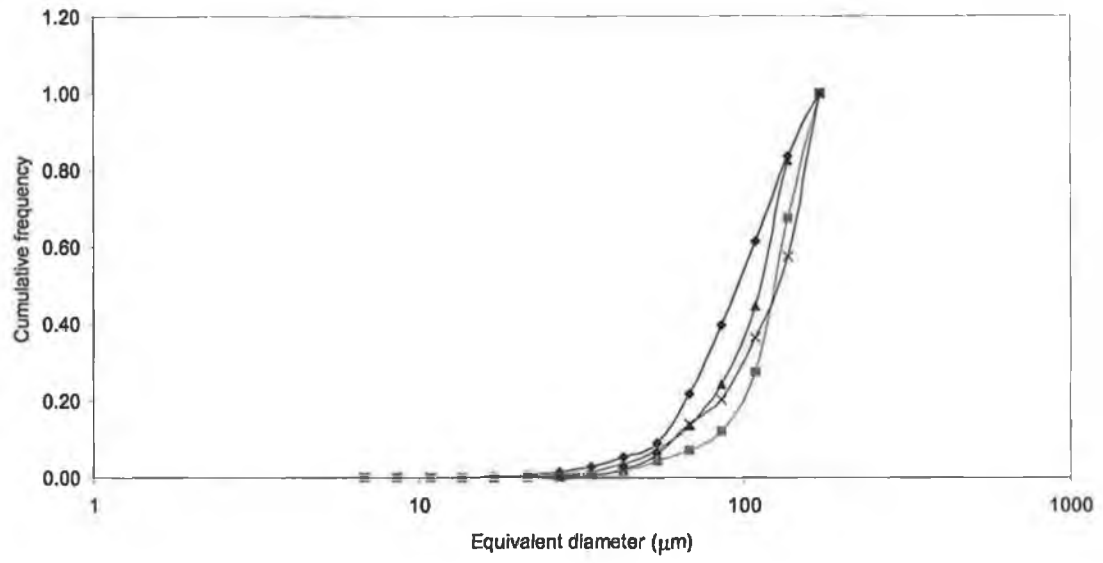

b)

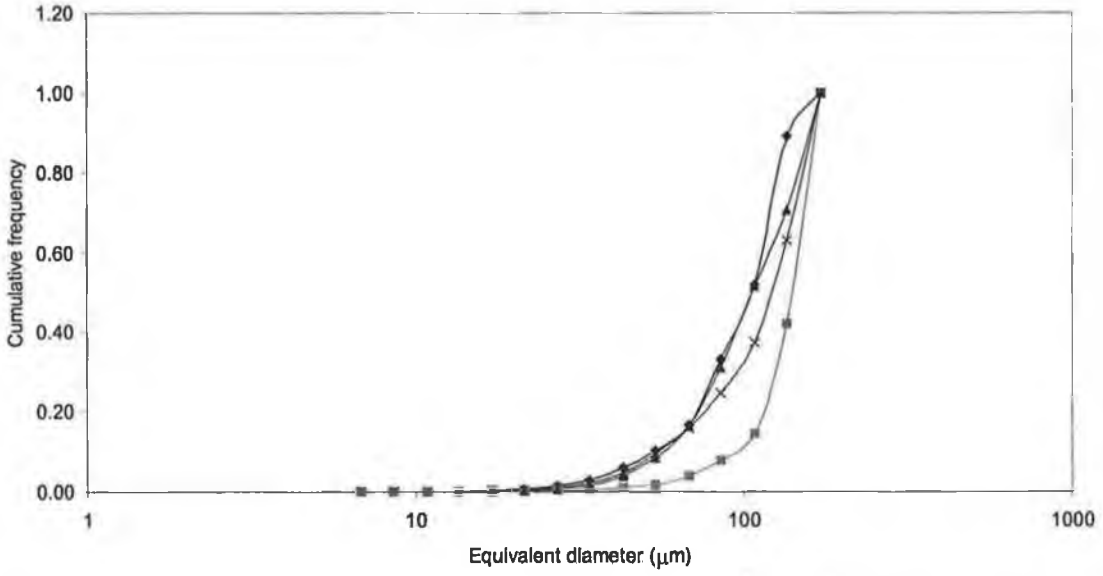

Figure 6.23 Development of a cumulative volume-based frequency distribution (P+C) for *S. natalensis* grown in YEME medium from a vegetative inoculum a) trial 1, b) trial 2. (◆ 12 hour, ■ 18 hour, ▲ 30 hour, ✕ 36 hour)

6.3 COMPARISON OF PERFORMANCE OF IMAGE ANALYSER AND LASENTEC FBRM PROBE

A preliminary investigation of the potential of a Lasentec®, Focused Beam Reflectance Measurement (FBRM) probe to characterise the morphological state of a filamentous organism grown in liquid culture was undertaken. Samples from the inoculum studies (section 6.2.1.1) were employed.

Specifically, the probe was used to analyse 18, 30 and 36 hour samples. The average number of entities counted per second, as a function of their size (chord length), was determined. It was hypothesised that the chord length, as determined by the Lasentec® FBRM probe, might be comparable, in trend, rather than absolute values, to the equivalent diameter measured by the image analyser. A comparison was made between these results and number-based frequency distributions obtained using the image analyser, based on all three morphological forms present in the samples (section 6.2.1.1). The FBRM probe results, for both trials 1 and 2 are presented in Figure 6.24 a) and b), respectively.

In both trials, the 18, 30 and 36 hour samples represent biomass levels of, on average, 0.7 g/L, 3.0 g/L and 4.9 g/L, respectively (Figure 6.12, Table A.22). Accordingly, variations between the FBRM count data for each of these broths might be expected to derive from (a) morphological differences, reflected in the relative distribution of the counts and (b) biomass concentration, reflected in the total number of counts recorded in a specified time interval. Figure 6.24 reflects both of these factors.

a)

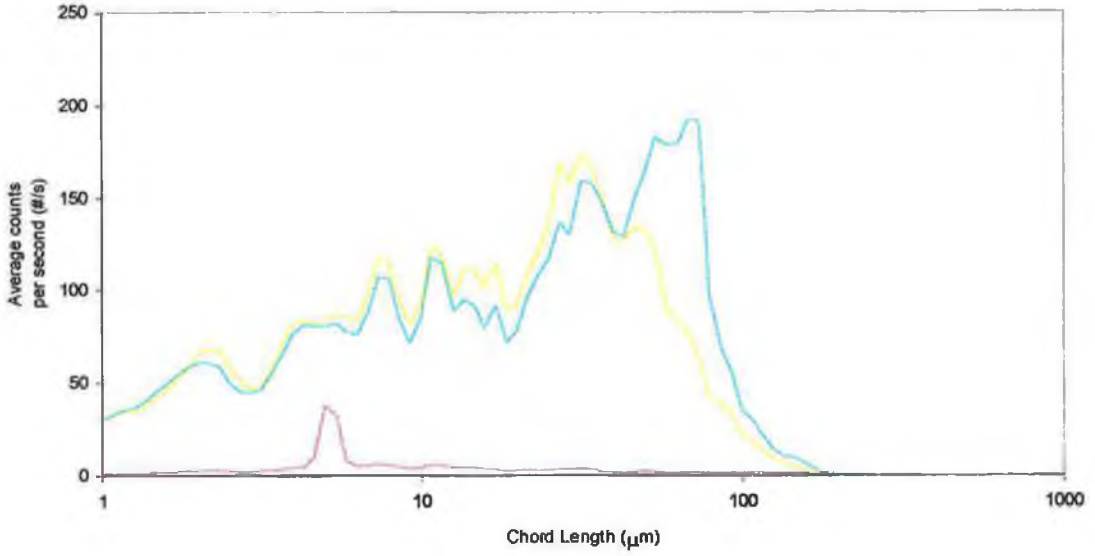

b)

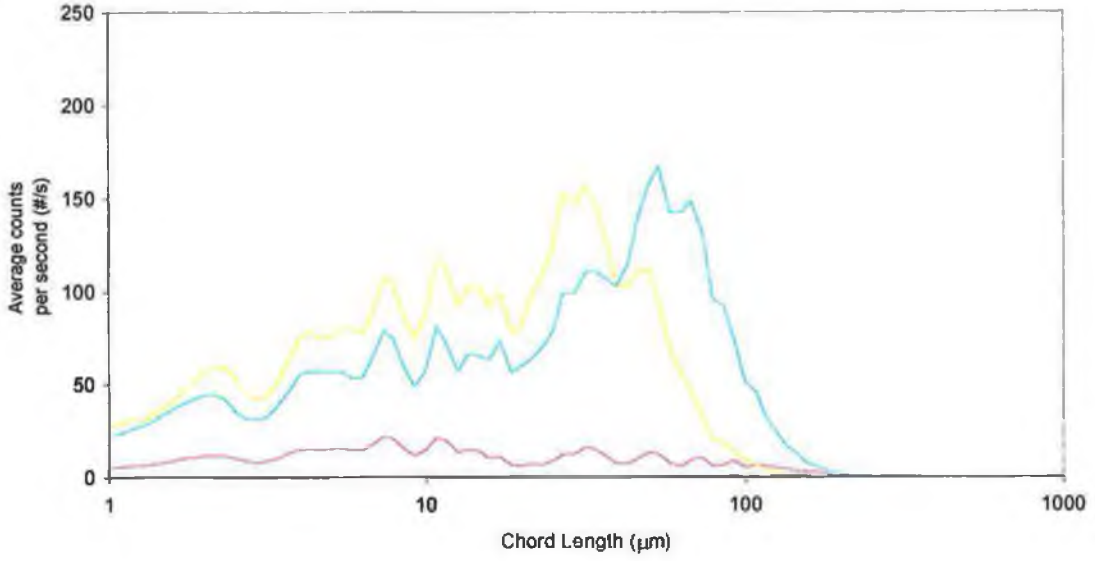

Figure 6.24 Development of an average particle number distribution using FBRM data (P+C+H)) for *S. natalensis* grown in YEME medium from a spore inoculum a) trial 1, b) trial 2. (— 18 hour, — 30 hour, — 36 hour)

A simple comparison between Figure 6.13 (image analysis) and Figure 6.24 reveals that, unlike the image analysis data, the FBRM distributions are not characterised by two distinct peaks representing 'most persistent' entity sizes. The 30 and 36 h distributions are all left-skewed and rise towards a mode at a chord length of approximately 31.62 μm (30 h) and 68.13 μm (36 h). For the 18 h samples, the biomass levels (and, thus, the count levels) are too low to permit any meaningful characterisation. With the exception of a small peak in the 18 h data for trial 1 at approximately 5.01 μm, there is good agreement between the shape and positioning of the distributions for trials 1 and 2.

A comparison between the range of equivalent diameters and chord lengths indicates that there is a smaller minimum detectable entity size for the FBRM than for the image analyser (2.85 μm). This is unsurprising when we consider the differences in sample preparation, entity detection and data processing. The image analysis algorithm is designed to measure dried material which has been spread on a slide. It specifically excludes all entities below a certain size limit as these are assumed (on the basis of prior visual observation) to represent non-hyphal particles. The FBRM data, however, represents in vivo measurements. The FBRM probe cannot distinguish between biological and non-biological material and the data may, thus, include other suspended solids. In a typical fermentation broth, particularly one employing an undefined medium, this might include particles of undissolved nutrients. Moreover, since an FBRM count represents the interruption of the laser signal as it is intersected by a freely moving particle, suspended in liquid, it is entirely possible that the laser may be directly intersected by a single hypha either isolated or extending from a clump. In this case, a chord length of the order of 1 μm might be expected.

At the other end of the scale, it can be seen (Table 6.3) that the maximum measured chord length (215 μm) is significantly smaller than the maximum equivalent diameter (286 μm) calculated.

The image analysis data (Figure 6.13) show a left shift in the distribution modes between 30 h and 36 h. It is postulated that this may reflect clump/pellet break-up or attrition

during the stationary phase. The FBRM data, on the other hand, show an upward shift during this time. This shift is certainly representative of a morphological change. However it is manifested differently. Further studies would be required to interrupt this trend.

	Trial 1		Trial 2	
Time (hours)	**FBRM probe (μm)**	**Image Analyser (μm)**	**FBRM probe (μm)**	**Image Analyser (μm)**
18	158	286	199	286
30	185	180	135	227
36	185	227	215	286

Table 6.3 Maximum entity size detected by the FBRM probe and Image Analyser, trials 1 and 2.

With the image analyser, the total number of entities is manually determined. Biomass levels are adjusted by dilution to ensure appropriate slide coverage by the sample. With the FBRM probe, however, the total number of counts recorded is a function of the concentration of the suspended material. Table 6.4 shows biomass level and total count rates (counts per second) for each of the six measurements performed. For both trials, between 18 and 30 h, as the biomass levels rise by a factor of approximately 5.7, the total count rate increases between 6-fold (trial 2) and 19-fold (trial 1). The level of between-trial consistency is obviously poor. However the data reflect a strong dependency of count rates on biomass level. Between 30 h and 36 h, biomass levels rise to a lesser extent (by a factor of 1.5 for trial 1 and a factor of 1.02 for trial 2). In both cases, the 36 h count rate is within ± 6 % of the 30 h count rate.

This limited series of preliminary trials clearly indicates the potential of the FBRM probe to detect changes in morphology and changes in biomass levels in suspension cultures of a filamentous organism. The attractions of this approach to morphological

characterisation are many: the biomass is measured in vivo and not artificially distorted by slide preparation; measurements may be performed in vivo and, as the probe may be sterilised, the potential for in-situ measurements in a STR certainly exists (work in this area is currently ongoing (Pearson *et al.*, ESBES poster, 2000)); each of the measurements undertaken here were of approximately 30 s in duration which image analysis of 600 entities requires up to 300 minutes.

However, as highlighted in Figure 6.24 and Table 6.3, optimisation of the measurement conditions for improved reproducibility is clearly required.

	Trial 1		Trial 2	
Time (hours)	**Biomass (g/L)**	**Total Count Rate (#/s)**	**Biomass (g/L)**	**Total Count Rate (#/s)**
18	0.6	286	0.8	736
30	3.4	5404	4.7	4644
36	5.1	5727	4.8	4468

Table 6.4 Biomass levels and FBRM Count Rate for trials 1 and 2.

CHAPTER 7
CONCLUSIONS AND RECOMMENDATIONS

7.1 CONCLUSIONS

The purpose of this research was to characterise both the growth and morphology of *S. natalensis* in submerged culture. This was achieved, firstly, by investigating the effect of different maintenance and cultivation techniques. Secondly, a program, using a semi-automated image analysis system, was written and validated and this was used, supported by data from a Lasentec FBRM probe, to morphologically characterise the organism.

In Study One, it was found that of the range of conditions investigated optimal growth occurs using YED medium as inoculum medium. Maximum biomass levels of 3.77 g/L were similar to levels reported by O' Shea (1998) for growth of the same organism in a medium rich in yeast extract. Inoculum age, (12, 18 or 24 hours) does not appear to influence the maximum biomass levels achieved (approximately 5g/L) when the inoculum is subsequently introduced into SPG medium. A similar result has been reported by El-Enhasey *et al.* (2000). In all cases investigated, maximum biomass production rates occur at the beginning of the fermentation, with pimaricin production commencing approximately 53 hours after inoculation. Maximum levels of 0.07 g/L were recorded.

In Study Two, use of SPG and defined phosphate-limited medium as the inoculum medium and fermentation/production medium, respectively, did not prove beneficial in terms of either growth or pimaricin production. Although substantial levels of biomass are recorded in the SPG medium, these are in striking contrast to those obtained in the defined phosphate-limited medium (where maximum levels of only about 1.2 g/L were measured). Again, the age of the inoculum was not found to have a significant effect on system performance. Pimaricin production was not detected and it was concluded that this was attributable to the very low levels of growth in the phosphate-limited medium.

Study Three focussed on an effort to increase levels of secondary metabolite production, to match those previously recorded by researchers using the phosphate-limited medium. YED medium was chosen as the inoculum medium, in place of the SPG medium. Biomass levels were increased to approximately 5 g/L, with maximum production rates observed at the beginning of the fermentation. Pimaricin production also commenced, after approximately 100 hours cultivation, reaching maximum levels (~ 0.06 g/L) similar to those found in Study One.

In Study Four, the introduction of an intermediate inoculum stage using SPG medium (inoculum biomass concentration of ~ 5 g/L) also failed to improve levels of growth in the phosphate-limited medium. As pimaricin production was only detected in a single flask, in one trial it is difficult to draw any conclusions about the potential of this cultivation technique.

Based on the results obtained for the four different maintenance and cultivation techniques described above, it is concluded that YED is the preferred inoculum medium in terms of biomass and subsequent pimaricin production levels. While both SPG and phosphate-limited medium appear to be suitable for secondary metabolite production, recorded levels in this work are significantly smaller than those obtained by other researchers using the same organism.

A major part of this work was directed towards development of a validation of a semi-automated image analysis technique for morphological characterisation of the organism. Mycelial elements were categorised as either hyphal entities, mycelial clumps or pellets. Dilution, magnification factor and sample size (*i.e.* number of entities to be counted) were the important validation steps. It was concluded that diluting a sample such that 10-15 % of the total area available in the region of interest was occupied by mycelial entities, as suggested by Treskatis *et al.* (1997), produced good quality images. It was determined that x10 (as opposed to x4) magnification gave a more accurate representation of the morphology. Also, upon using the image analysis algorithm to measure a total of 1000 entities, it was concluded that measurement of 600 entities was

sufficient to provide a meaningful representation of the morphological state of the organism.

Cultivation of the organism in YEME medium, using a spore inoculum, resulted in high levels of biomass (approximately 5 g/L). Analysis of number-based frequency distributions, highlighted the existence of two dominant groups of entities broadly classified as larger entities and smaller entities. The smaller entities were predominantly free hyphae. Although significant on a number basis, the hyphal contribution was less than 1 %, on a volume basis, and these entities were therefore, omitted from further statistical analysis.

Number-based analysis of pellet and clump data alone, suggested, during the early stages of the fermentation, a steady increase in the number and size of the most persistent entities due to continuing growth during the exponential phase. Conditions normally associated with the beginning of the stationary phase of the life cycle were thought to contribute to the recorded decrease in number and size of these entities. Also apparent at that time was the corresponding increase in the number of the 'smaller' entities present, thought to be fragments of the larger, disrupted entities.

Volume-based analysis of the data generally mirrored number-based trends. However it also highlighted the difficulties of applying a volume or weight basis to data which are inherently number-based.

A limited series of preliminary trials employing a Lasentec® FBRM probe highlighted the potential of this technique to detect, in real time, changes in both biomass levels and morphology.

7.2 RECOMMENDATIONS

- Although the use of the bioassay method for the quantitative determination of pimaricin levels proved satisfactory in this research, it is recommended that further work should involve an investigation into alternative methods used, such as UV- or HPLC-based techniques.
- Study Four should be repeated in order to determine, with confidence, the levels of pimaricin production by the organism using this cultivation technique.
- Future cultivation of the organism should be extended to track the secondary metabolite profile during the latter stages of the fermentation.
- Studies performed by El-Enhasey *et al.* (2000), have indicated that the type of inoculum can have a dramatic effect on the levels of pimaricin produced by *S. natalensis*. Results have indicated that use of a spore inoculum (2×10^8 spores/mL) has increased pimaricin levels to 1.6 g/L. Future trials should involve an examination of spore inoculum sizes and their effect on pimaricin production levels.
- The study performed by El-Enhasey *et al.* also referred to the potential influence of the morphology of the organism generated from the spore inoculum (typically a small pellet structure in a mycelial network) on subsequent antibiotic production levels. Future work should involve a thorough investigation into the influence of the spore inoculum sizes and their corresponding morphologies on secondary metabolite production.
- Farid *et al.* (2000), have reported on the combined effect of beef and yeast extract in the cultivation medium on growth and antibiotic production by *S. natalensis*. Future studies should involve a further investigation into the use of these two media types.
- Development of the image analysis algorithm, to minimise the manual editing stage would usefully reduce sampling time.
- Future work should involve a more detailed statistical analysis of the image analysis results allowing the contribution, on both a number and volume basis, to be determined for each of the three different morphological forms separately. This would result in a clearer portrait of the morphological state of the organism.

- In relation to the FBRM probe, further studies are required to reduce the variability in the data and optimise experimental conditions. Extension of the work to on-line measurements in a STR is an obvious and potentially valuable development.
- That a relationship exists between chord length distribution and morphology is evident from the work reported here. Elucidation of the nature of that relationship, however, requires further trials, involving both the FBRM and supporting image analysis data.

BIBLIOGRAPHY

Abraham, E.P. (1978). Developments in the chemistry and biochemistry of β-lactam antibiotics, 141-161. In Hutter, R., Leisinger, T., Nuesch, J. and Wehrli, W. (eds.), Antibiotics and other secondary metabolites. Biosynthesis and production Academic Press, London.

Adams, H.L. and Thomas, C.R. (1988). The use of image analysis for morphological measurements on filamentous microorganisms. *Biotechnol. Bioeng.*, **32**, 707-712.

Agger, T., Spohr, A.B., Carlsen, M. and Nielsen, J. (1998). Growth and product formation of *Aspergillus oryzae* during submerged cultivations: verification of a morphologically structured model using fluorescent probes. *Biotechnol. Bioeng.*, **57**, 321-329.

Aparicio, J.F., Fouces, R., Mendes, M.V., Olivera, N. and Martin, J.F. (2000). A complex multienzyme system encoded by five polyketide synthase genes is involved in the biosynthesis of the 26-membered polyene macrolide pimaricin in *Streptomyces natalensis*. *Chem. and Biol.*, **7**, 895-905.

Aparicio, J.F., Colina, A.J., Ceballos, E. and Martin, J.F. (1999). The biosynthetic gene cluster for the 26-membered ring polyene macrolide pimaricin. *J. Biol. Chem.*, **274**, 10133-10139.

Bader, F.G. (1986). Physiology and fermentation development. 281-322. In Queener, S.W. and Day, L.E. (eds.), The Bacteria. A treatise on structure and function, Antibiotic producing Streptomyces, **IX**. Academic Press, London.

Belmar-Campero, M.T. (1989). Influence of batch fermentation conditions on the morphology and clavulanic acid production of *Streptomyces clavuligerus*. PhD Thesis, University College London.

Belmar-Campero, M.T. and Thomas, C.R. (1988). The effect of stirrer speed on the morphology and clavulanic acid production of *S.clavuligerus*. Proceedings of the 2nd International conference on bioreactor fluid dynamics, 21-23 September.

Blyth, W. (1973). Farmer's lung disease, 261-273. In Sykes, G. and Skinner, F.A. (eds.). Actinomycetales: Characteristics and Practical Importance. Academic Press, London.

Borden, G.W., Maher, J.M. and Sklavounos, C. (1995). Process for natamycin recovery. International patent classification : C12P 19/62.

Bowel, P., Gibon, D., Coste, E., Daanen, V. and Rousseau, J. (1999). Automatic quality assessment protocol for MRI equipment. *Medical Physics*, **26**, 2693-2700.

Bowman, A.J. (2001). Quantitative morphological characterisation of submerged cultures of *Streptomyces natalensis* using semi-automated digital image analysis. Undergraduate project report, University College Dublin.

Brana, A.F., Wolfe, S. and Demain, A.L. (1986). Relationship between nitrogen assimilation and cephalosporin synthesis in *S.clavuligerus*. *Arch. Microbiol.*, **146**, 46-51.

Brana, A.F., Hu, W.S. and Demain, A.L. (1983). Involvement of aeration in carbon source regulation of cepham antibiotic biosynthesis in *S. clavuligerus*. *Biotechnol. Letters*, **5**, 791-794.

Braun, S. and Vecht-Lifshitz, S.E. (1991). Mycelial morphology and metabolite production. *TIBTECH.*, **9**, 63-68.

Bridger, H.J. (1968). Tetraene antibiotic purification. United States Patent, 3, 378,441.

Capitan-Valley, L.F., Checa-Moreno, R. and Navas, N. (2000). Rapid ultraviolet spectrophotometry and liquid chromatographic methods for the determination of natamycin in lactoserum matrix. *J. AOAC International*, **83**, 802-808.

Chater, K.F. (1972). A morphological and genetic mapping study of white colony mutants of *Streptomyces coelicolor*. *J. Gen. Microbiol.*, **72**, 9-28.

Christiansen, T., Spohr, A.B. and Nielsen, J. (1999). On-line study of growth kinetics of single hyphae of *Aspergillus oryzae* in a flow-through cell. *Biotechnol. Bioeng.*, **63**, 147-153.

Claridge, C.A. (1979). Aminoglycoside antibiotics, 151-238. In Rose, A.H. (ed.), Economic Microbiology, Secondary products of metabolism, **3**. Academic Press, London.

Crandall, L.W. and Hamill, R.L. (1986). Antibiotics produced by Streptomyces: Major structural classes, 355-391. In Queener, S.W. and Day, L.E. (eds.), The Bacteria. A treatise on structure and function, Antibiotic-producing Streptomyces, **IX**. Academic Press, London.

Cross, T. and Goodfellow, M. (1973), 11-91. Taxonomy and classification of the Actinomycetes. In Sykes, G. and Skinner, F.A. (eds.). Actinomycetales: Characteristics and Practical Importance. Academic Press, London.

Demain, A.L., (1988). Actinomycetes : What have you done for us lately?. *Biol. Actimomycetes*, 19-25.

Dietz, A. (1986), 1-26. Structure and taxonomy of Streptomyces. . In Queener, S.W. and Day, L.E. (eds.), The Bacteria. A treatise on structure and function, Antibiotic-producing Streptomyces, **IX**. Academic Press, London.

Dziezak, J.D. (1988). Microscopy and image analysis in R-and-D. *Food Technology*, **42**, 110-124.

Durant, G., Crawley, G. and Formisyn, P. (1994). A simple staining procedure for the characterisation of basidomycetes pellets by image analysis. *Biotechnol. Tech.*, **8**, 395-400.

El-Enhasey, H.A., Farid, M.A. and El-Sayed, E.A. (2000). Influence of inoculum type and cultivation conditions on natamycin production by *Streptomyces natalensis*. *J. Basic Microbiol.*, **40**, 333-342.

Fang, A., Keables, P. and Demain, A.L. (1996). Unexpected enhancement of β-lactam antibiotic formation in *S. clavuligerus* by very high concentrations of exogenous lysine. *Appl. Microbiol. Biotechnol.*, **44**, 705-709.

Farid, M.A., El-Enhasey, H.A., El-Diwany, A.I. and El-Sayed, E.A. (2000). Optimisation of the cultivation medium for natamycin production by *Streptomyces natalensis*. *J. Basic Microbiol.*, **40**, 157-166.

Fletouris, D.J., Botsoglou, N.A. and Mantis, J. (1995). Rapid spectrophotometric method for analysing natamycin in cheese and cheese rind. *J. AOAC International*, **78**, 1024-1029.

Gavaille, A., Bardy, B. and Andremant, A. (1994). Measurement of inhibition zone diameter in disk susceptibility tests by computerized image analysis. *Computers in Biology and Medicine*, **24**, 179-188.

Gonzales-Blanco, P.C., Larralde-Corona, C.P. and Viniegra-Gonzalez, G. (1993). *Biotechnol. Tech.*, **7**, 57-62.

Gottlieb, D. (1973), 1-9. General considerations and implications of the Actinomycetales. In Sykes, G. and Skinner, F.A. (eds.). Actinomycetales: Characteristics and Practical Importance. Academic Press, London.

Grisebach, H. (1978), 113-126. Biosynthesis of macrolide antibiotics. In Hutter, R., Leisinger, T., Nuesch, J. and Wehrli, W. (eds.), Antibiotics and other secondary metabolites. Biosynthesis and production Academic Press, London.

Holley, R.A. (1981). Prevention of surface mold growth on Italian dry sausage by natamycin and potassium sorbate. *Appl. Environ. Microbiol.*, 422-429.

Hopwood, D.A., Kieser, T., Lydiate, D.J. and Bibb, M.J. (1986), 159-230. Streptomyces plasmids: their biology and use as cloning vectors. In Queener, S.W. and Day, L.E. (eds.), The Bacteria. A treatise on structure and function, Antibiotic-producing Streptomyces, **IX**. Academic Press, London.

Kalakoutskii, L.V. and Pouzharitskaja, L.M. (1973), 155-178. The Streptomyces spore: Its distinct features and germinal behaviour. In Sykes, G. and Skinner, F.A. (eds.). Actinomycetales: Characteristics and Practical Importance. Academic Press, London.

Lebrihi, A., Lefebvre, G. and Germain, P. (1988). A study on the regulation of cephamycin C and expandase biosynthesis by *S. clavuligerus* in continuous and batch culture. *Appl. Microbiol. Biotechnol.*, **28**, 39-43.

Lebrihi, A., Germain, P. and Lefebvre, G. (1987). Phosphate repression of cephamycin and clavulanic acid production by *Streptomyces clavuligerus*. *Appl. Microbiol. Biotechnol.*, **26**, 130-135.

Lechevalier, H.A. and Lechevalier, M.P. (1981). Introduction to the order Actinomycetales. Section V, The Actinomycetes. 'The Prokaryotes. A handbook on habitats, isolation and identification of bacteria', **2**.

Lechevalier, H.A. and Lechevalier, M.P. (1967). Biology of the Actinomycetes. *Ann. review Microbiol.*, **21**, 71-100.

Lechevalier, H.A. and Lechevalier, M.P. (1965). Classification des actinomycetes aerobies basees sur leur morphologie et leur composition chimique. *Annales de L'Institut Pasteur*, **108**, 662-673.

Lejeune, R. and Baron, G.V. (1995). On the use of morphological measurements for the quantification of fungal growth. *Biotechnol. Tech.*, **9**, 327-328.

Lejeune, R., Nielsen, J. and Baron, G.V. (1995). Morphology of *Trichoderma reesei* QM9414 in submerged cultures. *Biotechnol. Bioeng.*, **47**, 609-615.

Lubbe, C., Wolfe, S. and Demain, A.L. (1985). Repression and inhibition of cephalosporin synthetases in *S. clavuligerus* by inorganic phosphate. *Arch. Microbiol.*, **140**, 317-320.

Mahon, D. (1990). Fermenter studies on the production of pimaricin by *Streptomyces natalensis*. M.Sc. Thesis, Dublin City University.

Martin, J.F. (1979), 239-286. Nonpolyene Macrolide Antibiotics. In Rose, A.H. (ed.), Economic Microbiology, Secondary Products of Metabolism, **3**. Academic Press, London.

Martin, J.F. (1978), 19-34. Manipulation of gene expression in the development of antibiotic production. In Hutter, R., Leisinger, T., Nuesch, J. and Wehrli, W. (eds.), Antibiotics and other secondary metabolites. Biosynthesis and production Academic Press, London.

Martin, J.F. and Mc Daniel, L.E. (1976). Biosynthesis of candicidin by phosphate-limited resting cells of *Streptomyces griseus*. *Eur. J. Appl. Microbiol.*, **3**, 135-144.

Martin, J.F. and Mc Daniel, L.E. (1975). Kinetics of biosynthesis of polyene macrolide antibiotics in batch cultures: Cell maturation time. *Biotechnol. Bioeng.*, **17**, 925-938.

Mendes, M.V., Recio, E., Fouces, R., Luiten, R., Martin, J.F. and Aparicio, J.F. (2001). Engineered biosynthesis of novel polyenes: a pimaricin derivative produced by targeted gene disruption in *Streptomyces natalensis*. *Chemistry and Biology*, **8**, 635-644.

Metz, B., de Bruijn, E.W. and van Suijdam, J.C. (1981). Methods for quantitative representation of the morphology of molds. *Biotechnol. Bioeng.*, **23**, 149-162.

Millis, J.R., Olson, P.T. and Reimer, M.H. (1992). Natamycin recovery. International Patent Classification : C12P 19/62

Mc Cabe, P. (1990). Production of Pimaricin by *Streptomyces natalensis* in submerged culture. M.Sc. Thesis, Dublin City University.

Mc Gowan, E., Douglas, G.C. and Parkinson, M. (1998). Morphological and physiological markers of juvenility and maturity in shoot cultures of oak (*Quercus robur* and *Q. petraea*). *Tree Physiology*, **18**, 251-257.

Mc Intyre, M., Berry, D.R., Eade, J.K., Cox, P.W., Thomas, C.R. and Mc Neil, B. (1998). Manual and semi-automated morphological analysis of *Penicillium chrysogenum* chemostat culture. *Biotechnol. Tech.*, **12**, 671-675.

Nabais, A.M.A., da Fonseca, M. and Manuela, R. (1995). The effect of solid medium composition on growth and sporulation of *S.clavuligerus*; spore viability during storage at 4°C. *Biotechnol. Tech.* **9**, 361-364.

Okami, Y. and Hotta, K. (1988), 33-67. Search and discovery of new antibiotics. In Goodfellow, M., Williams, S.T. and Mordarski, M. (eds.), Actinomycetes in Biotechnology. Academic Press, London.

O' Shea, M. (1998). Characterisation and growth optimisation of *Streptomyces natalensis*. M.Sc. Thesis, Dublin City University.

Packer, H.L. and Thomas, C.R. (1990). Morphological measurements on filamentous microorganisms by fully automatic image analysis. *Biotechnol. Bioeng.*, **35**, 870-881.

Palti, Y., Parsons, J.E. and Thorgaard, G.H. (1997). Assessment of genetic variability among strains of rainbow and cuttroat trout using multilocus DNA fingerprints. *Aquaculture*, **149**, 47-56.

Paul, G.C. and Thomas, C.R. (1997). Characterisation of mycelial morphology using image analysis. *Adv. Biochem. Eng. Biotechnol.*, 1-59.

Paul, G.C., Kent, C.A. and Thomas, C.R. (1994). Hyphal vacuolation and fragmentation in *P.chrysogenum*. *Biotechnol. Bioeng.*, **44**, 655-660.

Paul, G.C., Kent, C.A. and Thomas, C.R. (1993). Viability testing and characterisation of germination of fungal spores by automatic image analysis. *Biotechnol. Bioeng.*, **42**, 11-23.

Pearson, A., Glennon, B. and Kieran, P. (2000). In-line monitoring of the growth of filamentous organisms. Preceedings of 3rd European Symposium on Biochemical Engineering Science, Copenhagen, Denmark, Sept. 10-13th, p. 267.

Raab, W.P. (1972). Natamycin (Pimaricin). Its properties and possibilities in medicine. Georg Thieme publishers, Stuttgart.

Reichl, U., King, R. and Gilles, E.D. (1992). Characterisation of pellet morphology during submerged growth of *Streptomyces tendae* by image analysis. *Biotechnol. Bioeng.*, **39**, 164-170.

Rollins, M.J., Jensen, S.E. and Westlake, D.W.S. (1991). Effect of dissolved oxygen level on ACV synthetase synthesis and activity during growth of *S.clavuligerus*. *Appl. Microbiol. Biotechnol.*, **35**, 83-88.

Rollins, M.J., Jensen, S.E. and Westlake, D.W.S. (1989). Regulation of antibiotic production by iron and oxygen during defined medium preparation of *S.clavuligerus*. *Appl .Microbiol. Biotechnol.*, **31**, 390-396.

Rollins, M.J., Jensen, S.E. and Westlake, D.W.S. (1988). Effect of aeration on antibiotic production by *Streptomyces clavuligerus*. *J. Ind. Microbiol.*, **3**, 357-364.

Rose, A.H. (1979), 2-33. Production and industrial importance of secondary products of metabolism. In Rose, A.H. (ed.), Economic Microbiology, Secondary Products of Metabolism, **3**. Academic Press, London.

Ryoo, D. (1999). Fungal fractal morphology of pellet morphology in *Aspergillus niger*. *Biotechnol. Tech.*, **13**, 33-36.

Santarelli, M.F., Positano, V. and Landini, L. (2000). Combining high-performance computing and networking for advanced 3-D cardiac imaging. *IEEE Transactions on information technology in biomedics*, **4**, 58-67.

Singh, N., Slavik, M.F. and Wang, X, Li.Y. (1997). Image analysis as a rapid pathogen detection method for use in poultry industry. *J. Rapid Methods and Automation in Microbiol.*, **5**, 205-214.

Sokatch, J.R. and Ornston, L.N. (1986). Introduction. Antibiotic-producing Streptomyces. In Queener, S.W. and Day, L.E. (eds.), The Bacteria. A treatise on structure and function, Antibiotic-producing Streptomyces, **IX.** Academic Press, London.

Spohr, A., Dam-Mikkelsen, C., Carlsen, M., Nielson, J. and Villadsen, J. (1998). On-line study of fungal morphology during submerged growth in a small flow-through cell. *Biotechnol. Bioeng.*, **58**, 541-553.

Spohr, A., Carlsen, M., Nielsen, J. and Villadsen, J. (1997). Morphological characterisation of recombinant strains of *A. oryzae* producing α-amylase during batch cultivations. *Biotechnol. Letters*, **19**, 257-261.

Stanford, K., Richmond, R.J., Jones, S.D.M., Robertson, W.M., Price, M.A. and Gordon, A.J. (1998). Video image analysis for on-line classification of lamb carcasses. *Animal Science*, **67**, 311-316.

Struyk, A.P. and Waisvisz, J.M. (1975). Pimaricin and process of producing same. United States Patent.

Thomas, A.H. (1976). Analysis and assay of polyene antifungal antibiotics : A review. *The Analyst*, **101**, 321-340.

Treskatis, S.K., Orgeldinger, V., Wolf, H. and Gilles, E.D. (1997). Morphological characterisation of filamentous microorganisms in submerged cultures by on-line digital image analysis and pattern recognition. *Biotechnol. Bioeng.*, **53**, 191-201.

Tsutsumi, H., Kono, M., Takai, K., manabe, T., Haraguchi, M., Yamamoto, I. And Oppenheimer, C. (2000). Bioremediation on the shore after an oil spill from Nakhodka in the Sea of Japan. III. Field tests of a bioremediation agent with microobiological cultures for the treatment of an oil spill. *Marine Pollution Bulletin*, **40**, 320-324.

Tucker, K.G., Kelly, T., Delgrazia, P. and Thomas, C.R. (1992). Fully-automatic measurement of mycelial morphology by image analysis. *Biotechnol. Prog.*, **8**, 353-359.

Tuinstra, L.G.M.TH. and Traag, W.A. (1982). Liquid chromatographic determination of natamycin in cheese at residue levels. *J. Assoc. Off. Anal. Chem.*, **65**, 820-822.

Turner, W.B. (1973), 209-217. Secondary metabolisms in Actinomycetales. In Sykes, G. and Skinner, F.A. (ed.s). Actinomycetales: Characteristics and Practical Importance. Academic Press, London.

Vandevooren, J.G., Polder, G., Vanderheijden Gwan. (1991). Application of image analysis for variety testing of mushroom. *Euphytica*, **57**, 245-250.

Vecht-Lifshitz, S.E. and Ison, A.P. (1992). Biotechnological applications of image analysis : Present and future prospects. *J. Biotechnol.*, **23**, 1-18.

Vigneau, E., Loisel, C., Devaux, M.F. and Cantoni, P. (2000). Number of particles for the determination of size distribution from microscopic images. *Powder Technology*, **107**, 243-250.

Vitalis, S., Szalabo, G. and Valyi-Nagy, T. (1963). Comparison of the morphology of streptomycin-producing and non-producing strains of *Streptomyces griseus*. *ActaBiol. Hung.*, **14**, 1, 1-15.

Williams, S.T. (1990). Actinomycetes - The ray fungi. *Mycologist*, **4**, 110-115.

Woodward, R.B. (1957). Struktur und biogenese der makrolide, eine nelle klasse von naturstoffen. *Angew. Chem.*, **69**, 50-58.

Yang, Y.K., Morikawa, M., Shimizu, H., Shioya, S., Suga,K.I., Nihira, T. and Yamada, Y. (1996). Image analysis of mycelial morphology in virginiamycin production by batch culture of Streptomyces virginiae. *J. Ferment. Bioeng.*, **81**, 7-12.

Yegneswaran, P.K., Gray, M.P. and Thompson, B.G. (1991). Experimental simulation of dissolved oxygen fluctuations in large fermenters : Effect on S.clavuligerus. *Biotechnol. Bioeng.*, **38**, 1203-1209.

APPENDIX

A.1 IMAGE ANALYSIS: TERMINOLOGY AND PROGRAM CODE

Dilate filter	A common morphological operation in which the pixels covered by the structuring element (SE) are examined to identify the one with the highest numerical value. The central pixel in this SE is set to this maximum value in the output image. This produces two effects: firstly, the resulting image becomes brighter than the original image; and secondly, any darker details that are larger than the SE are eliminated.
Erode filter	The pixels covered by the SE are examined to identify the one with the lowest numerical value. The central pixel in this SE is set to this minimum value in the output image. This produces two effects: firstly, the resulting image becomes darker than the original image; and secondly, any brighter details that are smaller than the SE are eliminated.
Mask	A copy of the original binary image being processed.
Octagonal SE	A group of pixels arranged in the shape of an octagon.
Skeletonisation	Application of the erode filter which results in a 'skeleton' consisting of lines of pixels that mark the midlines of an object. When an object has branches or projections, this technique can be used to determine the number of branches or nodes.
Structuring Element	A group of pixels arranged in a definite shape.
Thinning filter	A morphological operation in which pixels are removed from a skeletonised object in order to reduce the presence of false branches.

```
//if(isobject("global_pellet"))
//pause();

global integer global_pellet;
//*************************************************************************
// define useful global variables

boolean pelletx_cores;

real core_area=0.0;
AreaCNVFactors[2:3] = -1.0:64.0;

//*************************************************************************
// define overall output variables

integer Total_No_Entities=0;
real Pellets_by_number;
real Clumps_by_number;
real Hyphae_by_number;
real Pellets_by_EVF;
real Clumps_by_EVF;
real Hyphae_by_EVF;
real Average_Area;
real Std_Dev_Area;
real Average_Perimeter;
real Std_Dev_Perimeter;
real Average_Conv_Area;
real Std_Dev_Conv_Area;
real Average_Roughness;
real Std_Dev_Roughness;
real Average_Fullness;
real Std_Dev_Fullness;
real Maximum_Hyphal_Length;
real Average_Hyphal_Length;

// Support function which determines if three points in array
// are in counter-clockwise order.
define ccw(REAL CHU_Array2D, INTEGER CHU_i,INTEGER CHU_j,INTEGER CHU_k){
 AUTO REAL  CHU_a=CHU_Array2D[CHU_i,0]-CHU_Array2D[CHU_j,0],
        CHU_b=CHU_Array2D[CHU_i,1]-CHU_Array2D[CHU_j,1],
        CHU_c=CHU_Array2D[CHU_k,0]-CHU_Array2D[CHU_j,0],
        CHU_d=CHU_Array2D[CHU_k,1]-CHU_Array2D[CHU_j,1];
  return((BOOLEAN)((CHU_a*CHU_d-CHU_b*CHU_c)<=0.));
}

// Requires 2D array of points structured like ArPoints, i.e.
// first point must be know to be in ConvexHull, points must be in
// clockwise order and last point must be same as first.  Status of
// process is shown as percentage on Status Bar.  Returns a selector
// of points in Array which make up ConvexHull.  This is slow, but
// thorough.

// - GL
// Points do not have to be in clockwise order anymore
// User created points will be sorted and the 1st point Pt[0]
// will be automatically found. (unnecessary for autocreated
```

```
// points, but necessary for user created point)
// - GL
define PtConvexHull(REAL CHU_Array2D){
AUTO INTEGER CHU_n=GetOneDimension(CHU_Array2D,0),
        CHU_i,CHU_j=0,CHU_order[CHU_n],CHU_min=0,
        CHU_s[CHU_n]=0..CHU_n;

 AUTO REAL CHU_angles[CHU_n], CHU_t;

//find Pt[0] -GL

 for (CHU_i=1;CHU_i<CHU_n;CHU_i++){
  if (CHU_Array2D[CHU_i,1]>CHU_Array2D[CHU_min,1]) CHU_min=CHU_i; /* find smallest y */
 }
 for (CHU_i=0;CHU_i<CHU_n;CHU_i++){
  if ((CHU_Array2D[CHU_i,1]==CHU_Array2D[CHU_min,1]) &&
(CHU_Array2D[CHU_i,0]>CHU_Array2D[CHU_min,0])) CHU_min=CHU_i ; /* find largest x */
 }

 // update Array2D and Pts for Pr[0] -GL
 CHU_t=CHU_Array2D[0,1];
 mPtPoints[0,0,1] =CHU_Array2D[0,1]=CHU_Array2D[CHU_min,1];
 mPtPoints[0,CHU_min,1]=CHU_Array2D[CHU_min,1] = CHU_t;

 CHU_t=CHU_Array2D[0,0];
 mPtPoints[0,0,0] =CHU_Array2D[0,0]=CHU_Array2D[CHU_min,0];
 mPtPoints[0,CHU_min,0]=CHU_Array2D[CHU_min,0] = CHU_t;




 for (CHU_i=1;CHU_i<CHU_n;CHU_i++){
  CreateLine(CHU_Array2D[0,0]:CHU_Array2D[0,1]:CHU_Array2D[CHU_i,0]:CHU_Array2D[CHU_i,1] );
  extract();
  CHU_angles[CHU_i]=360.0-LnAngleFromReference; /* find angles with Pt[0]*/
 }

 CHU_order=sort(CHU_angles,FALSE);/* sort angles with Pt[0] */

 //update Array2D -GL
 for (CHU_i=0;CHU_i<CHU_n;CHU_i++){
  CHU_Array2D[CHU_i,0] = mPtPoints[0,CHU_order[CHU_i],0];
  CHU_Array2D[CHU_i,1] = mPtPoints[0,CHU_order[CHU_i],1];
 }
clearscreen();
CreatePoints(CHU_Array2D); /* this is the sorted point set -GL */
 //extract();

 for(CHU_i=2;CHU_i<CHU_n;CHU_i++){
  for(CHU_j=SqueezeSelector(CHU_s==CHU_i)-1;CHU_j>0;CHU_j--){
    StatusBar=ToText(100*CHU_i/CHU_n):"%";
    if(!ccw(CHU_Array2D,CHU_i,CHU_s[CHU_j],CHU_s[CHU_j-1]))CHU_s[CHU_j]=FALSE;
   }
   CHU_s=SqueezeSelector(CHU_s);
 }
```

```
 StatusBar="";
clearscreen();
 return CHU_s;
}
//*************************************************************************
define Excel_Setup()
{
if((x=IsWindow("Microsoft Excel",true))>0)
        {
                PostMessage (x, 0x0010, 0L, 0L);
        }
Execute("c:/program files/microsoft office/office/excel.exe","c:\\windows\\desktop\\therese.xls");
Positionwindow("Microsoft Excel",-1);
Positionwindow("OPTIMAS",-2);
}

define Excel_Out(char sheet="Sheet1", integer row, integer col, val)
{
        hChanSheet1 = DDEInitiate ("Excel", sheet);
        DDEPoke (hChanSheet1, "R":totext(row):"C":totext(col), val);
        DDETerminate (hChanSheet1);
}

define Excel_Shutdown(newexcelfile="")
{
        if((x=iswindow("Microsoft Excel",true))>0)
        {
                Statusbar="Shutting down excel...";
                if(newexcelfile!="")
                {
                NewExcelFile1="D:\\therese\\":NewExcelFile:".xls";
                hChanSheet1 = DDEInitiate ("Excel", "Overall Results");
                DDEExecute (hChanSheet1, "[Save.As(\"":NewExcelFile1:"\")]");
                DDETerminate(hChanSheet1);
                }
                PostMessage (x, 0x0010, 0L, 0L);
                Statusbar="Ready...";
        }
}

//*************************************************************************
```

AQUISITION AND PROCESSING OF GREY IMAGE

```
define light_init(integer global_band=0,integer meanintens=200,boolean livestat=TRUE)
{
integer meanintensa=MEANINTENS;
if(global_band>0&&global_band<4)
{
        if(activeimage.colormode[0]!=1&&activeimage.colormode[0]!=2&&activeimage.colormode[0]!=3)
        {
                macromessage("Err001 - Selected Band is not available");
        }
}
```

```
if(livestat==TRUE)
IF(acquire(FALSE)==FALSE)
{
MACROMESSAGE("Err002 - Framegrabber not attached to current window");
return false;
}
integer global_colourstate=0;

if(global_band==0) global_colourstate=1;
ChangeCursor(1);
real rx;
if(global_band==0||global_band==4)
bandofinterest=0;
else
{
        if(global_band<=4)
        {
                bandofinterest=global_band;
        }
        else
        {
                Macromessage("Err004 - Selected value for Arg 0 is greater than those allowed");
                return false;
        }

}


if(livestat==TRUE)
{

real f_val = meanintensa;

for(xde=0;xde<3;xde++)
{
        Histogram(NULL);
        rx = ArROIHistogramStats[0];
        Beep();
        mytime=dostime();
        while(rx<(f_val-(f_val*0.025))||rx>(f_val+(f_val*0.025))&&(dostime()-mytime)<120)
                {
                Statusbar="Percentage of correct luminance":Totext(rx/f_val*100):"%";
                if(isobject("Lighting_info","char"))
                LIGHTING_Info="% Luminance=":Totext(rx/f_val*100):"%   Intensity=": ToText(rx);
                Histogram(NULL);
                rx = ArROIHistogramStats[0];
                }
        delayms(500);
}
freeze();

Statusbar="Percentage of correct luminance ":Totext(rx/f_val*100):"%";
if(isobject("Lighting_info","char"))
LIGHTING_Info="% Grayscale Luminance=":Totext(rx/f_val*100):"%   Intensity=": ToText(rx);
Histogram(NULL);
}
```

```
else
{
rx = ArROIHistogramStats[0];
meanintensa=rx;
}

INTEGER NEWmeanintens = ArROIHistogramStats[0];

if(global_colourstate==1)
{
        bandofinterest = 3;
        global byte bval=getpixelrect();
        bandofinterest = 2;
        global byte gval=getpixelrect();
        bandofinterest = 1;
        global byte rval=getpixelrect();
}
else
{
        if(global_band<4)
        {
                bandofinterest=global_band;
                global byte rval=getpixelrect();
                global byte bval=1;
                global byte gval=1;
        }
        else
        {       bandofinterest=0;
                SetColorMode (0 : 1 : 8 : 1 : 1 : 3);
                global byte rval=getpixelrect();
                global byte bval=1;
                global byte gval=1;
        }
}

global byte rval=getpixelrect();
integer lcount=vectorlength(rval);

Long lLowcount=Call(Lighting_MeanOfBytes,bval,gval,rval,lcount,NEWmeanintens,global_colourstate);
statusbar = "Luminance pattern recorded";
ChangeCursor(0);
if(livestat==TRUE)
Acquire(FALSE);
Beep();
return true;
}
define Light_adjust(integer global_band=0, boolean livestat=TRUE, boolean NEWIMAGEA=TRUE)
{

if(global_band>4||global_band<0)
{
        macromessage("Err004 - Illegal argument Arg 0");
        return false;
}

if(global_band==0&&bval==1)
```

```
{
        macromessage("Err002 - Initialisation completed on single band or grayscale image, Illegal Argument Arg
0");
        return false;
}

if(global_band>0&&bval!=1)
{
        macromessage("Err003 - Initialisation completed on colour image, Illegal Argument Arg 0");
        return false;
}


integer global_colourstate=0;

if(global_band==0) global_colourstate=1;



if(livestat==TRUE)
{

if(Acquire(FALSE)==FALSE)
{
        macromessage("Err005 - Selected image does not support live image display, Illegal argument Arg 1");
        return false;
}
integer xcv;

if(Acquire())
if(colormode!=1 : 1 : 8 : 1 : 3 : 3)
xcv=SetColorMode (1 : 1 : 8 : 1 : 3 : 3);
else
xcv==TRUE;

if(xcv==FALSE&&global_band==0)
{
macromessage("Err006 - Hardware does not support three band colour image, Illegal argument Arg 0");
return false;
}

}

Histogram(NULL);

ChangeCursor(1);
bandofinterest=1;
integer XC=GETSHAPE(getpixelrect());
byte a[,],b[,],c[,];
byte overall[xc[0],xc[1],3];

if(global_band==0)
{
bandofinterest=1;
a=getpixelrect();
bandofinterest=2;
```

```
b=getpixelrect();
bandofinterest=3;
c=getpixelrect();
Bandofinterest=0;
}

else

{
overall[,,]=0;
if(global_band<4)
{
bandofinterest=global_band;
a=getpixelrect();
b=1;
c=1;
}
else
{
bandofinterest=0;
SetColorMode (0 : 1 : 8 : 1 : 1 : 3);
a=getpixelrect();
b=1;
c=1;
}
bandofinterest=0;
}
if(vectorlength(a)==vectorlength(rval))
{
integer lcount=vectorlength(rval);
long aaa=Call(Lighting_Fixpixels,c,b,a,bval,gval,rval,lcount,global_colourstate,1);
//if(aaa==0)
//macromessage("This evaluation copy has expired...\r\n\r\nContact BOS now for a full version\r\n\r\nwww.bos.ie for
further details");
if(global_band==0)
{
IF(NEWIMAGEA==TRUE)
NEWIMAGE("SoftwareFixed", "Adjusted_Image", getshape(a[0,]) : getshape(a[,0]), 1 : 1 : 8 : 1 : 3 : 3, , ModelImage,
);
Overall[,,0]=a;
Overall[,,1]=b;
Overall[,,2]=c;
PutPixelRect(,Overall);
}
else
{

IF(NEWIMAGEA==TRUE)
NEWIMAGE("SoftwareFixed", "Adjusted_Image",  getshape(a[0,]) : getshape(a[,0]), 0 : 1 : 8 : 1 : 1 : 3, , ModelImage,
);

if(global_band<4)
{
bandofinterest=global_band;
Overall[,,0]=a;
SetColorMode (0 : 1 : 8 : 1 : 1 : 3);
```

```
PutPixelRect(,Overall[,,0]);
}
else
{
Overall[,,0]=a;
PutPixelRect(,Overall[,,0]);
}
}
}
else
{
Macromessage("Err001 - The image to be adjusted is not the same size as the initialised image.");
delete(overall,a,b,c);
}
ChangeCursor(0);
return true;
}

//*************************************************************************
```

PROCESSING OF RESULTING BINARY IMAGE
AUTOMATED EDITING-STAGE ONE

```
define process_areas()
{
        Calibrate (One_Pixel_per_Centimeter);        REMOVAL OF OBJECTS TOUCJING ROI
        OriginLockWhere = 1 : 2;
        areacnvfactors[7]=0;
        AreaCNVFactors[6]=0;
        roitobuffer();
        Threshold(0:165);
        x=createarea(,,true);
        if(getshape(x)==0)
        return false;
        clearscreen();
        if(isobject("bit"))
        bitmapdelete(bit);
        bit=ActiveImage.BitmapCreate (,,,TRUE);
        if(isobject("bit10"))
        bitmapdelete(bit10);
        bit10=bitmapprocess(bit,,20);
        if(isobject("bit1"))
        bitmapdelete(bit1);
        bit1=BitmapCreate(,,,,0,BitmapProcess (Bit, , 42, 20));          REMOVAL OF DEBRIS
        if(isobject("bit"))
        bitmapdelete(bit);
        bit=bitmapprocess(bit10,,20);
        clearscreen();
        if(isobject("bitzz"))
        bitmapdelete(bitzz);
        bitzz=bitmapprocess(bit,,20);

        bitmapprocess(bitzz,,36);
        zz=BitmapProcess(Bitzz, , 42,2000);          REMOVAL OF LARGER OBJECTS
        bitmapdelete(bitzz);
```

```
if(isobject("bitz"))
bitmapdelete(bitz);
if(zz!="")
{
bitz=BitmapCreate(,,,,0,zz);
}
clearscreen();
if(zz!="")
bitmapprocess(bit1,bitz,6);
clearscreen();
if(isobject("bit"))
bitmapdelete(bit);
bit=bitmapprocess(bit10,,20);

bitmapprocess(bit,bit1,8);
if(isobject("bit2"))
bitmapdelete(bit2);
bit2=bitmapprocess(bit1,,20);
bitmapprocess(bit2,bit,6);
bitmapprocess(bit2,bit1,8);
if(isobject("bit3"))
bitmapdelete(bit3);
bit3=Bitmapprocess(bit2,,20);
bitmapprocess(bit2,,30,1);
bitmapprocess(bit2,bit3,31,6);
if(isobject("bit3"))
bitmapdelete(bit3);
bit3=Bitmapprocess(bit1,,20);
bitmapprocess(bit3,,36);
bitmapprocess(bit2,bit3,6);
if(isobject("bit3"))
bitmapdelete(bit3);
bit3=Bitmapprocess(bit2,,20);
bitmapprocess(bit2,,30,3);
counter=0;
integer xcc;
```

AUTOMATED EDTITING-STAGE TWO

```
bitmapprocess(bit2,,30,1);
for(DF=0;DF<30;DF++)
{
        bitmapprocess(bit2,,30,1,,5,5,
                                0x8000: 0: 0: 0: 0x8000:
                                0: 0x8000: 0x8000: 0x8000: 0:
                        0: 0x8000: 0x8000: 0x8000: 0:
                                0: 0x8000: 0x8000: 0x8000: 0:
                                0x8000: 0: 0: 0: 0x8000,
                                2,2);
        if(isobject("bit7"))
        bitmapdelete(bit7);
        bit7=bitmapprocess(bit2,,20);

        GH=BitmapProcess (Bit2, , 42,500); // create large areas
        counter++;
        Threshold (253 : 254);
```

```
        if(isobject("bit5"))
        bitmapdelete(bit5);
        bit5=activeimage.BitmapCreate();
if(isobject("bit2"))
bitmapdelete(bit2);
        bit2=bitmapprocess(bit7,,20);
        if(getshape(gh)>0)
        {
        if(isobject("bit5"))
        bitmapdelete(bit5);
        bit5=BitmapCreate(,,,,0,gh);
        }
        else
        {
        if(isobject("bit5"))
        bitmapdelete(bit5);
        bit5=activeimage.BitmapCreate();
        }

                clearscreen();
                bitmapprocess(bit5,bit2,8);
                bitmapprocess(bit5,bit2,6);
                bitmapprocess(bit5,,30,1);
                bitmapprocess(bit5,bit2,31,5,true);
                bitmapprocess(bit2,bit5,6);

                if(counter==1||counter==6||counter==11||counter==16||counter==21||counter==26)
                {
                xcc=counter;
                if(isobject("bit":totext(10+xcc)))
                bitmapdelete(objectfromname("bit":totext(10+xcc)));
                objectfromname("bit":totext(10+xcc))=bitmapprocess(bit5,,20);
                }
                else
                {
                bitmapprocess(objectfromname("bit":totext(10+xcc)),bit5,14);
                }

}
if(isobject("bit2"))
bitmapdelete(bit2);
bit2=bitmapprocess(bit36,,20);

if(zz!="")
bitmapprocess(bit2,bitz,14);

if(isobject("bit110"))
bitmapdelete(bit110);
bit110=bitmapprocess(bit10,,20);

if(zz!="")
bitmapprocess(bit10,bitz,8);


bitmapprocess(bit2,bit3,31,10,TRUE);
bitmapprocess(bit2,bit31,14);
```

```
bitmapprocess(bit2,bit3,31,10,TRUE);
bitmapprocess(bit2,bit26,14);
bitmapprocess(bit2,bit3,31,10,TRUE);
bitmapprocess(bit2,bit21,14);
bitmapprocess(bit2,bit3,31,10,TRUE);
bitmapprocess(bit2,bit16,14);
bitmapprocess(bit2,bit3,31,10,TRUE);
bitmapprocess(bit2,bit11,14);
bitmapprocess(bit2,bit3,31,500,TRUE);



if(isobject("bit11"))
bitmapdelete(bit11);
bit11=bitmapprocess(bit,,20);

if(isobject("bit12"))
bitmapdelete(bit12);
bit12=bitmapprocess(bit2,,20);

bitmapprocess(bit12,bit11,31,10);
bitmapprocess(bit11,bit12,6);
bitmapprocess(bit2,bit11,14);
bitmapprocess(bit2,bit110,8);
bitmapprocess(bit2,bit110,31,50,TRUE);
bitmapprocess(bit2,bit110,14);

BitmapProcess(Bit2, , 42, 35);

if(zz!="")
bitmapprocess(bit,bit10,14);


calibrate(one_pixel_per_centimeter);
setexport(mararea,1,true);
setexport(marmajoraxislength,1,true);
setexport(marbreadth,1,true);
setexport(marhandle,1,true);
multipleextractall();
REAL xararea=mararea;
real xarfullness=mararea/(marmajoraxislength*marbreadth);
real xaraspectratio=marmajoraxislength/marbreadth;

xarhandle=marhandle;

BOOLEAN A=FALSE,B=FALSE,C=FALSE;          SIZE/SHAPE FILTERS APPLIED
for(x=0;x<getshape(xarhandle);x++)
{

        if(xararea[x]<450)
        {
        if((xararea[x]>50&&xarfullness[x]<0.5)||xararea[x]<=50)
        A=TRUE;
        if((xararea[x]<250&&xaraspectratio[x]>1.25)||xararea[x]>=250)
        B=TRUE;
        if(xararea[x]>60||(xararea[x]<60&&xaraspectratio[x]>4))
```

```
                C=TRUE;
                if(A==TRUE&&B==TRUE&&C==TRUE)
                {
                        xarhandle[x]=-1;
                }
                }
                else
                {
                xarhandle[x]=-1;
                }
        A=FALSE;B=FALSE;C=FALSE;
        }
        yarhandle=squeezeselector(xarhandle);
        clearscreen(yarhandle);
  setexport(marcentroid,1,true);
  multipleextract();
  TextToScreen ("*", mArCentroid);
```

MANUAL EDITING STAGE

```
        Macromessage("Select incorrectly outlined pellets or debris\r\nby clicking with the left hand mouse
button\r\nRight hand mouse + F2 to continue");

        while(keyhit()!=113)
        {
                select(-1);
                xhandle=select();
                if(xhandle>0)
                clearscreen(xhandle);
        }

        return true;
        for(xy=1;xy<50;xy++)
        IF(ISOBJECT("bit":totext(xy)))
        bitmapdelete(objectfromname("bit":totext(xy)));
}
```

//process_areas();

DETECTING FOR PRESENCE OF PELLETS

```
define create_cores()
{

        roitobuffer();
        setexport(marhandle,1,true);
        multipleextractall();
                if(isobject("bita"))
                bitmapdelete(bita);
        bita=BitmapCreate(,,,,0,marhandle);
        bitmapprocess(bita,bit,8);

        bitmapprocess(bita,,30,8,,5,5,
                                                0x8000: 0: 0: 0: 0x8000:
                                                0: 0: 0: 0: 0:
                                        0: 0: 0: 0: 0:
```

```
                                                0: 0: 0: 0: 0:
                                                0x8000: 0: 0: 0: 0x8000,
                                                2,2);
        bitmapprocess(bita,,22);
        bitmapprocess(bita,,31,8,,5,5,
                                                0x8000: 0: 0: 0: 0x8000:
                                                0: 0: 0: 0: 0:
                                        0: 0: 0: 0: 0:
                                                0: 0: 0: 0: 0:
                                                0x8000: 0: 0: 0: 0x8000,
                                                2,2);

        if(isobject("cores"))
        bitmapdelete(cores);
        cores=bitmapprocess(bita,,20);
        bitmapprocess(bita,,22);
        bitmapdelete(bita);
        roitolist(,"cores");
arithmeticop("copy","buffer");
}


//create_cores();


define check_for_double_cores()
{
        if(isobject("newareas"))
        delete(newareas);
        roitobuffer();
        setexport(marhandle,1,true);
        setexport(marpoints,1,true);
        multipleextract();
        xarpoints=marpoints;
        xarhandle=marhandle;

        for(x=0;x<getshape(xarhandle);x++)
        {
                clearscreen();
                ahan=createarea(xarpoints[x,,]);
                if(isobject("bita"))
                bitmapdelete(bita);
                bita=BitmapCreate(,,,,0,ahan);
                if(isobject("bitb"))
                bitmapdelete(bitb);
                bitb=bitmapprocess(bita,,20);
                bitmapprocess(bita,cores,8);
                clearscreen();
                if(isobject("bitc"))
                bitmapdelete(bitc);
                bitc=bitmapprocess(bita,,20);
                bhan=bitmapprocess(bita,,42);
                clearscreen();
                setexport(marpoints,1,true);
                multipleextract();
```

```
                if(getshape(bhan)>1)
                {
                        bitmapprocess(bitc,bitb,31,50,true);
                        chan=bitmapprocess(bitc,,42);
                        setexport(marpoints,1,true);
                        multipleextract();
                        if(!isobject("newareas"))
                        {
                                global real newareas=marpoints;
                        }
                        else
                        {
                                newareas::=marpoints;
                        }

                }
                else
                {
                        if(getshape(bhan)==1)
                        {
                                if(!isobject("newareas"))
                                {
                                        global real newareas=marpoints;
                                }
                                else
                                {
                                        newareas::=marpoints;
                                }

                        }
                        if(getshape(bhan==0))
                        {
                                if(!isobject("newareas"))
                                {
                                        global real newareas[,,];
                                        newareas=xarpoints[x,,];
                                }
                                else
                                {
                                        newareas::=xarpoints[x,,];
                                }
                        }
                 bitmapdelete(bita);
                 }

}

        clearscreen();
        createarea(newareas);
}


//check_for_double_cores();
```

```
define measurement_process()
{

        pellet_calib=6.32/10;
        real convexarea,convexperimeter;
        oldcnv=areacnvfactors;
        areacnvfactors[5]=0;
        areacnvfactors[6]=1;

        roitobuffer();
        clearscreen();
        xcv=getshape(newareas[,0,0]);
        ScalarToList (0.0);

        xhan=createarea(newareas[0,,]);
//      pause();

  pelletx_overallcount+=xcv;

        for(x=0;x<xcv;x++)
        {
                xhan=createarea(newareas[x,,]);
                imagemask(1,xhan);
                threshold(0:125);
                graytobinary();
                imagemask(4096);
                ArithmeticOp ("Min", "#0");
                imagemask(8192);
                imagemask(8);
                threshold(254:255);
                if(isobject("bitx"))
                bitmapdelete(bitx);
                bitx=ActiveImage.BitmapCreate(,,,TRUE);
                bitmapprocess(bitx,bit,31,10);
                bitmapprocess(bitx,,22);

//              Create and measure main area
                delete(points1);
                xhan=createarea(,,true);

//              convex area calculations

                SetExport (PtPoints, 1, TRUE);
                setexport(marpoints,1,true);
                setexport(marsampledpoints,1,true);
                multipleextract();
                xyarpoints=marpoints;
                ThickeningFilter(,1,8);
                DilateFilter(,2);
                ErodeFilter(,2);
                AreaCNVFactors[6]=-1;
                createarea(,,true);
                multipleextract();
                clearscreen();
                if(getshape(marsampledpoints)>0)
```

```
createpoints(marsampledpoints);
else
return false;
MultipleExtract();
clearscreen();
CreateArea(PtPoints[PtConvexHull(ptPoints),]);
setexport(mararea,1,true);
setexport(marperimeter,1,true);
multipleextract();
convexarea=mararea[0];
convexperimeter=marperimeter[0];
clearscreen();
undo();
undo();
undo();
xhan=createarea(xyarpoints);
AreaCNVFactors[6]=1;
```

// **convex area calculations**

```
setexport(mararea,1,true);
setexport(marperimeter,1,true);
setexport(marpoints,1,true);
multipleextractall();
area1=sum(mararea);
perimeter1=marperimeter;
points1=marpoints;
```

// **check for core region**

```
if(isobject("bita"))
bitmapdelete(bita);
bita=BitmapCreate(,,,,0,xhan);
bitmapprocess(bita,cores,8);
clearscreen();
bhan=bitmapprocess(bita,,42);
setexport(mararea,1,true);
multipleextract();
if(getshape(mararea)>0)
{
pelletx_cores=true;
core_area=mararea;
}
else
pelletx_cores=false;
clearscreen();
zhan=createarea(points1);
```

DETECTING FOR PRESENCE OF CLUMPS

// **Create Hole Areas**

```
imagemask(1,zhan);
```

```
threshold(0:125);
jhan=createarea(,,true);
setexport(mararea,1,true);
multipleextract();
if(getshape(mararea)>0)
{
area2=sum(mararea)*pow(pellet_calib,2);
holecount=getshape(mararea);
}
else
{
area2=0.0;
holecount=0.0;
}
fullness=1.0-(area2/(area1-area2));
imagemask(8);
arithmeticop("copy","buffer");



if(pelletx_cores==true)
{
Excel_Out("Pellet", pelletx_pelletcount, 1, area1*pow(pellet_calib,2));
Excel_Out("Pellet", pelletx_pelletcount, 2, perimeter1*pellet_calib);
Excel_Out("Pellet", pelletx_pelletcount, 3, convexarea*pow(pellet_calib,2));
Excel_Out("Pellet", pelletx_pelletcount, 4, convexperimeter*pellet_calib);
Excel_Out("Pellet", pelletx_pelletcount, 5, core_area*pow(pellet_calib,2));
Excel_Out("Pellet", pelletx_pelletcount, 6, perimeter1/convexperimeter);
Excel_Out("Pellet", pelletx_pelletcount, 7, fullness);
Excel_Out("Pellet", pelletx_pelletcount, 8, holecount);
Excel_Out("Pellet", pelletx_pelletcount, 9, area2);
statusbar="Pellet...";
pelletx_pelletcount++;
}
else
{
        if(holecount>0)
        {
        Excel_Out("Clump", pelletx_clumpcount, 1, area1*pow(pellet_calib,2));
        Excel_Out("Clump", pelletx_clumpcount, 2, perimeter1*pellet_calib);
        Excel_Out("Clump", pelletx_clumpcount, 3, convexarea*pow(pellet_calib,2));
        Excel_Out("Clump", pelletx_clumpcount, 4, convexperimeter*pellet_calib);
        Excel_Out("Clump", pelletx_clumpcount, 5, perimeter1/convexperimeter);
        Excel_Out("Clump", pelletx_clumpcount, 6, fullness);
        Excel_Out("Clump", pelletx_clumpcount, 7, holecount);
        Excel_Out("Clump", pelletx_clumpcount, 8, area2);
        pelletx_clumpcount++;
        }
        else
```

HYPHAL MEASURING PROCESS

```
        {
        Excel_Out("Hypha", pelletx_hyphacount, 1, area1*pow(pellet_calib,2));
        zhan=createarea(points1);
```

```
        if(isobject("bitd"))
        bitmapdelete(bitd);
                bitd=BitmapCreate(,,,,0,xhan);
                BitmapProcess (bitd, , 32, 1);
                BitmapProcess (bitd, , 22);
                threshold(254:255);
                AreaCNVFactors[12]=1;
                createarea(,,true);
                setexport(marperimeter);
                multipleextract();
                coolperimeter=marperimeter;
                Excel_Out("Hypha", pelletx_hyphacount, 2, coolperimeter/2.0*pellet_calib);
                ThinningFilter(,1,3);
        if(isobject("bitd"))
        bitmapdelete(bitd);
                bitd=BitmapCreate();
                ThinningFilter(,1,1);
                ZOOMFACTOR=-1;
        if(isobject("bite"))
        bitmapdelete(bite);
                bite=BitmapCreate();
                bitmapprocess(bitd,bite,6);
                bitmapprocess(bitd,,22);
                threshold(254:255);
                coolvals=createarea(,,true);

                integer aaaa,bbbb;
                real cccc;

                if(getshape(coolvals)<2)
                {
                        aaaa=0;
                        bbbb=0;
                        cccc=0;
                }
                else
                {
                        aaaa=getshape(coolvals);
                        bbbb=getshape(coolvals)-2;
                        cccc=(coolperimeter/2.0*pellet_calib)/getshape(coolvals);
                }

                Excel_Out("Hypha", pelletx_hyphacount, 3, aaaa);
                Excel_Out("Hypha", pelletx_hyphacount, 4, bbbb);
                Excel_Out("Hypha", pelletx_hyphacount, 5, cccc);

                imagemask(8);
                arithmeticop("copy","buffer");
                pelletx_hyphacount++;
                bitmapdelete(bitd);
                bitmapdelete(bite);
                }


        }
bitmapdelete(bitx);
```

```
        }
        areacnvfactors=oldcnv;
}

//measurement_process();
```

A.2 RAW DATA

Table A.1 Biomass and glucose data for *S. natalensis* grown in YED inoculum medium (Study One) (Figure 5.2)

Time (hours)	Biomass (g/L)	Glucose (g/L)
12.00	0.139	9.150
18.00	0.678	9.400
24.25	1.390	7.700
40.25	1.273	7.450
63.63	3.621	4.800
87.50	3.770	1.050
111.75	3.510	0.000
139.63	3.035	0.000
155.38	3.686	0.000
181.00	2.838	0.000
206.50	3.244	0.000
230.25	3.048	0.005

Table A.2 Biomass data for *S. natalensis* grown in SPG medium (Study One) (Figure 5.3a)

12 hour		18 hour		24 hour	
Time (hours)	Biomass (g/L)	Time (hours)	Biomass (g/L)	Time (hours)	Biomass (g/L)
0.00	0.014	0.00	0.068	0.00	0.139
28.25	2.181	22.25	2.070	16.25	1.442
51.63	2.603	45.63	2.656	39.63	2.695
75.50	3.128	69.50	2.777	63.50	2.937
99.75	3.193	93.75	3.260	87.75	3.088
127.63	3.928	121.63	3.885	115.63	3.781
145.88	4.310	139.88	4.142	133.88	4.040
171.50	4.227	165.50	4.150	159.50	4.328
196.00	4.022	190.00	4.628	184.00	4.598
219.75	4.781	213.75	4.800	205.75	4.812
243.50	5.210	237.50	4.767	229.50	5.154

Table A.3 Glucose data for *S. natalensis* grown in SPG medium (Study One) (Figure 5.3b)

12 hour		18 hour		24 hour	
Time (hours)	**Glucose (g/L)**	**Time (hours)**	**Glucose (g/L)**	**Time (hours)**	**Glucose (g/L)**
0.00	20.000	0.00	20.000	0.00	20.000
28.25	18.000	22.25	18.667	16.25	20.833
51.63	18.500	45.63	16.333	39.63	16.833
75.50	15.000	69.50	15.167	63.50	15.500
99.75	7.500	93.75	8.000	87.75	7.000
127.63	10.167	121.63	10.500	115.63	11.667
145.88	9.500	139.88	10.500	133.88	10.500
171.50	8.000	165.50	8.333	159.50	8.167
196.00	6.500	190.00	5.833	184.00	6.000
219.75	3.167	213.75	4.167	205.75	1.833
243.50	1.667	237.50	1.500	229.50	1.667

Table A.4 Pimaricin data for *S. natalensis* grown in SPG medium (Study One) (Figure 5.3c)

12 hour		18 hour		24 hour	
Time (hours)	**Pimaricin (g/L)**	**Time (hours)**	**Pimaricin (g/L)**	**Time (hours)**	**Pimaricin (g/L)**
0.00	0.000	0.00	0.000	0.00	0.000
28.25	0.000	22.25	0.000	16.25	0.000
51.63	0.003	45.63	0.004	39.63	0.000
75.50	0.007	69.50	0.005	63.50	0.006
99.75	0.011	93.75	0.004	87.75	0.004
127.63	0.008	121.63	0.008	115.63	0.007
145.88	0.016	139.88	0.013	133.88	0.009
171.50	0.026	165.50	0.020	159.50	0.014
196.00	0.029	190.00	0.031	184.00	0.020
219.75	0.053	213.75	0.037	205.75	0.070

Table A.5 $Y_{p/x}$ data for *S. natalensis* grown in SPG medium (Study One) (Figure 5.4)

12 hour		18 hour		24 hour	
Time (hours)	**$Y_{p/x}$ (g/g)**	**Time (hours)**	**$Y_{p/x}$ (g/g)**	**Time (hours)**	**$Y_{p/x}$ (g/g)**
0.00	0.000	0.00	0.000	0.00	0.000
28.25	0.001	22.25	0.002	16.25	0.000
51.63	0.002	45.63	0.002	39.63	0.002
75.50	0.004	69.50	0.001	63.50	0.001
99.75	0.002	93.75	0.002	87.75	0.002
127.63	0.004	121.63	0.003	115.63	0.002
145.88	0.006	139.88	0.005	133.88	0.003
171.50	0.007	165.50	0.007	159.50	0.005
196.00	0.011	190.00	0.008	184.00	0.015
219.75	0.008	213.75	0.000	205.75	0.003

Table A.6 $Y_{p/s}$ data for *S. natalensis* grown in SPG medium (Study One) (Figure 5.5)

12 hour		18 hour		24 hour	
Time (hours)	**$Y_{p/s}$ (g/g)**	**Time (hours)**	**$Y_{p/s}$ (g/g)**	**Time (hours)**	**$Y_{p/s}$ (g/g)**
0.00	0.000	0.00	0.000	0.00	0.000
28.25	0.002	22.25	0.001	16.25	0.000
51.63	0.001	45.63	0.001	39.63	0.001
75.50	0.001	69.50	0.000	63.50	0.000
99.75	0.001	93.75	0.001	87.75	0.001
127.63	0.001	121.63	0.001	115.63	0.001
145.88	0.002	139.88	0.002	133.88	0.001
171.50	0.002	165.50	0.002	159.50	0.001
196.00	0.003	190.00	0.002	184.00	0.004
219.75	0.002	213.75	0.000	205.75	0.001

Table A.7 Biomass and glucose data for *S. natalensis* grown in SPG inoculum medium (Study Two) (Figure 5.7)

Time (hours)	Biomass (g/L)	Glucose (g/L)
12.00	0.071	19.167
18.00	0.209	21.333
24.00	0.878	16.000
51.50	2.267	17.833
75.50	2.738	16.833
99.50	3.436	12.500
123.50	3.849	12.500
148.13	4.147	12.333
177.25	4.330	6.667
195.50	5.110	6.000

Table A.8 Biomass data for *S. natalensis* grown in P-limited medium (Study Two) (Figure 5.8a)

12 hour		18 hour		24 hour	
Time (hours)	Biomass (g/L)	Time (hours)	Biomass (g/L)	Time (hours)	Biomass (g/L)
0.00	0.007	0.00	0.021	0.00	0.088
27.50	0.411	21.50	0.487	15.50	0.407
51.50	0.656	45.50	0.643	39.50	0.722
75.50	0.720	69.50	0.767	63.50	0.868
99.50	0.834	93.50	0.864	87.50	0.893
123.63	0.841	117.63	0.841	111.63	0.923
153.13	0.853	147.13	0.791	141.13	0.851
171.50	0.696	165.38	1.164	159.38	0.770
195.50	1.043	189.38	1.089	183.38	0.993
219.13	1.101	213.00	1.067	207.00	1.043
246.38	1.094	240.25	1.238	234.25	1.119

Table A.9 Glucose data for *S. natalensis* grown in P-limited medium (Study Two) (Figure 5.8b)

12 hour		18 hour		24 hour	
Time (hours)	**Glucose (g/L)**	**Time (hours)**	**Glucose (g/L)**	**Time (hours)**	**Glucose (g/L)**
0.00	63.000	0.00	63.000	0.00	59.500
27.50	53.500	21.50	66.000	15.50	55.000
51.50	52.500	45.50	45.000	39.50	51.500
75.50	58.000	69.50	50.000	63.50	45.000
99.50	42.000	93.50	54.500	87.50	56.500
123.63	52.000	117.63	47.500	111.63	52.000
153.13	48.000	147.13	58.000	141.13	38.500
171.50	44.000	165.38	55.000	159.38	41.500
195.50	39.500	189.38	46.000	183.38	39.000
219.13	37.000	213.00	37.000	207.00	33.000
246.38	31.000	240.25	36.000	234.25	35.000

Table A.10 Biomass and glucose data for *S. natalensis* grown in P-limited medium (Study Three) (Figure 5.10)

Time (hours)	Biomass (g/L)	Glucose (g/L)
0.00	0.555	43.000
24.25	1.956	45.000
46.75	2.627	37.000
68.50	2.775	34.500
92.50	2.757	32.500
116.50	3.270	21.000
140.50	3.430	20.500
165.25	4.158	13.000
190.00	4.588	8.000
212.75	4.881	2.500

Table A.11 Pimaricin raw data for *S. natalensis* grown in P-limited medium (Study Three) (Figure 5.11)

Time (hours)	Pimaricin (g/L)
0.00	0.000
24.25	0.000
46.75	0.000
68.50	0.000
92.50	0.000
116.50	0.011
140.50	0.013
165.25	0.006
190.00	0.056
212.75	0.022

Table A.12 Biomass and glucose data for *S. natalensis* grown in P-limited medium (Study Four) (Figure 5.13)

Time (hours)	Biomass (g/L)	Glucose (g/L)
0.00	0.508	58.000
23.75	0.504	52.000
45.50	0.575	49.500
69.50	0.820	45.500
93.50	0.664	43.000
117.50	0.952	39.000
142.25	0.986	35.500
167.00	0.994	34.000
189.75	1.198	30.000
213.50	1.126	28.500
237.50	1.611	24.000

Table A.13 Recommended dilution factor for various biomass levels. (Figure 6.2)

Biomass (g/L)	Dilution Factor
0.0	0.0
0.4	20.0
0.7	50.0
4.0	150.0
5.0	200.0

Table A.14 Number-based frequency distribution data (Validation – Magnification factor) (Figure 6.3)

Eq. Diam. (μm)	x 10	x4
5.65	0.000	0.000
7.12	0.005	0.039
8.97	0.005	0.157
11.30	0.131	0.216
14.24	0.211	0.255
17.93	0.281	0.118
22.59	0.196	0.098
28.45	0.080	0.039
35.84	0.065	0.029
45.15	0.015	0.049
56.87	0.005	0.000
71.63	0.005	0.000
90.23	0.000	0.000
113.65	0.000	0.000

Table A.15 Cumulative number-based frequency distribution data (Validation – Magnification factor) (Figure 6.4)

Eq. Diam. (μm)	x10	x4
7.12	0.005	0.039
8.97	0.010	0.196
11.30	0.141	0.412
14.24	0.352	0.667
17.93	0.633	0.784
22.59	0.829	0.882
28.45	0.910	0.922
35.84	0.975	0.951
45.15	0.990	1.000
56.87	0.995	1.000
71.63	1.000	1.000
90.23	1.000	1.000
113.65	1.000	1.000

Table A.16 Volume-based frequency distribution data (Validation – Magnification factor) (Figure 6.5)

Eq. Diam. (μm)	x10	x4
7.12	0.000	0.001
8.97	0.000	0.012
11.30	0.014	0.032
14.24	0.044	0.075
17.93	0.118	0.070
22.59	0.165	0.116
28.45	0.135	0.093
35.84	0.220	0.139
45.15	0.101	0.463
56.87	0.067	0.000
71.63	0.135	0.000
90.23	0.000	0.000

Table A.17 Cumulative volume-based frequency distribution data (Validation – Magnification factor) (Figure 6.6)

Eq. Diam. (μm)	x10	x4
7.12	0.000	0.001
8.97	0.000	0.013
11.30	0.014	0.045
14.24	0.059	0.120
17.93	0.177	0.190
22.59	0.342	0.306
28.45	0.477	0.398
35.84	0.696	0.537
45.15	0.798	1.000
56.87	0.865	1.000
71.63	1.000	1.000
90.23	1.000	1.000

Table A.18 Number-based frequency distribution data (Validation – Number of entities) (Figure 6.7)

	No. of Entities							
Eq. Diam. (μm)	**300**	**400**	**500**	**600**	**700**	**800**	**900**	**1000**
2.71	0.000	0.000	0.000	0.000	0.000	0.000	0.000	0.000
3.41	0.000	0.003	0.008	0.008	0.007	0.007	0.008	0.007
4.30	0.037	0.030	0.032	0.033	0.034	0.039	0.039	0.040
5.41	0.083	0.073	0.068	0.075	0.075	0.070	0.066	0.067
6.82	0.090	0.093	0.092	0.106	0.117	0.116	0.118	0.112
8.59	0.090	0.110	0.129	0.124	0.134	0.132	0.135	0.138
10.81	0.090	0.093	0.092	0.088	0.090	0.095	0.102	0.101
13.62	0.070	0.080	0.080	0.073	0.070	0.075	0.075	0.080
17.15	0.053	0.055	0.052	0.050	0.051	0.047	0.042	0.045
21.60	0.053	0.053	0.046	0.045	0.041	0.042	0.038	0.036
27.21	0.023	0.023	0.024	0.022	0.021	0.021	0.021	0.019
34.27	0.053	0.043	0.042	0.040	0.038	0.035	0.032	0.034
43.16	0.066	0.063	0.062	0.060	0.054	0.052	0.052	0.050
54.37	0.073	0.075	0.072	0.070	0.064	0.060	0.057	0.053
68.48	0.076	0.068	0.066	0.068	0.067	0.068	0.064	0.064
86.26	0.037	0.038	0.038	0.036	0.037	0.037	0.038	0.037
108.66	0.033	0.030	0.028	0.027	0.030	0.034	0.035	0.033
136.87	0.017	0.023	0.024	0.025	0.024	0.026	0.024	0.027
172.40	0.023	0.020	0.018	0.020	0.018	0.020	0.022	0.023
217.16	0.027	0.023	0.018	0.018	0.016	0.015	0.022	0.025

Table A.19 Cumulative number-based frequency distribution data (Validation – Number of entities) (Figure 6.8)

	No. of Entities							
Eq. Diam. (μm)	**300**	**400**	**500**	**600**	**700**	**800**	**900**	**1000**
2.71	0.000	0.000	0.000	0.000	0.000	0.000	0.000	0.000
3.41	0.000	0.003	0.008	0.008	0.007	0.007	0.008	0.007
4.30	0.037	0.033	0.040	0.041	0.041	0.046	0.046	0.047
5.41	0.120	0.105	0.108	0.116	0.117	0.116	0.113	0.114
6.82	0.209	0.198	0.199	0.222	0.233	0.231	0.231	0.226
8.59	0.299	0.308	0.329	0.347	0.367	0.363	0.366	0.363
10.81	0.389	0.400	0.420	0.434	0.457	0.458	0.467	0.464
13.62	0.458	0.480	0.500	0.507	0.526	0.532	0.543	0.545
17.15	0.512	0.535	0.552	0.557	0.578	0.580	0.585	0.589
21.60	0.565	0.588	0.598	0.602	0.619	0.622	0.622	0.625
27.21	0.588	0.610	0.622	0.624	0.640	0.643	0.643	0.644
34.27	0.641	0.653	0.663	0.663	0.679	0.678	0.675	0.677
43.16	0.708	0.715	0.725	0.723	0.733	0.730	0.727	0.727
54.37	0.781	0.790	0.797	0.793	0.797	0.790	0.785	0.780
68.48	0.857	0.858	0.863	0.861	0.863	0.858	0.849	0.845
86.26	0.894	0.895	0.900	0.897	0.900	0.896	0.886	0.881
108.66	0.927	0.925	0.928	0.924	0.930	0.929	0.922	0.914
136.87	0.944	0.948	0.952	0.949	0.954	0.955	0.946	0.941
172.40	0.967	0.968	0.970	0.968	0.973	0.975	0.968	0.963
217.16	0.993	0.990	0.988	0.987	0.989	0.990	0.990	0.988
273.54	1.000	1.000	1.000	1.000	1.000	1.000	1.000	1.000

Table A.20 Volume-based frequency distribution data (Validation – Number of entities) (Figure 6.9)

	No. of Entities							
Eq. Diam. (μm)	**300**	**400**	**500**	**600**	**700**	**800**	**900**	**1000**
2.71	0.000	0.000	0.000	0.000	0.000	0.000	0.000	0.000
3.41	0.000	0.000	0.000	0.000	0.000	0.000	0.000	0.000
4.30	0.000	0.000	0.000	0.000	0.000	0.000	0.000	0.000
5.41	0.000	0.000	0.000	0.000	0.000	0.000	0.000	0.000
6.82	0.000	0.000	0.000	0.000	0.000	0.000	0.000	0.000
8.59	0.000	0.000	0.000	0.000	0.000	0.000	0.000	0.000
10.81	0.000	0.000	0.000	0.000	0.000	0.000	0.000	0.000
13.62	0.000	0.000	0.000	0.000	0.000	0.000	0.000	0.000
17.15	0.000	0.001	0.001	0.001	0.001	0.001	0.000	0.000
21.60	0.001	0.001	0.001	0.001	0.001	0.001	0.001	0.001
27.21	0.001	0.001	0.001	0.001	0.001	0.001	0.001	0.001
34.27	0.004	0.003	0.004	0.004	0.004	0.003	0.003	0.003
43.16	0.010	0.010	0.011	0.011	0.010	0.010	0.008	0.007
54.37	0.022	0.024	0.026	0.025	0.025	0.022	0.018	0.016
68.48	0.045	0.044	0.048	0.048	0.051	0.051	0.041	0.038
86.26	0.043	0.049	0.055	0.052	0.057	0.056	0.047	0.044
108.66	0.078	0.078	0.082	0.075	0.092	0.101	0.089	0.078
136.87	0.078	0.116	0.140	0.141	0.148	0.157	0.123	0.127
172.40	0.218	0.207	0.210	0.226	0.227	0.239	0.223	0.216
217.16	0.499	0.465	0.419	0.414	0.383	0.358	0.445	0.469
273.54	0.000	0.000	0.000	0.000	0.000	0.000	0.000	0.000

Table A.21 Cumulative volume-based frequency distribution data (Validation – Number of entities) (Figure 6.10)

	No. of Entities							
Eq. Diam. (μm)	**300**	**400**	**500**	**600**	**700**	**800**	**900**	**1000**
2.71	0.000	0.000	0.000	0.000	0.000	0.000	0.000	0.000
3.41	0.000	0.000	0.000	0.000	0.000	0.000	0.000	0.000
4.30	0.000	0.000	0.000	0.000	0.000	0.000	0.000	0.000
5.41	0.000	0.000	0.000	0.000	0.000	0.000	0.000	0.000
6.82	0.000	0.000	0.000	0.000	0.000	0.000	0.000	0.000
8.59	0.000	0.000	0.000	0.000	0.000	0.000	0.000	0.000
10.81	0.000	0.000	0.001	0.001	0.001	0.001	0.001	0.000
13.62	0.001	0.001	0.001	0.001	0.001	0.001	0.001	0.001
17.15	0.001	0.001	0.002	0.001	0.002	0.002	0.001	0.001
21.60	0.002	0.003	0.003	0.002	0.003	0.003	0.002	0.002
27.21	0.003	0.003	0.004	0.003	0.004	0.004	0.003	0.003
34.27	0.007	0.007	0.008	0.007	0.007	0.007	0.005	0.005
43.16	0.017	0.017	0.019	0.018	0.018	0.017	0.014	0.013
54.37	0.038	0.041	0.045	0.042	0.042	0.039	0.032	0.028
68.48	0.083	0.085	0.093	0.091	0.094	0.091	0.072	0.067
86.26	0.126	0.134	0.149	0.143	0.150	0.147	0.120	0.110
108.66	0.204	0.211	0.231	0.218	0.242	0.247	0.209	0.188
136.87	0.283	0.328	0.371	0.360	0.390	0.404	0.332	0.315
172.40	0.501	0.535	0.581	0.586	0.617	0.642	0.555	0.531
217.16	1.000	1.000	1.000	1.000	1.000	1.000	1.000	1.000
273.54	1.000	1.000	1.000	1.000	1.000	1.000	1.000	1.000

Table A.22 Biomass data for *S. natalensis* grown in YEME medium using a spore inoculum (Figure 6.12)

Trial 1		Trial 2	
Time (hours)	**Biomass (g/L)**	**Time (hours)**	**Biomass (g/L)**
6.00	0.500	12.00	0.700
18.00	0.600	18.00	0.800
30.00	3.400	24.00	2.500
36.00	5.100	30.00	4.700
42.00	3.900	36.00	4.800
48.00	4.600	48.00	4.200

Table A.23 Spore inoculum: Number-based frequency distribution data (trial 1) (Figure 6.13a)

Eq. Diam. (μm)	**12 hours**	**18 hours**	**30 hours**	**36 hours**
2.83	0.000	0.000	0.000	0.002
3.56	0.003	0.002	0.028	0.023
4.49	0.008	0.013	0.040	0.073
5.65	0.022	0.018	0.077	0.081
7.12	0.046	0.047	0.114	0.137
8.97	0.035	0.028	0.079	0.096
11.30	0.018	0.032	0.074	0.068
14.24	0.013	0.010	0.023	0.061
17.93	0.015	0.010	0.017	0.048
22.59	0.013	0.017	0.013	0.025
28.45	0.026	0.012	0.022	0.041
35.84	0.068	0.028	0.022	0.058
45.15	0.096	0.040	0.027	0.058
56.87	0.157	0.063	0.038	0.075
71.63	0.142	0.098	0.055	0.041
90.23	0.161	0.123	0.065	0.030
113.65	0.103	0.246	0.110	0.026
143.16	0.045	0.161	0.134	0.020
180.33	0.020	0.025	0.062	0.020
227.15	0.007	0.017	0.000	0.017
286.13	0.002	0.010	0.000	0.000

Table A.24 Spore inoculum: Number-based frequency distribution data (P+C+H) (trial 2) (Figure 6.13b)

Eq. Diam. (μm)	12 hours	18 hours	30 hours	36 hours
2.83	0.000	0.000	0.005	0.002
3.56	0.005	0.002	0.040	0.005
4.49	0.020	0.003	0.057	0.035
5.65	0.026	0.013	0.092	0.045
7.12	0.063	0.045	0.140	0.100
8.97	0.036	0.052	0.150	0.142
11.30	0.010	0.024	0.088	0.095
14.24	0.005	0.016	0.032	0.055
17.93	0.010	0.002	0.015	0.043
22.59	0.015	0.013	0.013	0.038
28.45	0.035	0.005	0.017	0.047
35.84	0.063	0.026	0.020	0.053
45.15	0.132	0.042	0.018	0.072
56.87	0.156	0.044	0.045	0.073
71.63	0.182	0.067	0.040	0.055
90.23	0.139	0.146	0.053	0.047
113.65	0.070	0.256	0.057	0.015
143.16	0.022	0.153	0.072	0.028
180.33	0.010	0.055	0.043	0.038
227.15	0.002	0.028	0.005	0.010
286.13	0.000	0.006	0.000	0.002

Table A.25 Spore inoculum: Cumulative number-based frequency distribution data (P+C+H) (trial 1) (Figure 6.14a)

Eq. Diam. (μm)	12 hours	18 hours	30 hours	36 hours
2.83	0.000	0.000	0.000	0.002
3.56	0.003	0.002	0.028	0.025
4.49	0.012	0.015	0.069	0.098
5.65	0.033	0.033	0.145	0.179
7.12	0.079	0.080	0.259	0.316
8.97	0.114	0.108	0.338	0.412
11.30	0.132	0.140	0.411	0.480
14.24	0.146	0.150	0.435	0.541
17.93	0.161	0.160	0.452	0.589
22.59	0.174	0.176	0.465	0.614
28.45	0.200	0.188	0.487	0.656
35.84	0.268	0.216	0.508	0.714
45.15	0.364	0.256	0.535	0.772
56.87	0.522	0.319	0.574	0.846
71.63	0.664	0.418	0.629	0.887
90.23	0.825	0.541	0.694	0.917
113.65	0.927	0.787	0.804	0.944
143.16	0.972	0.948	0.938	0.964
180.33	0.992	0.973	1.000	0.983
227.15	0.998	0.990	1.000	1.000
286.13	1.000	1.000	1.000	1.000

Table A.26 Spore inoculum: Cumulative number-based frequency distribution data (P+C+H) (trial 2) (Figure 6.14b)

Eq. Diam. (μm)	12 hours	18 hours	30 hours	36 hours
2.83	0.000	0.000	0.005	0.002
3.56	0.005	0.002	0.045	0.007
4.49	0.025	0.005	0.101	0.042
5.65	0.051	0.018	0.193	0.087
7.12	0.114	0.063	0.333	0.187
8.97	0.151	0.115	0.483	0.328
11.30	0.161	0.140	0.571	0.423
14.24	0.166	0.156	0.602	0.478
17.93	0.175	0.157	0.617	0.522
22.59	0.190	0.170	0.631	0.560
28.45	0.225	0.175	0.647	0.607
35.84	0.288	0.201	0.667	0.660
45.15	0.421	0.244	0.686	0.732
56.87	0.576	0.287	0.730	0.805
71.63	0.758	0.354	0.770	0.860
90.23	0.897	0.500	0.824	0.907
113.65	0.967	0.756	0.880	0.922
143.16	0.988	0.909	0.952	0.950
180.33	0.998	0.964	0.995	0.988
227.15	1.000	0.992	1.000	0.998
286.13	1.000	0.998	1.000	1.000
360.41	1.000	1.000	1.000	1.000

Table A.27 Spore inoculum: Number-based frequency distribution data (P+C) (trial 1) (Figure 6.15a)

Eq. Diam. (μm)	12 hours	18 hours	30 hours	36 hours
5.09	0.000	0.004	0.000	0.000
6.41	0.002	0.006	0.011	0.007
8.07	0.002	0.006	0.011	0.015
10.16	0.008	0.010	0.017	0.011
12.79	0.006	0.004	0.014	0.033
16.11	0.017	0.015	0.020	0.055
20.29	0.035	0.015	0.037	0.070
25.56	0.048	0.023	0.023	0.088
32.19	0.083	0.042	0.040	0.136
40.55	0.161	0.052	0.057	0.151
51.08	0.175	0.102	0.086	0.147
64.35	0.177	0.107	0.089	0.074
81.06	0.152	0.226	0.158	0.066
102.10	0.071	0.274	0.230	0.044
128.61	0.044	0.079	0.181	0.044
162.00	0.015	0.017	0.023	0.033
204.06	0.004	0.013	0.000	0.022
257.04	0.002	0.006	0.000	0.000
323.77	0.000	0.000	0.000	0.000

Table A.28 Spore inoculum: Number-based frequency distribution data (P+C) (trial 2) (Figure 6.15b)

Eq. Diam. (μm)	12 hours	18 hours	30 hours	36 hours
6.78	0.000	0.006	0.020	0.009
8.54	0.004	0.002	0.024	0.016
10.76	0.002	0.008	0.028	0.035
13.55	0.014	0.004	0.024	0.044
17.06	0.014	0.013	0.020	0.047
21.49	0.035	0.006	0.036	0.085
27.07	0.065	0.027	0.040	0.094
34.10	0.150	0.042	0.048	0.129
42.96	0.165	0.049	0.103	0.142
54.11	0.215	0.066	0.083	0.110
68.15	0.189	0.148	0.139	0.094
85.85	0.094	0.282	0.115	0.041
108.14	0.039	0.220	0.175	0.035
136.21	0.012	0.076	0.135	0.075
171.58	0.002	0.036	0.012	0.035
216.12	0.000	0.015	0.000	0.006
272.23	0.000	0.002	0.000	0.000
342.94	0.000	0.000	0.000	0.000

Table A.29 Spore inoculum: Cumulative number-based frequency distribution data (P+C) (trial 1) (Figure 6.16a)

Eq. Diam. (μm)	12 hours	18 hours	30 hours	36 hours
6.41	0.002	0.006	0.011	0.007
8.07	0.004	0.011	0.023	0.022
10.16	0.012	0.021	0.040	0.033
12.79	0.017	0.025	0.055	0.066
16.11	0.035	0.040	0.075	0.121
20.29	0.069	0.056	0.112	0.191
25.56	0.117	0.079	0.135	0.279
32.19	0.200	0.121	0.175	0.415
40.55	0.361	0.172	0.233	0.566
51.08	0.536	0.274	0.319	0.713
64.35	0.712	0.381	0.408	0.787
81.06	0.864	0.607	0.566	0.853
102.10	0.935	0.881	0.796	0.897
128.61	0.979	0.960	0.977	0.941
162.00	0.994	0.977	1.000	0.974
204.06	0.998	0.990	1.000	0.996
257.04	1.000	0.996	1.000	0.996
323.77	1.000	1.000	1.000	1.000

Table A.30 Spore inoculum: Cumulative number-based frequency distribution data (P+C) (trial 2) (Figure 6.16b)

Eq. Diam. (μm)	12 hours	18 hours	30 hours	36 hours
8.54	0.004	0.002	0.024	0.016
10.76	0.006	0.009	0.052	0.050
13.55	0.020	0.013	0.075	0.094
17.06	0.033	0.027	0.095	0.142
21.49	0.069	0.032	0.131	0.226
27.07	0.134	0.059	0.171	0.321
34.10	0.283	0.100	0.218	0.450
42.96	0.449	0.150	0.321	0.591
54.11	0.663	0.216	0.405	0.701
68.15	0.852	0.364	0.544	0.796
85.85	0.947	0.646	0.659	0.836
108.14	0.986	0.866	0.833	0.871
136.21	0.998	0.941	0.968	0.947
171.58	1.000	0.977	0.980	0.981
216.12	1.000	1.000	1.000	1.000

Table A.31 Spore inoculum: Volume-based frequency distribution data (P+C) (trial 1) (Figure 6.17a)

Eq. Diam. (μm)	12 hours	18 hours	30 hours	36 hours
6.41	0.000	0.000	0.000	0.000
8.07	0.000	0.000	0.000	0.000
10.16	0.000	0.000	0.000	0.000
12.79	0.000	0.000	0.000	0.000
16.11	0.000	0.000	0.000	0.000
20.29	0.001	0.000	0.000	0.001
25.56	0.002	0.000	0.000	0.003
32.19	0.006	0.002	0.002	0.008
40.55	0.023	0.004	0.004	0.018
51.08	0.050	0.015	0.013	0.035
64.35	0.101	0.031	0.028	0.035
81.06	0.173	0.132	0.099	0.063
102.10	0.162	0.320	0.287	0.084
128.61	0.202	0.183	0.451	0.167
162.00	0.140	0.080	0.115	0.251
204.06	0.070	0.125	0.000	0.335
257.04	0.070	0.107	0.000	0.000
323.77	1.000	1.000	1.000	1.000

Table A.32 Spore inoculum: Volume-based frequency distribution data (P+C) (trial 2) (Figure 6.17b)

Eq. Diam. (μm)	12 hours	18 hours	30 hours	36 hours
8.54	0.000	0.000	0.000	0.000
10.76	0.000	0.000	0.000	0.000
13.55	0.000	0.000	0.000	0.000
17.06	0.000	0.000	0.000	0.000
21.49	0.001	0.000	0.000	0.002
27.07	0.005	0.001	0.001	0.004
34.10	0.022	0.002	0.002	0.010
42.96	0.050	0.004	0.011	0.022
54.11	0.129	0.012	0.017	0.035
68.15	0.227	0.052	0.058	0.060
85.85	0.226	0.200	0.095	0.052
108.14	0.189	0.311	0.289	0.087
136.21	0.113	0.214	0.447	0.380
171.58	0.038	0.204	0.079	0.348

Table A.33 Spore inoculum: Cumulative volume-based frequency distribution data (P+C) (trial 1) (Figure 6.18a)

Eq. Diam. (μm)	12 hours	18 hours	30 hours	36 hours
6.41	0.000	0.000	0.000	0.000
8.07	0.000	0.000	0.000	0.000
10.16	0.000	0.000	0.000	0.000
12.79	0.000	0.000	0.000	0.000
16.11	0.000	0.000	0.000	0.001
20.29	0.001	0.000	0.001	0.002
25.56	0.003	0.001	0.001	0.004
32.19	0.008	0.002	0.003	0.012
40.55	0.032	0.006	0.007	0.030
51.08	0.082	0.021	0.021	0.065
64.35	0.183	0.052	0.048	0.100
81.06	0.356	0.184	0.147	0.163
102.10	0.518	0.504	0.434	0.247
128.61	0.720	0.687	0.885	0.414
162.00	0.860	0.768	1.000	0.665
204.06	0.930	0.893	1.000	1.000
257.04	1.000	1.000	1.000	1.000

Table A.34 Spore inoculum: Cumulative volume-based frequency distribution data (P+C) (trial 2) (Figure 6.18b)

Eq. Diam. (μm)	12 hours	18 hours	30 hours	36 hours
8.54	0.000	0.000	0.000	0.000
10.76	0.000	0.000	0.000	0.000
13.55	0.000	0.000	0.000	0.000
17.06	0.000	0.000	0.000	0.001
21.49	0.002	0.000	0.001	0.002
27.07	0.007	0.001	0.002	0.006
34.10	0.029	0.003	0.004	0.016
42.96	0.079	0.007	0.015	0.039
54.11	0.208	0.019	0.032	0.073
68.15	0.434	0.071	0.090	0.133
85.85	0.661	0.271	0.185	0.185
108.14	0.849	0.582	0.474	0.272
136.21	0.962	0.796	0.921	0.652
171.58	1.000	1.000	1.000	1.000

Table A.35 Biomass data for *S. natalensis* grown in YEME medium using a vegetative inoculum (Figure 6.19)

Time (hours)	Biomass (g/L)	Time (hours)	Biomass (g/L)
0.00	0.450	0.00	0.450
6.00	0.500	6.00	0.600
12.00	1.100	12.00	1.350
20.00	0.800	20.00	1.450
27.00	0.550	27.00	0.600
30.00	0.900	30.00	1.250
37.00	1.450	37.00	1.400
43.00	1.300	43.00	2.300

Table A.36 Vegetative inoculum: Number-based frequency distribution data (P+C) (trial 1) (Figure 6.20a)

Eq. Diam. (μm)	12 hours	20 hours	30 hours	43 hours
6.78	0.003	0.016	0.011	0.017
8.54	0.023	0.036	0.039	0.033
10.76	0.029	0.036	0.028	0.041
13.55	0.074	0.073	0.022	0.071
17.06	0.100	0.042	0.072	0.046
21.49	0.087	0.063	0.088	0.062
27.07	0.119	0.052	0.055	0.041
34.10	0.109	0.099	0.099	0.046
42.96	0.090	0.094	0.127	0.112
54.11	0.071	0.104	0.116	0.154
68.15	0.119	0.073	0.094	0.141
85.85	0.084	0.057	0.083	0.062
108.14	0.051	0.089	0.077	0.075
136.21	0.026	0.115	0.072	0.050
171.58	0.010	0.047	0.017	0.050

Table A.37 Vegetative inoculum: Number-based frequency distribution data (P+C) (trial 2) (Figure 6.20b)

Eq. Diam. (μm)	12 hours	20 hours	30 hours	43 hours
6.78	0.009	0.011	0.012	0.000
8.54	0.016	0.044	0.028	0.021
10.76	0.019	0.039	0.040	0.035
13.55	0.059	0.055	0.045	0.084
17.06	0.122	0.088	0.045	0.108
21.49	0.144	0.039	0.069	0.077
27.07	0.094	0.061	0.121	0.098
34.10	0.116	0.050	0.077	0.101
42.96	0.116	0.083	0.113	0.119
54.11	0.078	0.072	0.126	0.115
68.15	0.056	0.066	0.101	0.077
85.85	0.078	0.072	0.097	0.052
108.14	0.044	0.061	0.069	0.038
136.21	0.044	0.127	0.032	0.038
171.58	0.006	0.133	0.024	0.028

Table A.38 Vegetative inoculum: Cumulative number-based frequency distribution data (P+C) (trial 1) (Figure 6.21a)

Eq. Diam. (μm)	12 hours	20 hours	30 hours	43 hours
6.78	0.003	0.016	0.011	0.017
8.54	0.026	0.052	0.050	0.050
10.76	0.055	0.089	0.077	0.091
13.55	0.129	0.161	0.099	0.162
17.06	0.228	0.203	0.171	0.207
21.49	0.315	0.266	0.260	0.270
27.07	0.434	0.318	0.315	0.311
34.10	0.543	0.417	0.414	0.357
42.96	0.633	0.510	0.541	0.469
54.11	0.704	0.615	0.657	0.622
68.15	0.823	0.688	0.751	0.763
85.85	0.907	0.745	0.834	0.826
108.14	0.958	0.833	0.912	0.900
136.21	0.984	0.948	0.983	0.950
171.58	0.994	0.995	1.000	1.000
216.12	1.000	1.000	1.000	1.000

Table A.39 Vegetative inoculum: Cumulative number-based frequency distribution data (P+C) (trial 2) (Figure 6.21b)

Eq. Diam. (μm)	12 hours	20 hours	30 hours	43 hours
6.78	0.009	0.011	0.012	0.000
8.54	0.025	0.055	0.040	0.021
10.76	0.044	0.094	0.081	0.056
13.55	0.103	0.149	0.126	0.140
17.06	0.225	0.238	0.170	0.248
21.49	0.369	0.276	0.239	0.325
27.07	0.463	0.337	0.360	0.423
34.10	0.578	0.387	0.437	0.524
42.96	0.694	0.470	0.551	0.643
54.11	0.772	0.541	0.676	0.759
68.15	0.828	0.608	0.777	0.836
85.85	0.906	0.680	0.874	0.888
108.14	0.950	0.740	0.943	0.927
136.21	0.994	0.867	0.976	0.965
171.58	1.000	1.000	1.000	0.993
216.12	1.000	1.000	1.000	1.000

Table A.40 Vegetative inoculum: Volume-based frequency distribution data (P+C) (trial 1) (Figure 6.22a)

Eq. Diam. (μm)	12 hours	20 hours	30 hours	43 hours
6.78	0.000	0.000	0.000	0.000
8.54	0.000	0.000	0.000	0.000
10.76	0.000	0.000	0.000	0.000
13.55	0.001	0.000	0.000	0.000
17.06	0.002	0.000	0.001	0.000
21.49	0.003	0.001	0.002	0.001
27.07	0.008	0.001	0.002	0.001
34.10	0.015	0.005	0.008	0.003
42.96	0.024	0.010	0.021	0.015
54.11	0.038	0.023	0.038	0.041
68.15	0.127	0.032	0.062	0.075
85.85	0.179	0.050	0.109	0.066
108.14	0.220	0.154	0.204	0.159
136.21	0.220	0.398	0.378	0.212
171.58	0.165	0.325	0.174	0.424

Table A.41 Vegetative inoculum: Volume-based frequency distribution data (P+C) (trial 2) (Figure 6.22b)

Eq. Diam. (μm)	12 hours	20 hours	30 hours	43 hours
6.78	0.000	0.000	0.000	0.000
8.54	0.000	0.000	0.000	0.000
10.76	0.000	0.000	0.000	0.000
13.55	0.001	0.000	0.000	0.001
17.06	0.002	0.000	0.001	0.001
21.49	0.005	0.000	0.002	0.002
27.07	0.006	0.001	0.006	0.005
34.10	0.016	0.002	0.007	0.011
42.96	0.031	0.006	0.021	0.025
54.11	0.042	0.010	0.047	0.048
68.15	0.060	0.018	0.076	0.064
85.85	0.168	0.039	0.146	0.087
108.14	0.188	0.066	0.207	0.128
136.21	0.375	0.278	0.195	0.256
171.58	0.107	0.579	0.292	0.372

Table A.42 Vegetative inoculum: Cumulative volume-based frequency distribution data (P+C) (trial 1) (Figure 6.23a)

Eq. Diam. (μm)	12 hours	20 hours	30 hours	43 hours
6.78	0.000	0.000	0.000	0.000
8.54	0.000	0.000	0.000	0.000
10.76	0.000	0.000	0.000	0.000
13.55	0.001	0.000	0.000	0.000
17.06	0.002	0.001	0.001	0.001
21.49	0.005	0.001	0.003	0.002
27.07	0.013	0.003	0.005	0.003
34.10	0.028	0.008	0.013	0.006
42.96	0.052	0.019	0.034	0.021
54.11	0.090	0.041	0.073	0.062
68.15	0.217	0.073	0.135	0.138
85.85	0.396	0.123	0.244	0.204
108.14	0.616	0.277	0.447	0.363
136.21	0.835	0.675	0.826	0.576
171.58	1.000	1.000	1.000	1.000

Table A.43 Vegetative inoculum: Cumulative volume-based frequency distribution data (P+C) (trial 2) (Figure 6.23b)

Eq. Diam. (μm)	12 hours	20 hours	30 hours	43 hours
6.78	0.000	0.000	0.000	0.000
8.54	0.000	0.000	0.000	0.000
10.76	0.000	0.000	0.000	0.000
13.55	0.001	0.000	0.000	0.001
17.06	0.003	0.001	0.001	0.002
21.49	0.008	0.001	0.003	0.004
27.07	0.014	0.002	0.008	0.009
34.10	0.029	0.004	0.016	0.020
42.96	0.060	0.009	0.037	0.045
54.11	0.102	0.019	0.084	0.093
68.15	0.163	0.037	0.160	0.157
85.85	0.330	0.077	0.307	0.244
108.14	0.518	0.143	0.514	0.372
136.21	0.893	0.421	0.708	0.628
171.58	1.000	1.000	1.000	1.000

Table A.44 Vegetative Inoculum: FBRM data (P+C+H) for *S. natalensis* grown in YEME medium from a spore inoculum (Figure 6.4 a) and b))

Chord Length (µm)	1.00	1.08	1.17	1.26	1.36	1.47	1.59	1.71	1.85	2.00	2.15	2.33	2.51	2.71	2.93	3.16	3.42
Trial 1																	
18 hour	1.441	1.556	1.671	1.704	1.840	2.208	2.475	2.599	2.775	3.211	3.335	3.362	2.812	2.487	2.577	2.662	3.204
30 hour	31.127	33.610	35.896	34.740	37.511	41.897	45.810	52.200	57.533	66.086	67.888	67.621	60.196	51.643	48.054	48.969	58.041
36 hour	30.224	32.635	35.140	36.949	39.896	44.815	49.101	53.752	58.353	61.126	61.473	59.494	50.960	46.011	44.645	47.445	56.021
Trial 2																	
18 hour	5.463	5.899	6.346	6.621	7.150	8.194	9.041	10.109	11.063	11.752	12.085	12.074	10.408	8.933	8.214	8.817	10.626
36 hour	22.338	24.120	25.986	27.462	29.653	33.331	36.527	39.529	42.719	45.037	44.838	42.705	36.153	32.294	31.174	33.158	39.031
30 hour	26.871	29.015	31.037	30.537	32.974	36.721	40.107	46.020	50.849	57.701	59.616	59.859	52.754	45.737	42.628	43.574	51.852

Chord Length (µm)	3.69	3.98	4.30	4.64	5.01	5.41	5.84	6.31	6.81	7.36	7.94	8.58	9.26	10.00	10.80	11.66	12.59
Trial 1																	
18 hour	3.815	4.684	5.097	10.312	37.819	33.145	8.436	5.518	5.703	6.784	6.313	4.932	3.847	4.502	6.355	5.970	4.429
30 hour	70.893	83.380	84.687	82.659	83.204	87.326	86.677	84.427	96.316	117.018	115.366	94.603	82.133	92.317	123.715	118.955	98.351
36 hour	66.548	77.188	81.292	81.206	80.987	82.024	78.217	76.632	89.124	107.968	105.920	85.657	72.058	85.709	117.821	114.945	88.738
Trial 2																	
18 hour	13.098	15.072	15.412	15.027	15.639	16.149	15.275	14.753	18.081	22.409	21.115	15.921	12.186	14.744	21.899	19.810	13.538
36 hour	47.290	54.953	57.471	56.368	57.062	57.256	53.913	54.325	65.315	79.409	74.700	58.937	48.966	57.576	81.206	72.491	57.774
30 hour	63.453	75.144	77.481	75.171	76.475	79.888	79.580	77.450	88.515	107.600	105.211	86.120	75.471	86.900	117.349	111.999	93.150

Chord Length (µm)	13.59	14.68	15.85	17.11	18.48	19.95	21.54	23.26	25.12	27.12	29.29	31.62
Trial 1												
18 hour	4.402	4.336	3.713	3.740	2.598	2.698	3.027	2.826	3.238	3.566	3.545	3.906
30 hour	109.663	112.217	101.979	114.281	90.096	92.895	110.094	120.959	136.059	168.429	158.993	172.625
36 hour	94.944	91.935	80.457	92.273	71.785	78.794	97.636	109.031	117.714	136.687	130.506	159.320
Trial 2												
18 hour	15.006	14.352	10.804	11.202	6.630	5.908	7.506	7.065	8.933	12.952	12.897	16.070
36 hour	66.493	65.969	63.357	73.485	56.841	59.760	63.943	70.070	78.786	99.508	99.126	110.591
30 hour	101.837	103.066	91.975	100.055	78.428	80.724	98.900	108.230	125.026	153.205	146.498	156.649

Chord Length (µm)	34.15	36.87	39.81	42.99	46.42	50.12	54.12	58.43	63.10	68.13	73.56	79.43
Trial 1												
18 hour	3.578	2.568	2.063	1.670	2.197	2.622	2.605	1.673	1.383	2.086	2.411	1.562
30 hour	167.749	150.353	128.371	127.773	135.092	132.403	121.650	90.190	83.174	78.240	62.012	42.702
36 hour	158.263	147.378	132.063	129.384	149.869	165.057	182.662	178.582	179.976	192.156	191.687	97.152
Trial 2												
18 hour	15.009	11.144	7.418	7.352	10.448	13.603	12.443	7.202	6.094	9.847	10.457	5.813
36 hour	111.168	106.994	103.181	116.036	139.605	157.983	167.317	142.240	142.811	149.620	131.699	96.268
30 hour	147.065	126.653	103.309	103.811	111.548	112.290	95.802	67.923	57.824	46.556	32.398	20.920

Chord Length (µm)	85.77	92.61	100.00	107.98	116.59	125.89	135.94	146.78	158.49	171.13	184.79	199.53
Trial 1												
18 hour	1.722	2.553	1.585	2.127	1.944	1.707	1.793	1.581	1.144	0.932	0.602	0.330
30 hour	39.166	33.306	21.942	18.903	12.885	9.179	6.435	4.594	3.039	2.271	1.398	0.913
36 hour	70.697	56.194	35.123	29.999	20.751	14.378	10.793	9.576	7.060	3.204	1.482	0.890
Trial 2												
18 hour	6.882	8.882	5.136	6.933	5.901	4.927	4.434	3.797	2.830	2.672	1.614	1.026
36 hour	92.567	76.488	51.684	46.542	32.541	24.673	17.486	12.392	7.350	4.970	3.166	1.879
30 hour	18.308	14.299	8.841	6.816	4.303	2.768	1.520	0.934	0.468	0.239	0.138	0.089

Chord Length (µm)	541.17	584.34	630.96	681.29	735.64	794.33	857.70	926.12	1000.000
Trial 1									
18 hour	0.000	0.000	0.000	0.000	0.000	0.000	0.000	0.000	0.000
30 hour	0.000	0.000	0.000	0.000	0.000	0.000	0.000	0.000	0.000
36 hour	0.000	0.000	0.000	0.000	0.000	0.000	0.000	0.000	0.000
Trial 2									
18 hour	0.003	0.000	0.000	0.000	0.000	0.000	0.000	0.000	0.000
36 hour	0.003	0.000	0.000	0.000	0.000	0.000	0.000	0.000	0.000
30 hour	0.000	0.000	0.000	0.000	0.000	0.000	0.000	0.000	0.000